Sedimentological, petrographic, and geochemical characterization of Ediacaran platform carbonates (Tamengo Formation, Corumbá Group)

Maria Eduarda Alves Ferreira Ramos
(17/0171264)

Advisor: Prof. Dr. Martino Giorgioni

Co-advisor: Prof. Dr. Detlef Walde

Examination committee: Prof. Dr. Shuhai Xiao

Prof. Dr. Carlos José S. Alvarenga

Graduate Program in Geochemistry

Brasília, August 2019

ACKNOWLEDGEMENT

First, I thank my mother, Maria José, for having always encouraged me to be the scientist I am today. I thank my father, Ronaldo, for teaching me about the strength of being a woman. I thank my sister, Maria Clara, for the advice and for all her love. I thank my partner, Jordana, for helping me with the graphics and for giving me strength on the hard days, for laughing with me on fun days and for being by my side in every trivial day. I thank my friends for always sounding interested and enthusiastic when hearing the news on the Corumbá Ediacaran Ramp.

Thanks to Prof. Detlef for the attention and kindness with which he welcomed me in Brasília, for presenting me this masters project and for his willingness and help in all the fieldwork. Thanks to my advisor Prof. Martino for the opportunity to be his student, for the trust over these two years, for being always available and for your patience and serenity. Thanks also to the colleagues involved in the EDIACARANO group for all the support and exchange of knowledge. Special thanks to friends Matheus Denezine, Rodrigo Adôrno and Gabriella Fazio for the help in collecting samples and for the most pleasant company in the fieldwork.

I thank FAPDF, which funded this research through the grant with process n. 0193.001609/2017 and CAPES for granting the scholarship.

ABSTRACT

The Tamengo Formation crops out in the southern portion of the Paraguay Belt and presents continuous geological record of the late Neoproterozoic in Brazil, with its carbonate and siliciclastic sediments being the remnants of a period marked by many environmental changes. Even though its paleontological, structural and stratigraphic features had been broadly studied, there is still a deficiency on sedimentological characterization. This study presents new detailed stratigraphic sections, facies analysis, and carbon isotopic data from two sections of the Tamengo Formation (Corcal and Laginha), aiming to enhance the understanding of the Corumbá Ediacaran Ramp palaeodepositional environment. The unit comprises mainly dark limestones with marl and mudstone intercalations, in addition to a remarkable fossil record, including the Ediacaran marker taxa *Cloudina lucianoi* (Beurlen & Sommer, 1957) and *Corumbella werneri* (Hahn *et al*., 1982). The $\delta^{13}C_{PDB}$ results in Laginha reveal a complex signal, with highly variable values, including negative ones, not observed in neighbour sections. This record might be influenced both by primary and diagenetic processes. Nevertheless, the Corcal section bears a primary signal, steady and correlative to other renowned upper Ediacaran reference sections. The facies analysis in the Corcal section revealed a gently dipping ramp setting with sea level fluctuations, as well as peritidal to inner ramp structures, which indicate an environment shallower than previously outlined. On the other hand, the Laginha section displays a diverse facies association, marked by terrigenous contributions, suggesting a setting with a steeper topography, probably controlled by extensional tectonics. The results suggest that the Tamengo Formation deposited in graben type setting, with a complex topography.

Keywords Ediacaran; C and O isotopes; Paraguay Belt; Corumbá Group; Corumbá Graben System

TABLE OF CONTENTS

TABLE OF FIGURES

1. INTRODUCTION

This work presents new contributions concerning the sedimentological characterization, facies analysis and isotopic geochemistry of the Tamengo Formation, part of the Corumbá Group, which outcrops in the southern Paraguay Belt. It is composed of carbonate and siliciclastic rocks, with fossil content of great geological relevance. Paleontological studies and dating place the Tamengo Formation at the end of the Ediacaran Period.

This dissertation begins with the presentation of the study area, its location, motivation and aims. The second chapter presents theoretical basis related to the Ediacaran period and the carbon isotope geochemistry. The third chapter contains results, discussion and conclusion in the form of a scientific paper.

1.1. STUDY AREA

The research was developed in the surroundings of the city of Corumbá, located in the extreme northwest of the state of Mato Grosso do Sul, in southwest Brazil, near the border with Bolivia. It is located 1500 km from Brasília, with access by highways BR-060 followed by BR-262. The studied outcrops are located in two mining areas of the cement industry. The Corcal Mine is located 4 km west of the center of Corumbá, with access via Highway Ramon Gomes, and Laginha Mine is 18 km south, with access via BR-262. The coordinates of the mines, with Datum WGS 84, Zone 21K, are respectively 428170/7897070 and 432261/7885946 (Figure 1). The geological setting of the studied area is presented in chapter 3.3, page 8.

1.2. MOTIVATION AND AIMS

The characterization of Ediacaran carbonate environments has fundamental implications not only in carbonate sedimentology, but also for constraining the origin of the chemostratigraphic signal and the conditions that prompted the rise of the early animals on Earth. The paleontological, structural, and stratigraphic features of the Tamengo Formation have been extensively studied, however, there is still a deficiency on the sedimentological characterization. Here we enhance the sedimentological characterization of this unit and contribute to bring its study up to a level comparable with that of the most studied Ediacaran carbonates. This study focuses on two stratigraphic sections of the Tamengo Formation to perform a detailed facies characterization and reach the following aims:

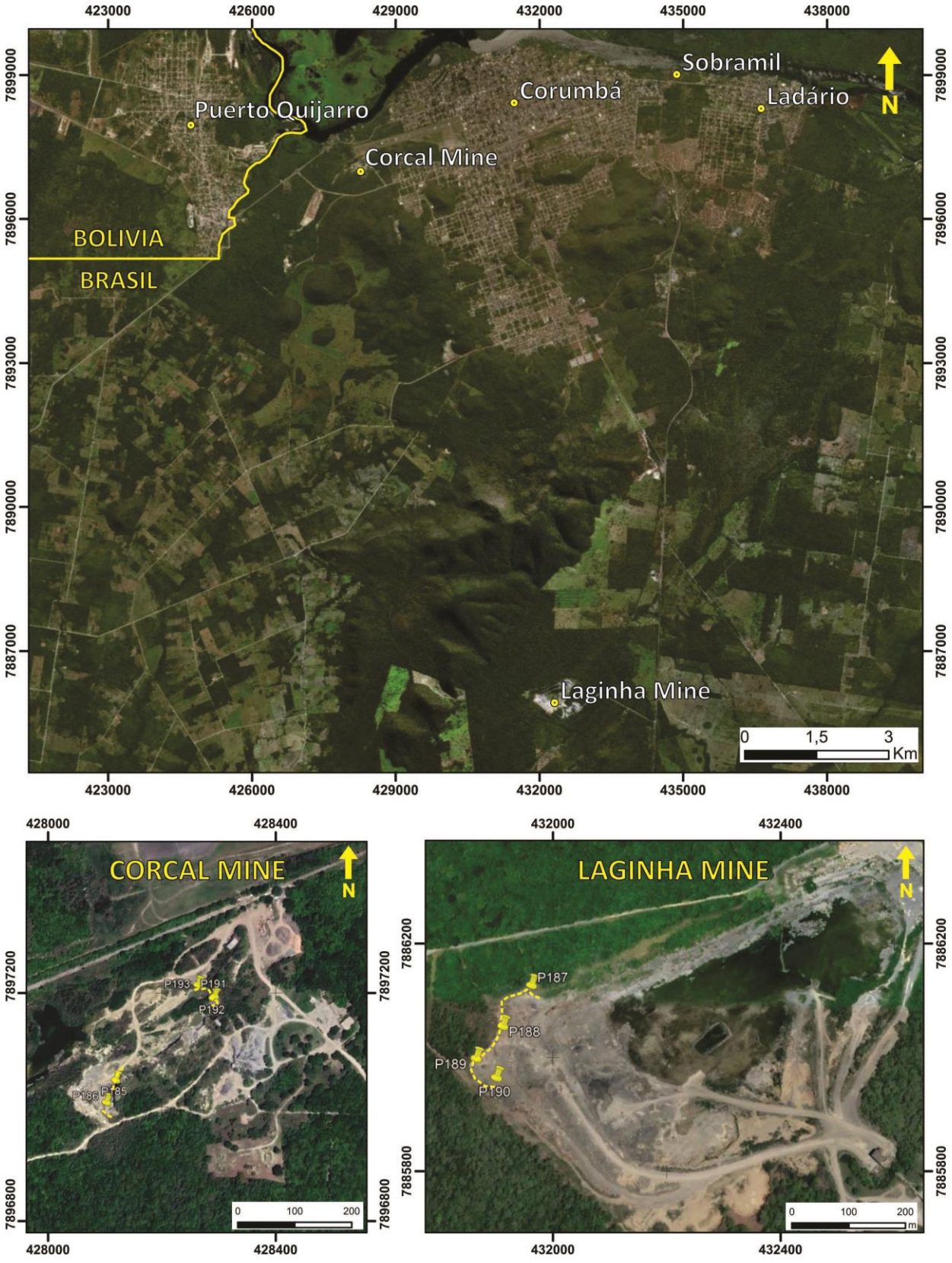

Figure 1: Satellite images of the study area showing the position of Corumbá and Ladário cities plus Corcal, Laginha and Sobramil outcrops. Below, there are mapping track of the mining walls described for Corcal and Laginha lithostratigraphic sections.

1) Characterize the details of the depositional setting and conditions of the Tamengo Formation;

2) Unravel the factors controlling the stable isotopic composition of the different lithofacies of the Tamengo Formation

2. THEORETICAL BASIS

2.1 THE EDIACARAN PERIOD

The Neoprotezoic Era is characterized by profound environmental and climatic changes related to the break-up of Rodinia Supercontinent and associated to the emergence of complex forms of life on Earth. Halverson *et al.* (2005) propose three major glacial events during this era: Sturtian, Marionoan and Gaskiers. The Ediacaran (635-541 Ma) is the final period of the Neoproterozoic, occurring after the Marinoan glaciation, including the Gaskiers glaciation, and preceding the remarkable evolutionary radiation of the Cambrian Period. In the sedimentary record shallow and deep post-glacial marine carbonate deposits predominate, particularly cap carbonates. These are rocks typical for this period as they record the termination of glaciations. The fossil record shows that after 4 Ga of evolutionary inertia, the planet inhabited predominantly by protozoa - simple microbial forms, such as cyanobacteria, acritarchs and microalgae - witnesses the emergence and global settlement of the first complex and macroscopic multicellular beings: the metazoan, early ancestors of animals.

In Phanerozoic successions, it is common to use the fossils as a tool to determine the age of rocks and for stratigraphic correlation; however, this approach does not work well with the enigmatic pre-Cambrian fossils. Xiao *et al.* (2016) recommend a holistic approach, integrating biostratigraphy, chemostratigraphy and geochronological data. Knoll *et al.* (2006) acknowledge that the isotopic carbon record can be an excellent tool, allowing correlations more precise than those offered by invertebrate fossils. Furthermore, the isotopic carbon record of the Neoproterozoic shows particular features. It is characterized by average values of $\delta^{13}C$ about 5‰, very high when compared to the Mesoproterozoic and Phanerozoic averages, which are on the order of 0 to 1‰ (Halverson *et al.*, 2010). In addition, variations in $\delta^{13}C$ occur with large amplitudes (Figure 2), some larger than 10‰, not observed in other geological periods (Grotzinger *et al.*, 2011).

2.2 CARBON ISOTOPE GEOCHEMISTRY

Carbon isotope geochemistry is the study of variations of the isotopic ratio between the heavy and the light isotopes of carbon, which are ^{13}C and ^{12}C, respectively. From the isotopic point of view, ^{12}C composes 98.93% of the terrestrial reservoir and ^{13}C makes up the remaining 1.07%. The isotopic composition of the various substances, especially natural ones, is subjected to variations that are a reflection of the physical, chemical and biological processes to which they are submitted. This variation occurs through isotope fractionation, which is the selection of a specific isotope of an element in a process and thus generates products enriched in that specific isotope. Fractionation occurs in the processes that compose the carbon cycle, so that each component has characteristic values of isotopic composition, according to the geochemical pathways through which it originated. The isotopic composition is function of the ratio between the heavy and the light isotope and is expressed by the conventional δ notation, which increases when a substance gets enriched in the heavier isotope.

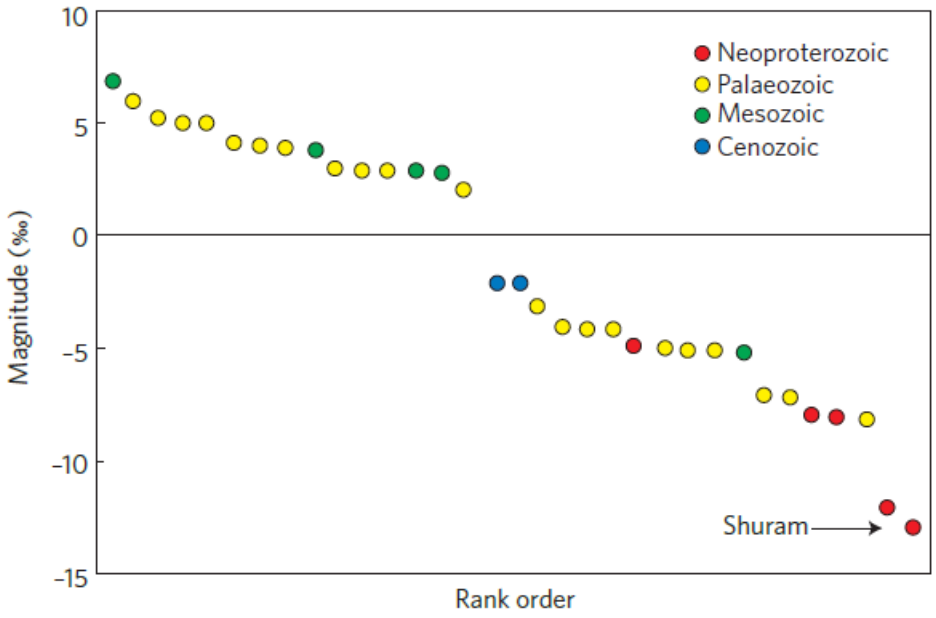

Figure 2: Historical variability of carbon isotopic composition in sedimentary rocks. Ranking of excursions exceeding 2‰ over the last 1000 Ma in terms of signal and magnitude. The most intense excursions predominate in the Neoproterozoic, indicating large-scale carbon cycle disturbances at that time. (Grotzinger *et al.*, 2011).

The carbon isotope composition is expressed as $\delta^{13}C$ and its main application in sedimentary rocks is as proxy for carbon cycle and environmental parameters at the time of deposition. In carbonate sedimentary environments the $\delta^{13}C$ depends on the isotopic composition of the dissolved inorganic carbon (DIC) in the seawater, which in turn is a

function of atmospheric $\delta^{13}C$, primary productivity, weathering and runoff. Thus, changes in the $\delta^{13}C$ of ancient carbonate sediments can be used to trace local and global climatic and environmental changes related to the carbon cycle, depending on the geographic distribution and the time scale considered. (Falkowski, 2003; Sundquist & Visser, 2004). Isotopic studies of carbon in carbonates are the most frequently performed in Neoproterozoic rocks, due to carbon resilience to post-depositional changes, simplicity of measurement and large variations that generate strong isotopic signals (Halverson *et al.*, 2010). However, the interpretation of a $\delta^{13}C$ record is bound to our understanding of the C-cycle processes that acted in the respective period of the geological past. These can be relatively well constrained in the Phanerozoic, especially in the Cenozoic, but are much more enigmatic in the Precambrian. There is noteworthy debate on the authenticity of the primary $\delta^{13}C$ signal in Neoproterozoic marine carbonates, due to the anomalous both positive and negative values (Frimmel *et al.*, 2010; Grotzinger *et al.*, 2011; Cui *et al.*, 2018). So far, it is not clear whether they reflect the $\delta^{13}C$ of the seawater DIC, environmental disequilibrium, or post-depositional fractionation processes, especially fluid-rock interaction (Bristow & Kennedy, 2008; Knauth & Kennedy, 2009; Derry, 2010; Frimmel *et al.*, 2010). Probably, in most case they come from a combination of the three factors. On the other hand, the origin of the $\delta^{13}C$ signal in a record must be clarified prior to use it as chemostratigraphic tool.

3. SCIENTIFIC PAPER

Sedimentological, petrographic, and geochemical characterization of an Ediacaran carbonate platform: a new facies model for the Tamengo Formation (Corumbá Group, SW Brazil)

Maria E.A.F. Ramos[a,*], Martino Giorgioni[a], Dermeval A. do Carmo[a], Detlef H.G. Walde[a], Gabriella Fazio[a], Lucieth C. Vieira[a], Matheus Denezine[a], Roberto V. Santos[a], Rodrigo R. Adôrno[a,b]

[a] University of Brasília, Institute of Geosciences, Campus Darcy Ribeiro, Brasília, DF CEP 70.910-900, Brazil

[b] Geological Survey of Brazil – Center for Technological Development-CEDES, Setor Bancário Norte, Brasília, DF. Brazil. Postal Code: 70040-904 E-mail: rodrigo.Adôrno@cprm.gov.br

[*] Corresponding author at: University of Brasília, Institute of Geosciences, Campus Darcy Ribeiro, Brasília, DF CEP 70.910-900, Brazil. *E-mail address:* meaframos@gmail.com (M.E.A.F. Ramos).

3.1. ABSTRACT

The Tamengo Formation crops out in the meridional portion of the Paraguay Belt and presents continuous geological record of the late Neoproterozoic in Brazil, with its carbonate and siliciclastic sediments being the remnants of a period marked by many environmental changes. Even though its paleontological, structural and stratigraphic features had been broadly studied, there is still a demand on sedimentological characterization. This study presents new detailed stratigraphic sections paired with facies analysis and carbon isotopic data aiming to enhance the understanding of the Corumbá Ediacaran Ramp palaeodepositional environment. The unit comprises mainly dark limestones with marl and mudstone intercalations, in addition to a remarkable fossil record, including the *Cloudina lucianoi*. The $\delta^{13}C_{PDB}$ values vary from -3.11‰ to 6.97‰, nevertheless chemostratigraphic correspondence to renowned upper Ediacaran sections is possible. There are alternating carbonate, mixed and siliciclastic lithofacies, containing fine matrix and grains ranging in size from silt to boulder. The predominant facies are carbonate mudstones and grainstones, nevertheless, other remarkable features such as breccias and desiccation-related structures provide critical evidence for the paleoenvironment reconstruction. The facies analysis revealed minor and major sea level fluctuations in peritidal to mid-ramp settings, shallower than previously outlined. In addition, the role of extensional tectonics, formerly underrated, is embraced on a novel depositional model proposal.

Keywords Ediacaran; C and O isotopes; Paraguay Belt; Corumbá Group; Corumbá Graben System

3.2. INTRODUCTION

The Neoproterozoic geological record discloses a period of remarkable tectonic, climatic and evolutionary changes on Earth. The paleogeographic transformations since Rodinia fragmentation followed by Gondwana assembly triggered glaciations and extensive volcanism, inducing major oceanic and climatic perturbations (Hoffman *et al.*, 1998; Fike *et al.*, 2006; Li *et al.*, 2013; Gernon *et al.*, 2016). Furthermore, the fossil record reveals a noteworthy radiation of metazoans during the Ediacaran Period (Knoll & Carroll, 1999; Walde *et al.*, 2015; Xiao *et al.*, 2016).

The Ediacaran is marked by strong fluctuations in the carbon isotopic record, which are observed at both global and local level, and reach amplitudes greater to 10 ‰ (Halverson *et al.*, 2010; Grotzinger *et al.*, 2011). Variations of this intensity are not observed in other geological periods and possibly reflect rare biogeochemical conditions woth major impact in the carbon cycle. Evidence and information about Ediacaran environments are mostly from shallow water carbonate sediments due to their high potential of preservation (e.g. Grotzinger & James, 2000). However, sedimentological studies on Ediacaran carbonates are challenging since they had been deposited in conditions with no present day analogues. Firthermore, they always present some degree of diagenetic and metamorphic alteration that overprints primary signals (Derry, 2010; Frimmel, 2010; Narbonne *et al.*, 2010). Hence, uncertainties in the interpretation of the geochemical and paleontological data limit their potential applications in chemo- and biostratigraphy (Kaufman & Knoll, 1995). Therefore, the characterization of Ediacaran carbonate environments has fundamental implications not only in carbonate sedimentology, but also for constraining the origin of their unique chemostratigraphic signal and the conditions that prompted the rise of the early animals on Earth.

In Brazil, the most important Ediacaran geological record can be found in the Corumbá Group, specifically in Tamengo Formation, which hosts late Ediacaran typical fossils (Walde *et al.*, 2015). For this reason, there are many studies concerning the fossil record of the Corumbá Group (Beurlen & Sommer, 1957; Fairchild, 1978; Hahn *et al.*, 1982; Walde *et al.* 1982, 2015; Zaine & Fairchild, 1985; Zaine, 1991; Hidalgo, 2002; Gaucher *et al.*, 2003; Kerber *et al.*, 2013; Tobias, 2014; Adôrno *et al.*, 2017; Becker-Kerber *et al.*, 2017; Parry *et al.*, 2017). Likewise, as the Corumbá Group sits in the Paraguay Fold Belt, there is extensive research on stratigraphy and structural geology done in this region (Barbosa, 1949; Almeida,

1964, 1965, 1984; Alvarenga & Trompette, 1992; Boggiani & Alvarenga, 2004; Gaucher *et al.*, 2003; Babinski *et al.*, 2008; Boggiani *et al.*, 2010; Meira, 2011; D'el- Rey *et al.*, 2016; Sial *et al.*, 2016). However, sedimentological and paleoenvironmental studies are still scarse and not much detailed (Boggiani *et al.*, 1993; Boggiani, 1998; Oliveira, 2010; Campanha *et al.*, 2011; Fontanela, 2012; Spangenberg *et al.*, 2014).

In this work we present new detailed stratigraphic sections and facies analyses of the Tamengo formation, which provide an enhanced characterization of this Ediacaran carbonate paleoenvironment. Results point to a heterogeneous ramp, with changeable topography, influenced in different degrees by extensional tectonics. In addition, we provide new carbon isotopic data that contributes to the validation of the Tamengo Formation's $\delta^{13}C$ curve as possible chemostratigraphic reference, and elevate it to an international standard level.

3.3. GEOLOGICAL SETTING AND LITHOSTRATIGRAPHY

The carbonate and associated siliciclastic sedimentary rocks of the Tamengo Formation (Corumbá Group) are exposed in outcrops nearby the city of Corumbá, Mato Grosso do Sul, in western Brazil, close to the Bolivian border. These units are included in the southern portion of the Paraguay Belt, a thrust-and-fold belt generated during the Pan-African-Brasiliano Tectonic Cycle (Boggiani & Alvarenga 2004). It extends for about 1000 km with an approximate N-S orientation, and is surrounded to the north by the Amazon Craton, to the east by the Pantanal Basin, to the south by the Rio Apa Block, and to the west by the Tucavaca-Chiquitos Aulacogen. Jones (1985) and Walde (1988) consider that the Corumbá region sits on a tectonic triple junction, where the southern and northern branches of the Paraguay Belt, and the Tucavaca-Chiquitos Aulacogen intersect (Figure 3). These basins formed after extensional tectonics related to the breakup of the Rodinia supercontinent, between 650 and 540 Ma (Babinski *et al.*, 2013). This led the evolution of a rift system, which formed the southern Paraguay Basin, filled with the sediments of the Jacadigo and Corumbá groups (Trompette *et al.*, 1998; Alvarenga *et al.*, 2009; Figures 3 and 4). In the Early Paleozoic, the tectonic regime reversed and these sequences got affected by the Brasiliano Orogeny, with ductile to brittle deformation and low-grade metamorphism, in greenschist facies (Trompette *et al.*, 1998; D'el-Rey *et al.* 2016).

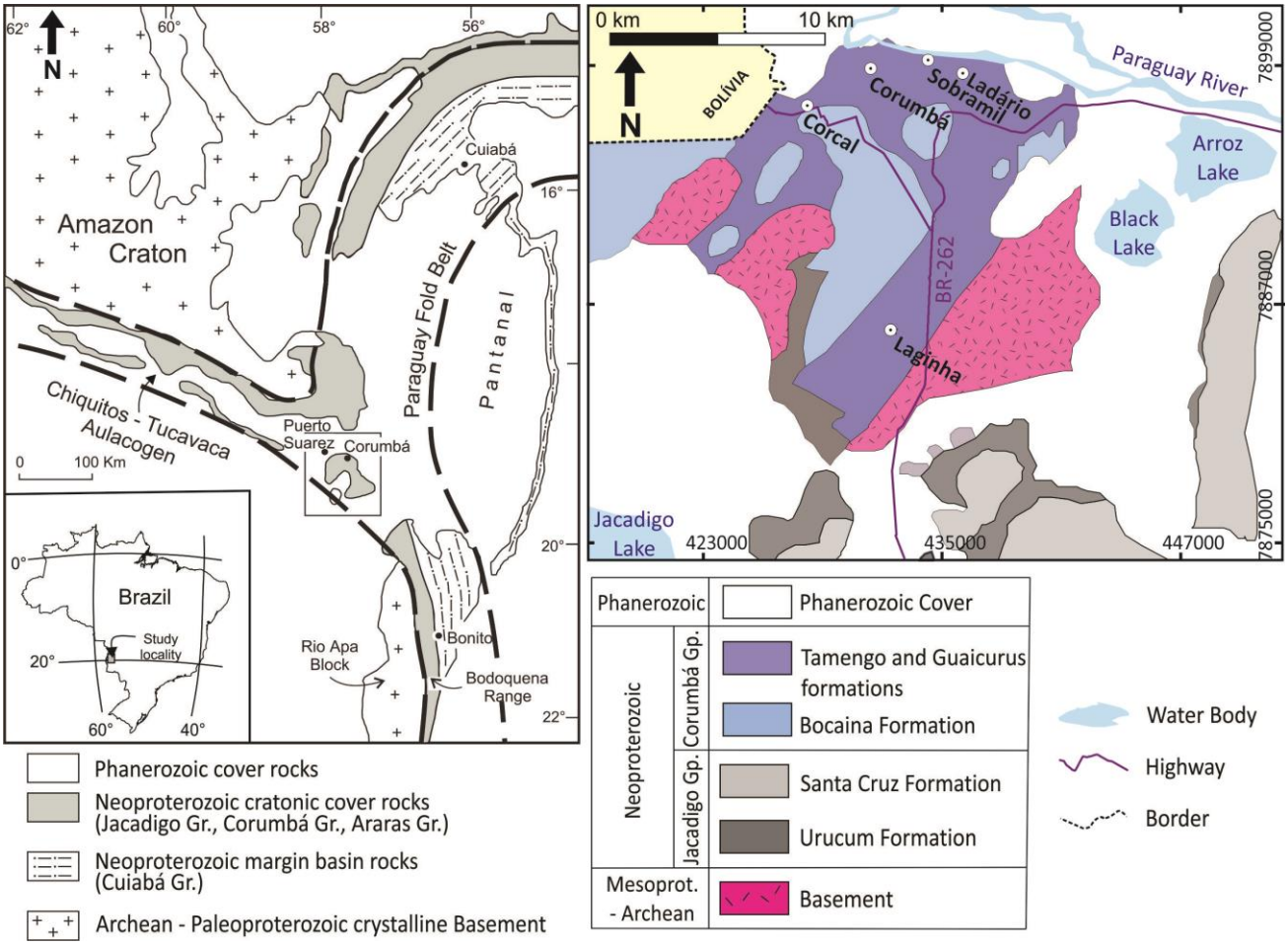

Figure 3: Left - Geological map and geotectonic context of the Paraguay Fold Belt and the Chiquitos-Tucavaca Aulacogen showing the location of Corumbá in Mato Grosso do Sul, southwestern Brazil. Right – detailed geological map of the studied area showing the location of mines Corcal, Laginha and Sobramil, as well as Corumbá and Ladário cities.

The Jacadigo Group comprises diamictites, arkoses, and volcanogenic rocks of the basal Urucum Formation, followed by hematite-jaspilites with manganese ore horizons and dropstones of the Santa Cruz Formation, with minimum depositional age of 587 ± 7 Ma ($^{40}Ar/^{39}Ar$ in cryptomelane; Piacentini *et al.*, 2013). The Corumbá Group includes carbonate and siliciclastic facies arranged in five units (Almeida, 1965; Boggiani, 1998; Figure 3). The basal Cadiueus and Cerradinho formations consist of conglomerates, arkoses, siltstones, and occasionally limestones. These basal units do not outcrop in the region of Corumbá. The overlying Bocaina Formation, of greater extension, consists of stromatolitic dolostones and subordinate phosphorite levels. These units are interpreted as a transgressive sequence, beginning with alluvial fan deposits followed by a vast tidal flat with high evaporation rates (Boggiani, 1998; Sial *et al.*, 2016; Fontanela, 2012; Oliveira, 2010).

The upper part of the Corumbá Group is represented by the Tamengo and Guaicurus formations. The former includes basal breccias and sandstones, followed by thick sets of

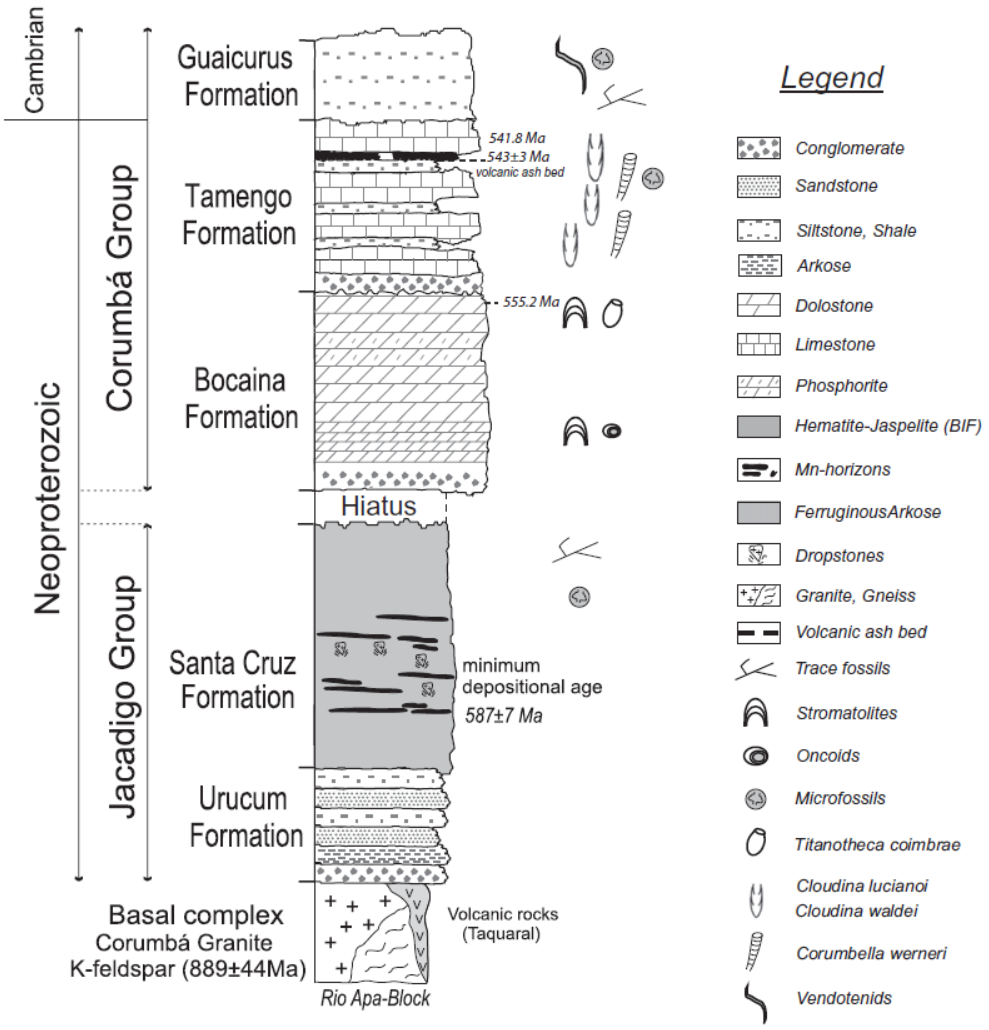

Figure 4: Lithostratigraphic column of the Jacadigo and Corumbá groups at Corumbá (Walde *et al.*, 2019). Age data follow Babinski *et al.* (2008), Piacentinni *et al.* (2013) and Parry *et al.* (2017). New trace fossil occurrences in the Santa Cruz Formation based on Walde *et al.* (2015) and Parry *et al.* (2017) for the Guiaicurus Formation.

dark fossil-rich limestones alternated with marls and mudstones. Dolostones and phosphorites occur locally. The paleontological content includes macroscopic skeletal fossils, especially *Cloudina lucianoi* (Beurlen & Sommer 1957) and *Cloudina carinata* (Cortijo *et al*., 2010), an index fossil for the late Ediacaran (eg Grant, 1990), and *Corumbella werneri* (Hahn *et al.*, 1982), first described in Corumbá, besides the occurrences of ichnofossils, vendotaenids and organic-walled microfossils (Adôrno, 2019). *Cloudina lucianoi* is usually found in limestones, whereas *Corumbella werneri ans Cloudina carinata* occur only in mudstones (Adôrno *et al.*, 2017; Adôrno, 2019 and references therein). Boggiani (1998) suggests that this unit overlaid the Bocaina Formation during a transgression, establishing a slope-break ramp system marked by reworking of the shallower sediment. On the other hand, Oliveira *et al.* (2019) proposes a shallower setting, with oolitic bars and storm-derived deposits. The Guaicurus Formation comprises a thick set

of laminated siltstones, which mark the end of carbonate deposition, related to climatic or tectonic changes. This unit was probably deposited in a deeper environment, below fair weather wave base (Boggiani, 1998; Gaucher *et al.*,2003; Oliveira, 2010; Fazio *et al.*, 2019).

Concerning the age of the Corumbá Group, zircons from volcanic tuff beds were dated using the U-Pb method. Parry *et al.* (2017) provide ages of ~555 Ma for the top of the Bocaina Formation and ~542 Ma for the top of the Tamengo Formation, in agreement with the 543 ± 3 Ma age provided before by Babinski *et al.* (2008). Furthermore, the presence of the index-fossil *Cloudina lucianoi* and *Cloudina carinata* in the Tamengo Formation supports an upper Ediacaran age (Adôrno *et al.*, 2017; Adôrno, 2019).

3.4. METHODOLOGY

3.4.1. Fieldwork and lithostratigraphy

The studied outcrops are located in two open-pit mines near the city of Corumbá, in western Brazil. Even though there are many other good outcrops of the Tamengo Formation in this region, Corcal and Laginha were elected for this detailed work due to their great vertical continuity, fresh rock exposures and popularity. These sites were visited in June 2018 and detailed lithostratigraphic logs were measured and described with a cm to dm resolution. Some intervals were completed using the lithostratigraphic logs of Adôrno *et al.* (2017) and Fazio *et al.* (2019). Descriptions of the observed lithofacies at microscopic scale were performed and a total of 225 samples were collected for petrographic characterization and geochemical analyses.

3.4.2. Petrography

Petrographic characterization was performed using a ZEISS petrographic microscope at the University of Brasília (UnB). Seventy-nine thin sections were studied, being 10 from samples collected during fieldwork and the remaining from samples collected previously by other colleagues. Of them, 40 are from the Corcal and 36 from the Laginha mines. As many carbonate thin sections displayed some degree of recrystallization, a plain white paper was placed underneath the thin section and used as a light diffuser in order to clarify textural features under the microscope (Delgado, 1977). The following abbreviations are used along the results: PPl - plane-polarized light; XPL - cross-polarized light; DPL - diffused polarized light; Qz – quartz; Bt – biotite; Cal – calcite; Ap – fluorapatite; Alm – almandine; Op – opaque

minerals.

The revised carbonate classification by Wright (1992) was adopted in this study, as well as Wentworth (1922) grain size classification for siliciclastic facies. In addition, the term “marl” is used for sedimentary rock containing a mix of clay and calcium carbonate.

3.4.3. Scanning electron microscopy

SEM analyses were made on 9 thin sections, selected as representative of the main lithofacies. Prior to the analysis the sections were coated with carbon, and then analyzed at the University of Brasília (UnB) using a FEI QUANTA 450 scanning electron microscope with a BSE detector, 20kV accelerating voltage, working distance of 10-12 mm and high-vacuum mode.

3.4.4. Carbon and oxygen isotopes geochemistry

For the isotopic analysis, 116 samples from Corcal and 54 from Laginha were collected at every 20 to 40 cm, always tracking facies variation. Additionally, areas containing veins, fractures and other post-depositional features, likely to interfere with the primary isotopic signal, were avoided. Fresh rock samples were powdered using a drill with 3 mm-diameter bit. Prior to the analysis about 300 µg of material were put in glass vials, acclimatized at 72 ºC, and flushed with He in order to eliminate atmospheric gases. Afterwards, carbonate samples were reacted with concentrated phosphoric acid during 1 h and the released CO_2 was analyzed for O and C isotopes by mass spectrometry. All isotope determinations were performed with a Thermo® Gasbench II connected to a Thermo® Delta V^{Plus} mass spectrometer at the University of Brasília (UnB). The isotopic ratios are reported in per mil (‰), using the conventional δ notation, relative to the Vienna Pee Dee Belemnite (VPDB) standard. The analytical precision is ±0.1‰ for $\delta^{13}C$ and ±0.1‰ for $\delta^{18}O$.

3.4.5. Sedimentary facies

The sedimentary facies study relied primarily on macroscopic and thin section descriptions, integrated by geochemical and paleontological data. After extensive observation, samples were categorised in sedimentary facies according to similar mineralogical composition, texture and structural features.

3.5. RESULTS

The Corcal and Laginha rocks differ markedly from each other. For this reason, results are presented independently.

3.5.1. Lithostratigraphy

Corcal

The Corcal section is *ca* 55 m thick and sedimentation is marked by ten meters thick packages of limestones interbedded with cm thick beds of mudstone and marl, alternated to metric packages of mudstones (Figures 5 and 6). Neither the base nor the top of the Tamengo Formation is exposed at this site. Despite the presence of folds and a fault in the outcrops, it was possible to reconstruct the lithostratigraphic stacking.

The lower section begins with a meter-thick package of massive mudstones, lying above a limestone bed, and followed by limestones arranged in sets of centimeter to decimeter-thick tabular wavy beds, interchanged with decimeter to meter-scale massive tabular beds. Flaser bedding occurs between 6.10 m and 7.40 m. At 7.38 m there is a 21 cm-thick package of mudstone grading to marl, followed by a 50 cm-thick massive limestone bed, and a 54 cm-thick massive mudstone bed. Above, there are 10 m of limestones arranged in sets of centimeter to decimeter-thick tabular wavy beds interchanged with centimeter-scale beds of marl, at the base, and mudstone toward the top.

The middle section lithostratigraphy was described in detail by Adôrno *et al.* (2017). This interval starts at 18.60 m, where the limestone deposition is replaced by a 1.9 m-thick package of massive mudstone. Then, there are 2.25 m of limestones, followed by two alternated decimeter-thick mudstone and limestone beds, and then a 2.90 m-thick package of massive mudstone.

Figure 5: (next page) Corcal lithostratigraphic section.

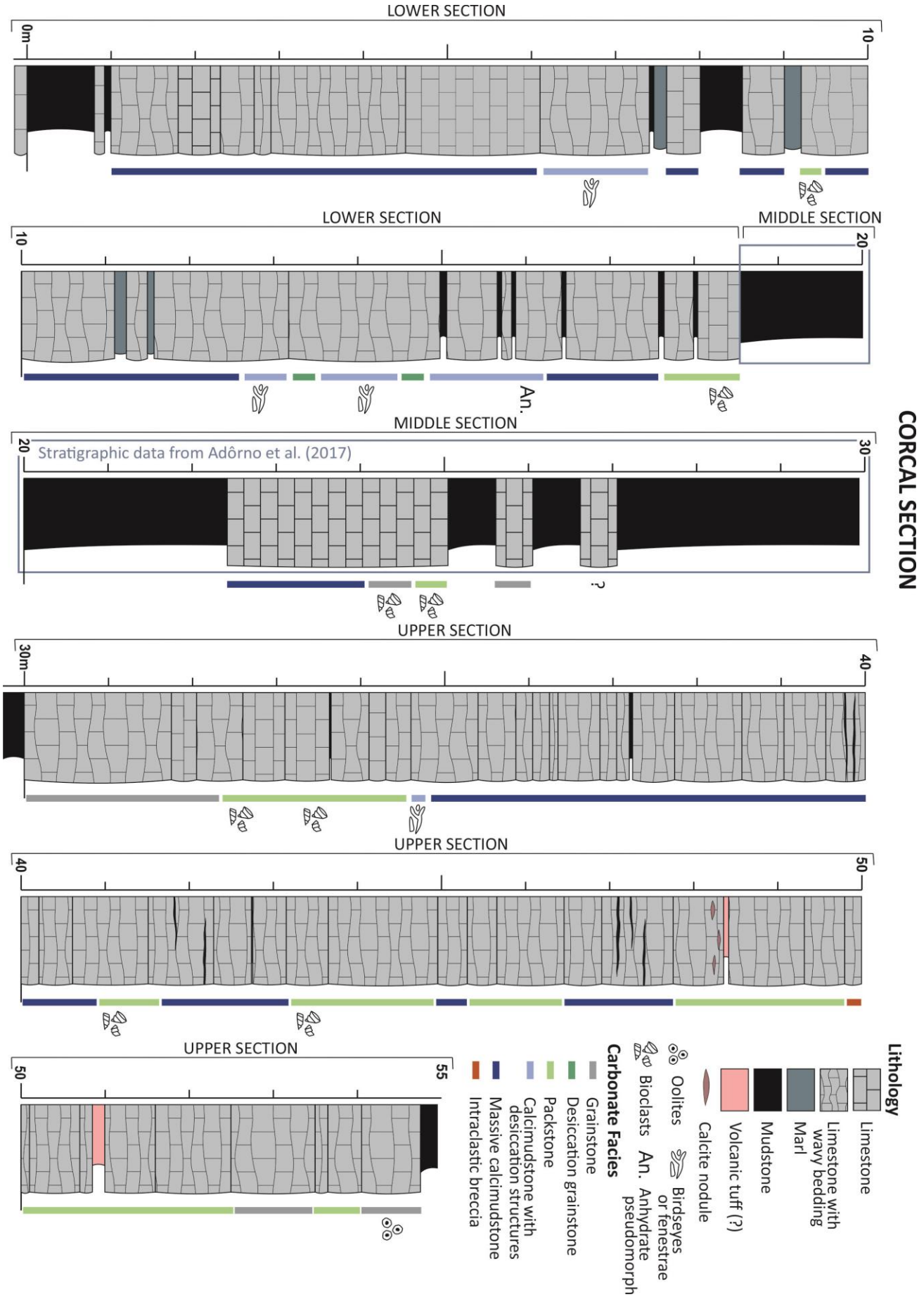
CORCAL SECTION
LOWER SECTION
0m
10
LOWER SECTION
MIDDLE SECTION
10
20
An.
MIDDLE SECTION
20
30
Stratigraphic data from Adôrno et al. (2017)
?
UPPER SECTION
30m
40
UPPER SECTION
40
50
UPPER SECTION
50
55
Lithology
Limestone
Limestone with wavy bedding
Marl
Mudstone
Volcanic tuff (?)
Calcite nodule
Oolites
Birdseyes or fenestrae
Bioclasts
An. Anhydrate pseudomorph
Carbonate Facies
Grainstone
Desiccation grainstone
Packstone
Calcimudstone with desiccation structures
Massive calcimudstone
Intraclastic breccia

The upper section consists of 24.75 m of limestone arranged in sets of centimeter to decimeter-thick tabular wavy beds, interchanged with rare millimeter to centimeter scale-thick mudstone beds. Occasionally mudstone lenses occur. At 18.38 m and 20.88 m there are tabular centimeter scale-thick beds of light, clayey sediment, different from the other mudstones, described as possible volcanic tuffs. In addition, at 18.30 m, there are pinkish calcite nodules. The latest limestone bed is a massive oolitic grainstone, followed by a massive mudstone package with carbonate lenses, which description is provided by Fazio *et al.* (2019).

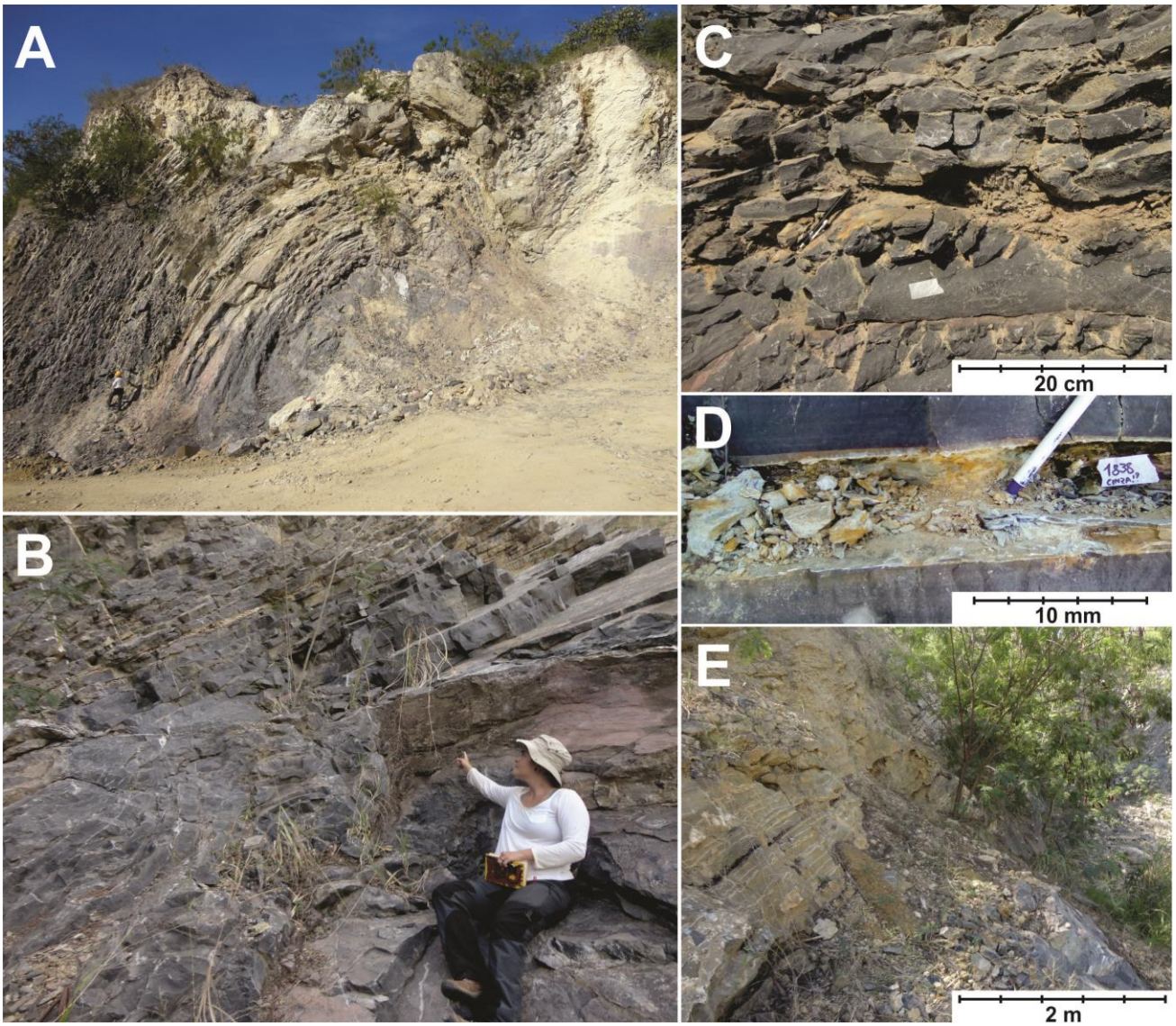

Figure 6: Corcal outcrops. A – Panoramic view of mine wall displaying a fold. At this site, the lower section was described. B – Fresh outcrop displaying dark gray limestones of the upper section. C – Detail of the wavy bedding present in Corcal, in addition to fine siliciclastic intercalations. D – Close view of the possible volcanic

tuff in the upper section. E – Oolitic grainstone outcropping at the left-hand side with distinct texture.

Laginha

The Laginha section is about 100 m thick. In this location both the lower and the upper boundaries of the Tamengo Formation are exposed. Carbonates range from pure to marly, comprising dolostones and limestones, as well as mixed siliciclastic – carbonate rocks and terrigenous sediments (Figures 7, 8 and 9).

The lower section starts with a 2.50 m thick massive bed of light gray dolostone followed by a 2.00 m thick massive bed of dark gray sandstone with dolomitic matrix. The contact between these beds is very irregular, apparently karstified. Above, there is a 50 cm thick bed of dark gray dolomite, and then a *ca* 15 m-thick massive polymictic breccia containing carbonate and granitoid basement clasts, with micritic matrix and erosional contact at the base (Figure 8). Above the breccia there is a 25 cm thick friable yellowish-brown muddy sandstone with lithoclasts and argillaceous matrix, grading into a yellow massive sandstone.

Following occurs a mainly carbonate succession, starting with 4.5 m of massive dolostones with numerous randomly oriented fractures, with millimeter to centimeter size and filled with white sparry calcite. Above, there are 2.80 m of dolostones arranged in sets of centimeter to decimeter scale-thick tabular beds with occasional limestone and mudstone horizons. At 22.75 m there is a 7 cm-thick bed of polymictic breccia, followed by a 3.40 m thick package of dolostones grading to limestones, containing cm thick mudstone and marl intercalations. Lastly, there is a 15 cm-thick bed of limestone with intraclasts. Following, there is an irregular body of massive polymictic breccia, with maximum thickness estimated in 5 m and erosional contact at the base. Laterally, it grades into a light gray limestone.

The middle section starts with a package of dark gray limestone wich overlies the breccia with a very irregular contact, erosional and perhaps karstified. This 5.35 m interval is massive, comprising intraclasts at the base and a 20 cm-thick bed of silty laminated limestone at 13.70 m. The last 3.75 m of the middle section comprise dark gray limestone arranged in sets of centimeter to decimeter-thick tabular wavy beds.

Figure 7: (next page) Laginha lithostratigraphic section.

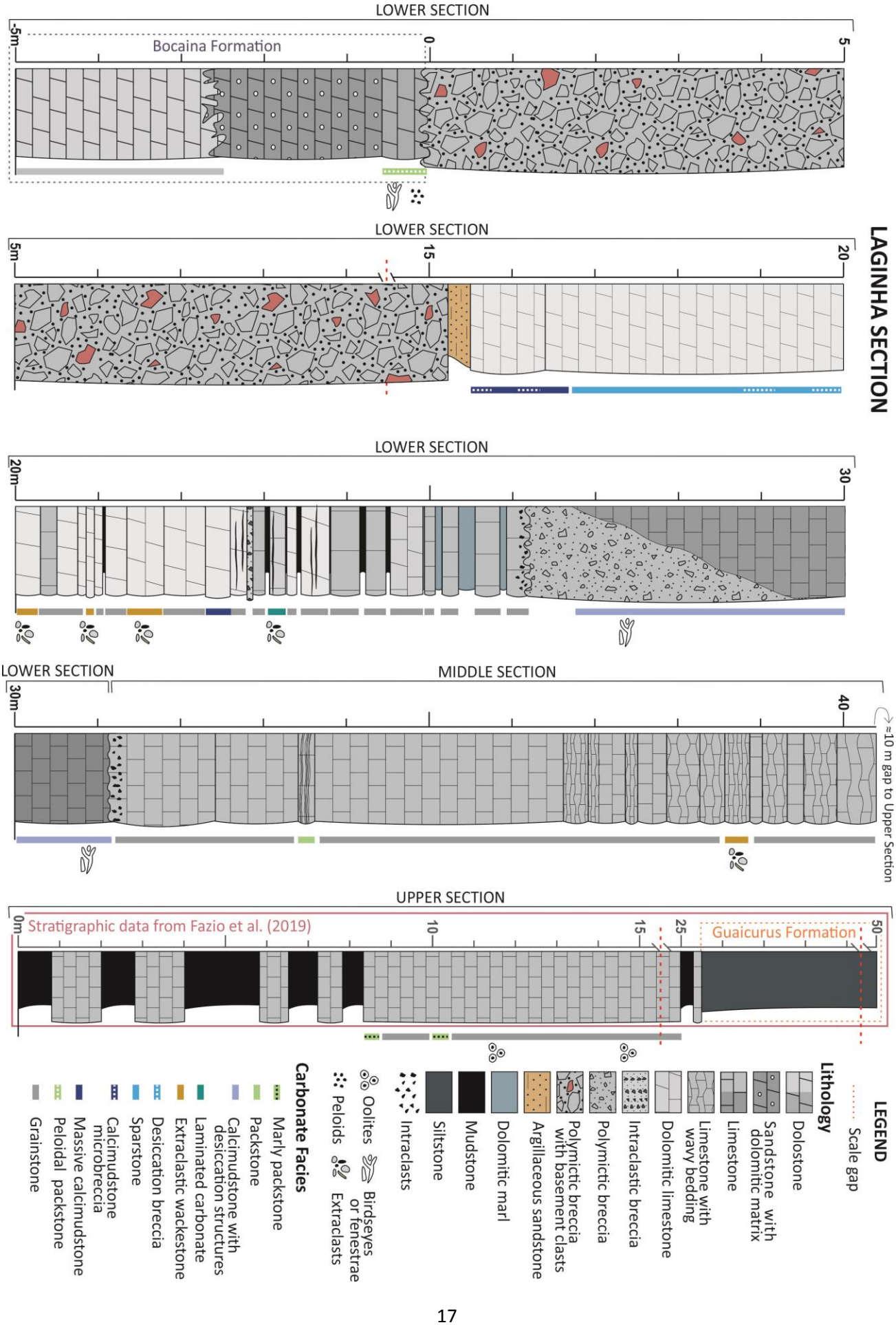
LAGINHA SECTION
LOWER SECTION
-5m
Bocaina Formation
0
5
LOWER SECTION
5m
15
20
LOWER SECTION
20m
30
LOWER SECTION
MIDDLE SECTION
30m
40
≈10 m gap to Upper Section
UPPER SECTION
0m
Stratigraphic data from Fazio et al. (2019)
10
15
25
Guaicurus Formation
50
LEGEND
Scale gap
Lithology
Dolostone
Sandstone with dolomitic matrix
Limestone
Limestone with wavy bedding
Dolomitic limestone
Intraclastic breccia
Polymictic breccia
Polymictic breccia with basement clasts
Argillaceous sandstone
Dolomitic marl
Mudstone
Siltstone
Intraclasts
Oolites
Birdseyes or fenestrae
Peloids
Extraclasts
Carbonate Facies
Marly packstone
Packstone
Calcimudstone with desiccation structures
Laminated carbonate
Extraclastic wackestone
Desiccation breccia
Sparstone
Calcimudstone microbreccia
Massive calcimudstone
Peloidal packstone
Grainstone

Figure 8: Starting point of Laginha section, displaying, from bottom to top, the light gray dolomitic grainstone in karstified contact with the dark gray sandstone with dolomitic matrix, which grades to the dark gray peloidal packstone, which has erosional contact with the polymictic breccia with basement clasts. Sharp contacts highlighted by yellow dotted lines.

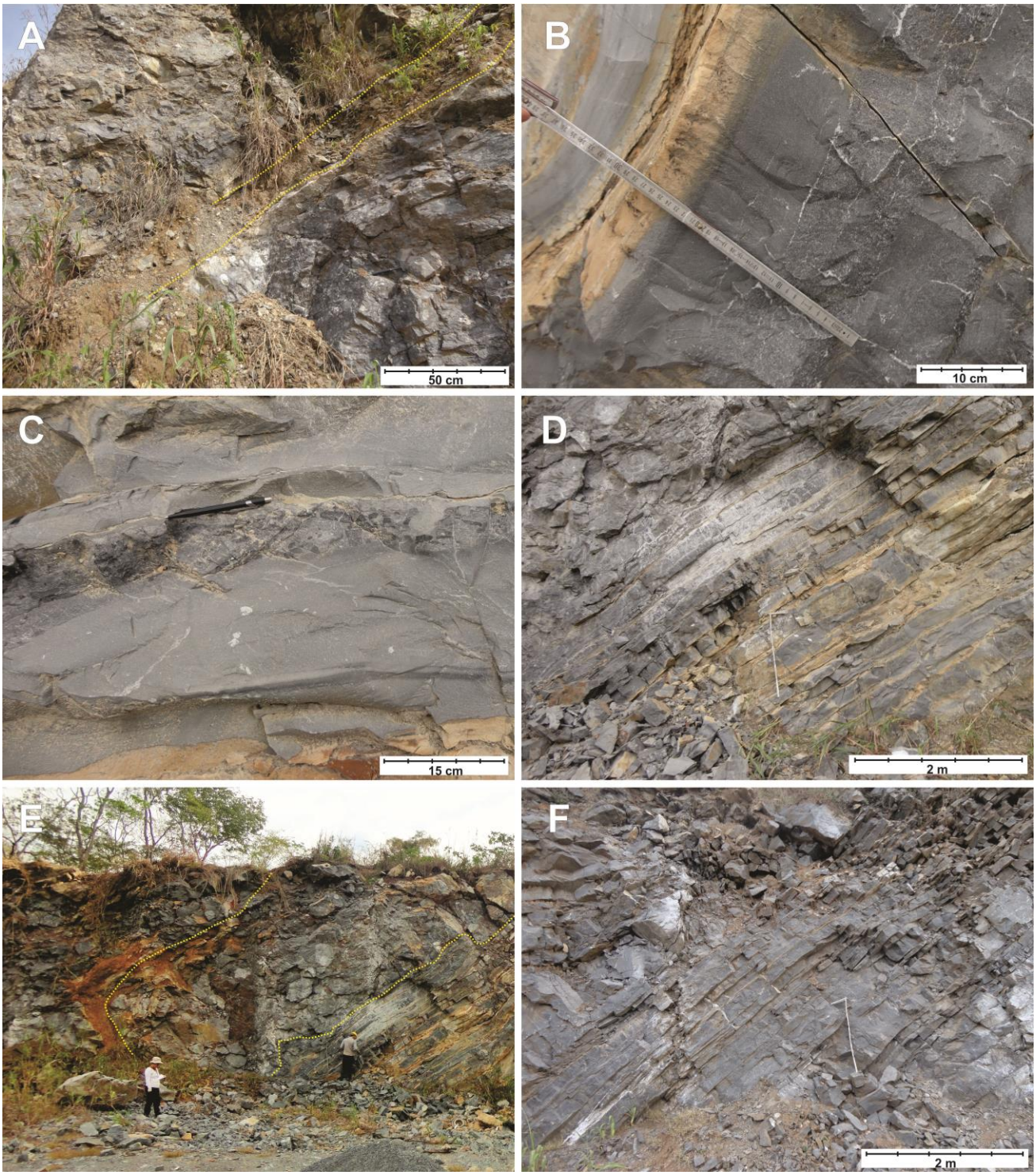

Figure 9: Laginha outcrops. A – Contact of the polymictic breccia with the dirty sandstone, followed by the first Tamengo's carbonates. B – Facies heterogeneity in lower section represented by the dark gray fine grainstone, dark gray coarse lithic sandstone with carbonate matrix and the light gray dolomitic wackestone. C – Level of intraclastic breccia in the lower section. D - Panoramic view of the tabular bedding in the lower section. E – Contact between the limestones and the polymictic breccia, overlaid by dark gray limestone. F – Panoramic view of the top of the lower section. Chaotic bedding towards the top.

Is was not possible to precisely link the upper section with the middle section, however, a 10 m gap is considered between both. According to Fazio *et al.* (2019) description, the upper section comprises 30 m of limestone, of which the lower half is represented by alternating limestone and laminated mudrocks, ranging from carbonate to siliciclastic composition. Overlying the limestones there are *ca* 24 m of siltstone from the Guaicurus Formation.

3.5.2. Petrography

Corcal

The following petrofacies has been recognized in the Corcal section (Figure 10):

Calcimudstones, often rather recrystallized and subdivided in two groups: 1) massive calcimudstones and 2) calcimudstones with desiccation structures. Both groups present extraclasts (Qz, Bt, Op), bioclasts, intraclasts, compaction-related segregation structures, heterolithic structure calcite-filled fractures, and stylolites. Nevertheless, group 1 have dissolution porosity and group 2 display fenestral fabrics, birdseyes, anhydrate pseudomorph, silicification, dolomitization and micritization.

Packstones are formed by bioclasts, intraclasts, and extraclasts (Op). Grain size is from sand to granule and the intergranular space is filled with micrite. Occasionally recrystallization or dolomitization is present. The structure is massive, with lenticular veins (Cal, Qz, Op) and calcite-filled fractures.

Grainstones, are formed by bioclasts, intraclasts, ooids and extraclasts (Qz, Op, Ap, Alm) of sand to granule size, cemented by calcite. They have calcite-filled fractures, stylolites and can be recrystallized. The desiccation grainstones occur near to desiccation structures and the irregular form and fabrics of the intraclasts within them suggest very little transportantion, in addition to ones that seem to fit together.

The intraclastic breccia is composed of angular to rounded intraclasts. Grain size is from sand to granule, and the intergranular space is filled with micrite. Stylolites, calcite-filled fractures and compaction-related segregation structures are present.

Marls are formed by clay to silt-size detrital grains, especially quartz, in a mixed siliciclastic-carbonate matrix. The structure is massive to laminated. Carbonate concretions

and nodules, opaque grains and heterolithic structures are present.

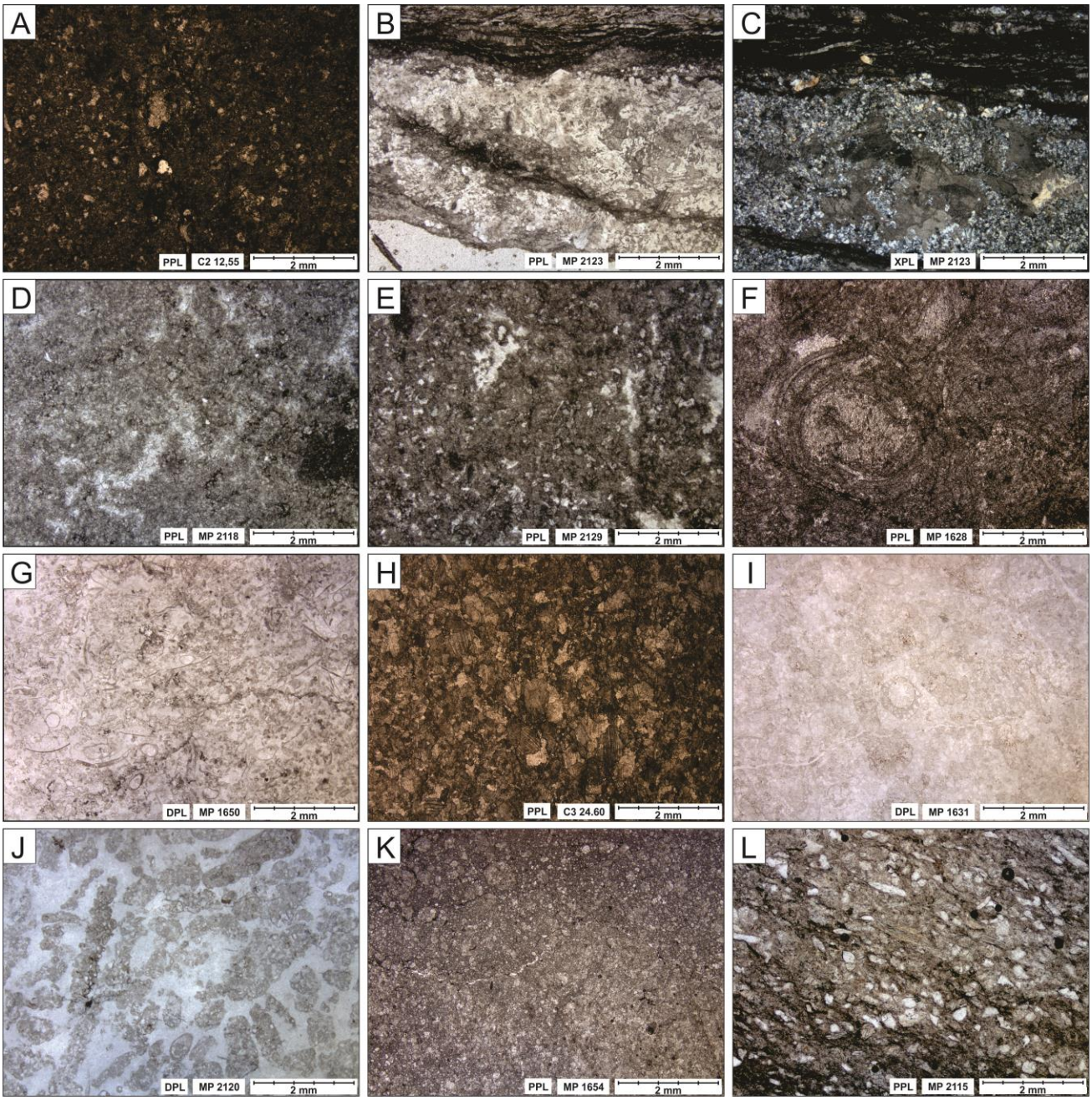

Figure 10: Carbonate microfacies in Corcal thin sections. Light type, sample identification and scale at the right-hand bottom corner of pictures. A - Massive calcimudstone with extraclasts. B and C: Calcimudstone with desiccation structures displaying silica anhydrate pseudomorphs. D and E – Calcimudstones with desiccation structures displaying fenestral porosity. F and G – Packstones displaying different sized bioclasts. H – Recrystallized oolitic grainstone. I – Intraclastic grainstone. J – Desiccation grainstone. K – Intraclastic breccia with micritic matrix. L – Marl with quartz and biotite grains and mixed carbonate-clay matrix.

Mudstones are formed by clay to silt-size detrital grains, and with plane lamination or foliation. There are seldom opaque grains, compaction-related segregation structures, calcite and quartz-filled fractures, and silicification nodules.

The SEM analysis revealed the presence of fluorapatite in 4 different levels of the Corcal section: 6.50 m, 10.40 m, 2.55 m, and 18.42 m.

Laginha

Laginha thin sections reveal a wide variety of microfacies, marked by terrigenous contribution (Figures 11 and 12). Calcimudstones occur in two habits: 1) micritized to recrystallized, presenting desiccation structures and silicification nodules; and 2) mottled, dolomitized, with extraclasts (Qz, Op) plus calcite-filled fractures. There are microbreccias of these calcimudstone with fractures and very angular intraclasts cemented by at least two generations of calcite cement: isopachous on the borders and sintaxial on the center.

Sparstones, dolomitic to calcitic, massive to laminated, containing stylolites and calcite-filled veins, locally associated with fluorite. Some dolomitic sparstones are fractured and host millimeter to centimeter-scale calcimudstone angular and broken intraclasts.

Packstones are of three types: 1) peloidal, dolomitized, with desiccation cracks; 2) heterogeneous, calcitic, containing intraclasts, muddy extraclasts, bioclasts, and enigmatic sub-rounded features; 3) rather recrystallized marly packstones with intraclasts.

Grainstones are grain-supported and cemented by calcite. The grains are predominantly concentric ooids, occurring as single or compound, often micritized or completely recrystallized. There are also rare aggregate grains. Stylolites are frequent, occasionally generating condensed oolitic grainstones.

There are laminated carbonates with interchanged crystalline and sandy horizons. The first are crystalline, calcitic to dolomitic, with sparse extraclasts (Qz, Bi); the latter are grain-supported, with calcitic to dolomitic matrix, sand-size extraclasts varying in composition from quartz to k-feldspar. Authigenic pyrite and phosphatized grains are present, besides, SEM-EDS revealed traces of zircon and possible anatase. Late compaction structures such as stylolites and calcite-filled veins occur frequently.

Wackestones are matrix-supported and bear a great amount of extraclasts, especially quartz and muscovite grains ranging from fine to coarse sand-size.

Breccias with carbonate matrix comprise: 1) basal polymictic breccia with basement clasts (level 0 m); 2) fine intraclastic breccia with quartz and phosphatized grains (at 2.75 m);

and 3) coarse polymictic breccia with quartz and phosphatized grains (at 6.45 m). The former bears clasts ranging in size from sand to boulder, and with composition of quartz, dolostone, limestone, chert, phosphorite, and granite type rocks. They are poorly sorted, with chaotic distribution and with a rounded to very angular shape. The matrix is dolomitic and dark gray, there are irregular voids filled with white spatic calcite. Breccia 2 is grain-supported, with micritic matrix and angular grains, ranging in size from fine sand to granule, with the larger grains of tabular shape. Quartz grains are predominant; but there are also clasts of dolomite, phosphorite, mudstone, k-feldspar, and pyrite. Breccia 3 is also grain-supported and have similar composition to breccia 2. The main difference between them is the texture, as breccia 3 has angular grains, not oriented, and varying in size from sand to cobble, in addition to mire extraclasts.

Marls are composed of siliciclastic and carbonate mud. They often show rounded to lenticular carbonate concretions and have both empty and calcite-filled fractures.

The argillaceous sandstone is massive, composed of sand-size quartz grains and lithoclasts bonded by argillaceous matrix. The sandstone with dolomitic matriz is mostly composed of very well rounded quartz grains with approximatelly equal ammounts of grains and matrix.

The SEM analysis showed fluorapatite in levels -0.1 m, 3.10 m, 6.45 m and 10.75 m.

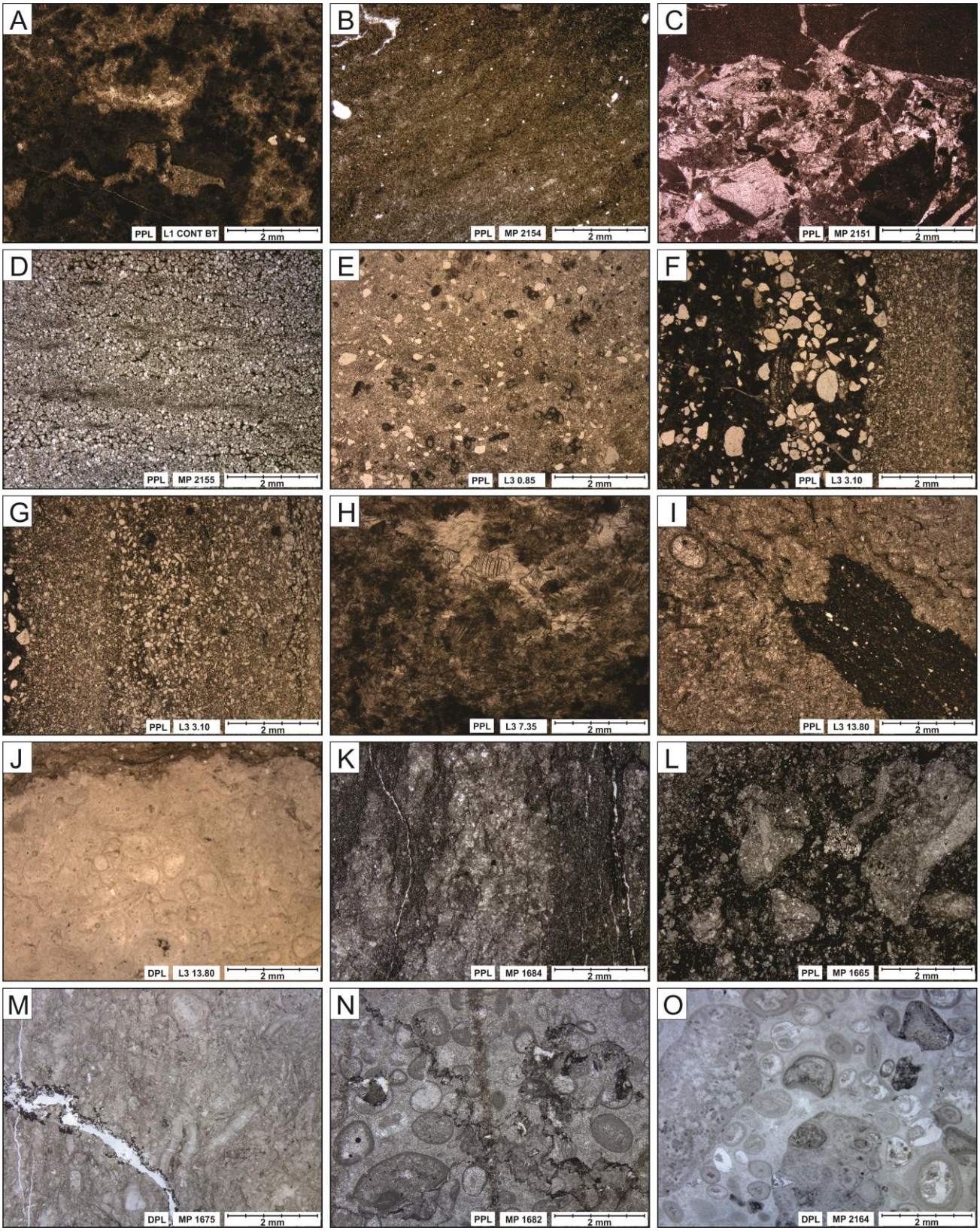

Figure 11: Carbonate microfacies in Laginha thin sections. Light type, sample identification and scale at the right-hand bottom corner of pictures. A- Dolomitized peloidal packstone with fenestral porosity. B – Massive calcimudstone with quartz extraclasts. C – Calcimudstone microbreccias with sparite cement. D – Dolomitic sparstone. E – Lithic sandstone with micritic matrix. F and G – Laminated carbonate showing alternate layers of pure and impure dolostone and limestone. H – Calcimudstone with desiccation structures showing fenestral porosity. I and J – Intraclastic packstone displaying enigmatic sub-rounded features. K – Marl with local

compositional segregation. L and M – Marly packstone with angular intraclasts. N and O – Oolitic grainstone with stylolites.

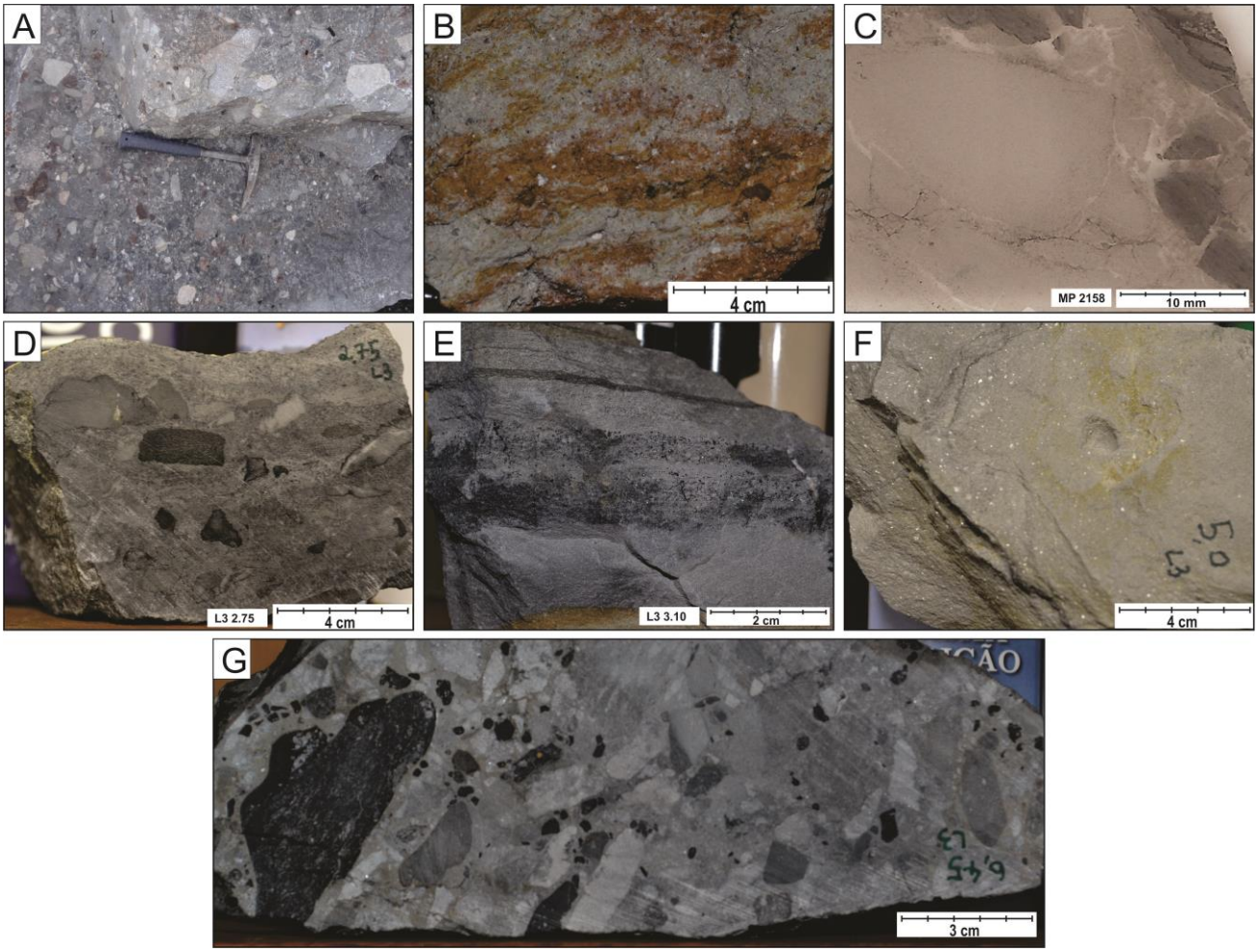

Figure 12: Macroscopic view of Laginha sedimentary facies. Sample identification and scale at the right-hand bottom corner of pictures. A – Basal polymictic breccia with poorly sorted clasts and micritic matrix. B – Dirty sandstone with quartz grains and lithoclasts. C – Thin section macroscopic view of a dolomitized desiccation breccia. Note the broken dark grains still positioned next to each other counterparts. D – Intraclastic breccia I showing tabular clasts. E – Laminated carbonate with alternated fine and coarse layers. F – Dolomitic marl displaying mica extraclasts. G – Intraclastic breccia II displaying chaotic structure.

3.5.3. Carbon and oxygen stable isotopes geochemistry

High-resolution carbon isotopic compositions are very diverse between Corcal and Laginha sections.

Corcal

Corcal samples provide very consistent $\delta^{13}C_{PDB}$ values (Figure 13), ranging from 0.70‰ to 6.97‰ and with average of 4.60‰. Values are around 3.5‰ in the lower part of the section, increase gradually to about 5‰ at 10 m, and then persist through to the middle and upper

part. At 52 m, values start to decrease to 2.83‰ at 54.3 m. There are minor positive peaks of 5.33‰, 6.97‰, and 5.75‰ at 10 m, 12.95 m, and 15.95 m, respectively, a negative peak of 4.16‰ at 32.85 m, as well as few outliers

$\delta^{18}O_{PDB}$ values range from -10.47‰ to -4.75‰ and show average of -7.67‰. In the lower part of the section values are quite dispersed, but become steadier in the mid and upper part. The cross-plot between $\delta^{13}C_{PDB}$ and $\delta^{18}O_{PDB}$ shows no linear correlation nor facies-related clustering (Figure 14).

Laginha

Laginha samples yield $\delta^{13}C_{PDB}$ values from -3.11‰ to 4.92‰ (Figure 13). Below 0 m, values show a linear increase from 1.53‰ to 3.14‰. Above the polymictic breccia, which was not analyzed for stable isotopes, values start at 0.79‰ and decrease to -3.00‰ at 21 m, then increase again to 0.13‰ at 27.35 m and 1.92‰ at 30.75 m. In this last interval the values are scattered, showing no clear trend. The middle part of the section has values around -1.00‰, with a distinct negative peak of -2.14‰ at 34.8 m. The upper part of the section starts with values around 4‰, which increase to 4.80‰ at 12 m and decrease to around 2‰ at 17m, persisting until the end. The average for lower and middle sections is -1.01‰ and 3.29‰ to the upper section

$\delta^{18}O_{PDB}$ values range from -10.09‰ to -2.12‰, with average of -6.84‰. They are dispersed through lower and middle section, showing no clear trends, and stay between -8 and -6‰ in the upper section. The cross-plot between $\delta^{13}C_{PDB}$ and $\delta^{18}O_{PDB}$ shows no linear correlation nor facies-related clustering (Figure 14).

Figure 13: (next page) Corcal and Laginha simplified lithostratigraphic sections paired with high-resolution chemostratigraphic (C, O) data.

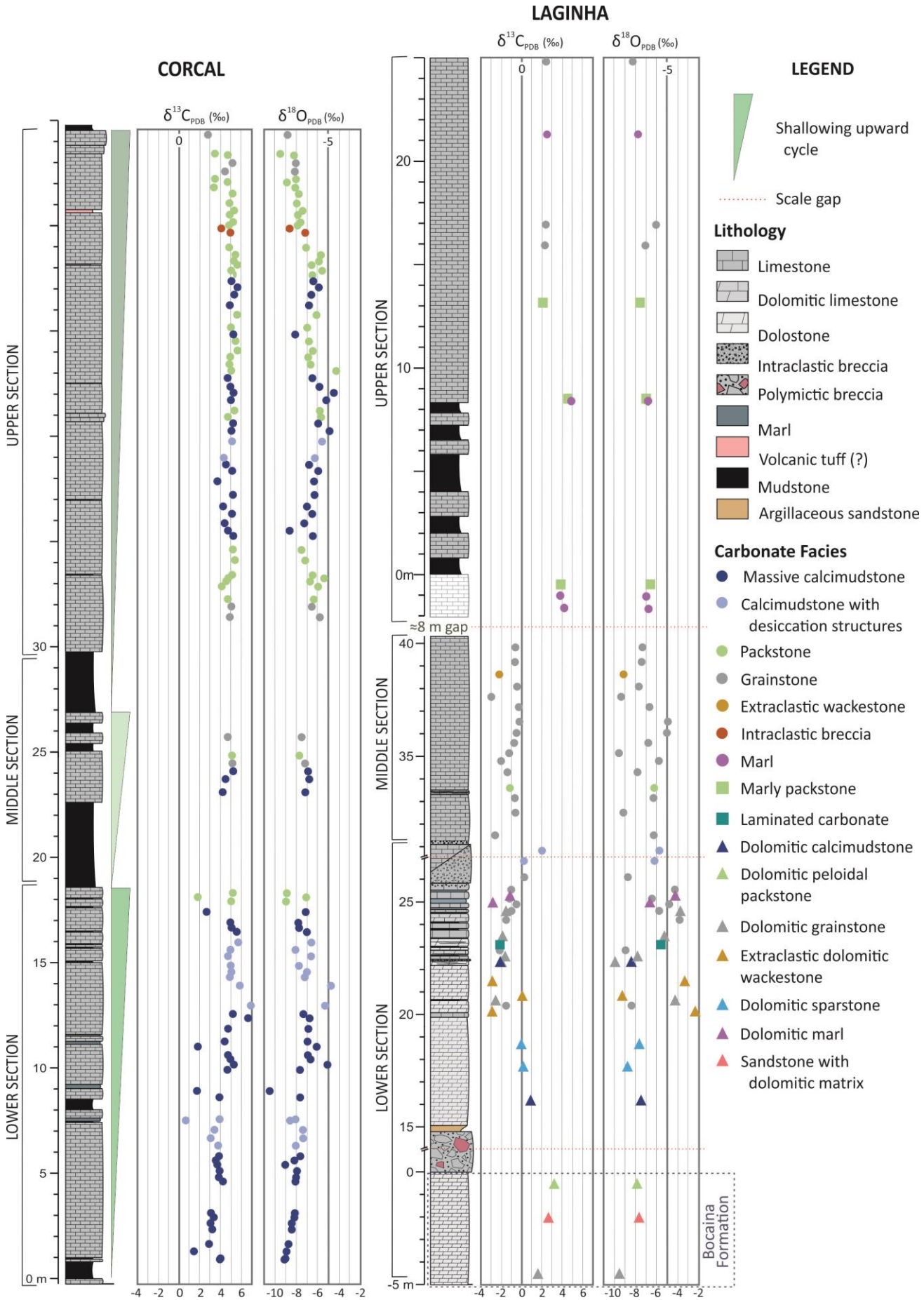
CORCAL
LAGINHA
δ13CPDB (‰)
δ18OPDB (‰)
UPPER SECTION
MIDDLE SECTION
LOWER SECTION
≈8 m gap
Bocaina Formation
LEGEND
Shallowing upward cycle
Scale gap
Lithology
Limestone
Dolomitic limestone
Dolostone
Intraclastic breccia
Polymictic breccia
Marl
Volcanic tuff (?)
Mudstone
Argillaceous sandstone
Carbonate Facies
Massive calcimudstone
Calcimudstone with desiccation structures
Packstone
Grainstone
Extraclastic wackestone
Intraclastic breccia
Marl
Marly packstone
Laminated carbonate
Dolomitic calcimudstone
Dolomitic peloidal packstone
Dolomitic grainstone
Extraclastic dolomitic wackestone
Dolomitic sparstone
Dolomitic marl
Sandstone with dolomitic matrix

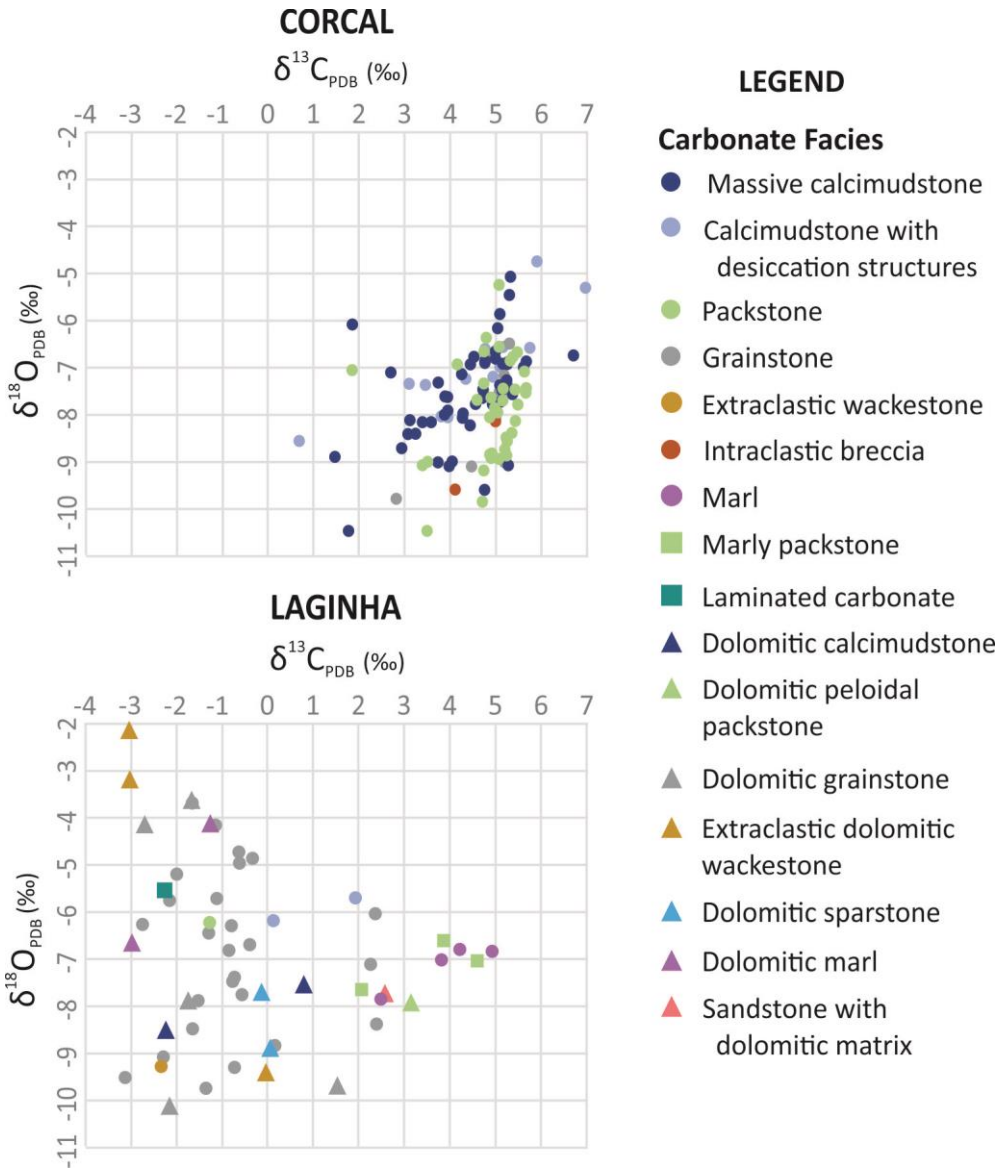

Figure 14: Corcal and Laginha cross-plots of C versus O isotopic data.

3.5.4. Sedimentary facies

Nine facies were recognized at Corcal and twenty at Laginha, which are summarized in tables 1 and 2 and positioned at figures 5 and 7.

Table 1: Corcal sedimentary facies.

FACIES	DESCRIPTION
Mudstone	Centimeter to meter-scale tabular beds composed of massive to fissile siliciclastic mudstone, beige to gray. They locally host *Corumbella werneri* and ichnofossils.
Massive calcimudstone	Sets of decimeter-scale thick wavy tabular beds composed of massive dark gray carbonate mudstone. They locally display bioclasts, intraclasts, interstitial concentration of clay and extraclasts (Qz, Op).
Calcimudstone with desiccation structures	Sets of centimeter to decimeter-scale thick beds with tabular or flaser bedding, composed of massive carbonate mudstone, dark gray, with desiccation structures. They locally display bioclasts, intraclasts and extraclasts (Qz, Ap, Bt, Op).
Marl	Centimeter to decimeter-scale thick tabular beds with both siliciclastic and carbonate fine components. They range from brown to light gray, massive to fissile.
Packstone	Sets of centimeter to decimeter-scale thick tabular wavy beds of massive dark gray packstone composed of intraclasts and bioclasts in micritic matrix. They locally display sparse extraclasts, pelitic levels, nodules and mild dolomitization.
Grainstone	Sets of centimeter to decimeter-scale thick tabular wavy beds of massive dark gray grainstone composed of bioclasts, intraclasts and oolites cemented by sparite.
Intraclastic breccia	Centimeter-scale thick tabular bed of recrystallized breccia composed of rounded, poorly sorted intraclasts in micritic matrix.
Desiccation grainstone	Centimeter-scale thick tabular bed of grainstone composed of non-oriented intraclasts cemented by sparite.
Volcanic tuff (?)	Centimeter-scale thick tabular beds of claystone, white, with shades of pink to orange and very friable.

Table 2: Laginha sedimentary facies.

FACIES	DESCRIPTION
Dolomitic grainstone	Meter-scale thick tabular bed composed of massive light gray dolomitic grainstone.
Sandstone with dolomitic matrix	Meter-scale thick tabular bed composed of massive dark gray sandstone with dolomitic matrix. The grains are predominantly quartz, coarse sand sized and very well rounded. In addition, there a few lithoclasts.
Peloidal packstone	~50 cm tabular bed composed of massive dark gray peloidal packstone with birdseyes.
Polymictic breccia with basement clasts	Approximately 15 m thick bed composed of massive polymictic breccia. The matrix is fine, dolomitic, dark gray. Clasts range in size from sand to boulder, vary from rounded to very angular and include limestones, dolostones, silexites, phosphorites and granitoids.
Argillaceous sandstone	Centimeter-scale thick tabular bed composed of massive dirty sandstone, yellowish-brown when weathered, containing poorly sorted grains of quartz and lithoclast bonded by argillaceous matrix.
Massive calcimudstone	Centimeter to decimeter-scale thick tabular beds composed of massive gray carbonate mudstone. They locally display extraclasts (Qz).
Calcimudstone microbreccia	Centimeter-scale thick beds of brecciated gray carbonate mudstone cemented by at least two generations of calcitic cement. The clasts are very angular and rage in size from fine sand to gravel.
Dolomitic sparstone	Centimeter to decimeter-scale thick tabular beds composed of massive to laminated crystalline dolostone. They are gray, locally displaying extraclasts (Qz) and fractures.
Dolomitic desiccation breccia	Centimeter-scale thick bed of gray desiccation breccia composed of crystalline dolostone with carbonate mudstone intraclasts and sintaxial calcite cement filling the cracks.
Extraclastic wackestone	Centimeter to decimeter-scale thick beds of light gray massive wackestone with with poorly sorted quartz, mica and phosphate grains bonded by micritic matrix
Intraclastic breccia	Centimeter-scale thick wavy bed of massive breccia with abundant extraclasts (Qz). Grains are poorly sorted and angular.
Laminated carbonate	Centimeter-scale thick bed of gray laminated carbonate. It has interchanged fine crystalline and poorly sorted extraclastic levels. They vary from dolomitic to calcitic.
Polymictic breccia	Meter-scale thick irregular body of polymictic breccia. The matrix is micritic, dark gray. Clasts range in size from sand to pebble, vary from rounded to angular and include quartz, limestones, dolostones, siliciclastic mudstones and phosphorites.
Calcimudstone with desiccation structures	Centimeter to decimeter-scale thick tabular beds composed of massive, gray, recrystallized carbonate mudstone with desiccation structures. They locally display micritization and silicification nodules.

FACIES	DESCRIPTION
Packstone	Decimeter-scale thick bed of dark gray packstone with intraclasts and bioclasts.
Marl	Centimeter to decimeter-scale beds with both siliciclastic and carbonate fine components. They occur as thin horizons within carbonates or as thick massive tabular beds.
Marly packstone	Decimeter-scale thick bed of dark gray massive marly packstone with intraclasts.
Grainstone	Sets of decimeter-scale thick beds of dark gray massive grainstones with oolites. They show evidence of intense chemical compaction.
Mudstone	Centimeter scale-thick beds of laminated beige mudstone interbedded with carbonates

3.6. DISCUSSION

The detailed petrographic study revealed important and distinct sedimentary features, which allow us to make a detailed characterization of the sedimentary facies and improve the paleoenvironmental interpretation of the Tamengo Formation. The facies analysis and interpretation were done according to Flügel (2004) and references therein. According to Sumner & Grotzinger (1993) carbonate ramps prevail over rimmed shelves during the Neoproterozoic, for this reason this work uses the Carbonate Ramp Model from Burchette & Wright (1992) for means of depositional setting analysis (Figure 15).

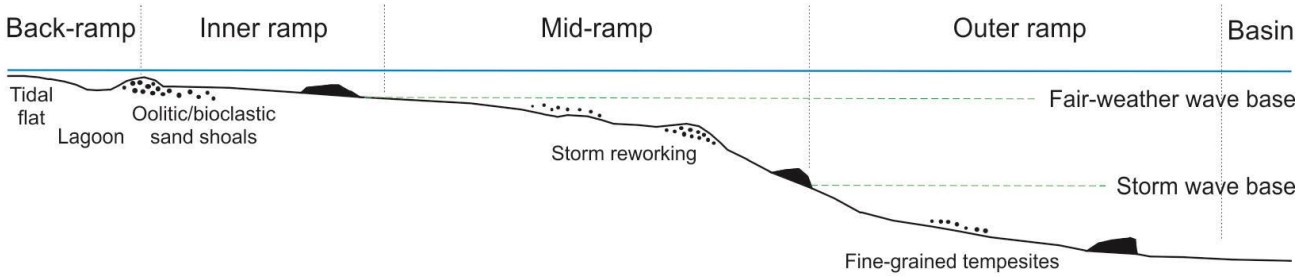

Figure 15: Carbonate Ramp Modelo of a homoclinal ramp. Adapted from Flügel (2004, modified from Burchette & Wright, 1992).

3.6.1. Corcal

The Corcal section comprises massive calcimudstones, calcimudstones with desiccation structures, marls, packstones, and mudstones in the lower part. This facies association suggests a low-energy environment, where fine sediment would settle from suspension. In terms of sedimentary structures, the thin wavy to flaser bedding is characteristic of peritidal to inner ramp settings. Additionally, the presence of fenestral and birdseyes structures indicates a shallow environment, supra to intertidal. The anhydrate pseudomorphs indicate a supratidal hypersaline environment, and the desiccation breccias require exposition, in a supra to intertidal environment. The silicification observed in some levels also supports a shallow water environment, with silica supplied by continental runoff (Laschet, 1984 in Flügel, 2004). All this evidence suggests a peritidal environment for the lower Corcal section.

The meter scale-thick packages of mudstone alternated with the limestones are probably a response to sea level rise, as they required much lower energy conditions, well below the fair-weather wave base, such as in the mid to outer ramp.

The middle part of the section comprises a thinner package of limestones. Initially there are massive calcimudstones, followed by packstones and grainstones, with two mudstone beds intercalated. The facies association shows a shallowing-upward trend, maybe recording the transition from the deeper inner ramp to a sand shoal setting, with the thin mudstone beds deposited on the lee side of the sand bars (Oliveira et al., 2019; Walker, 1984). The second meter scale-thick package of mudstone can represent another phase of sea level rise.

The upper part of the section is the thickest and with more abundant carbonate. There are, from base to top: grainstones, packstones, massive calcimudstones, calcimudstones with fenestral porosity, packstones, massive calcimudstones, packstones, intraclastic breccia, grainstones, packstones, and a final massive bed of oolitic grainstone. This succession indicates variable water energy and proximity to the carbonate factory, suggesting an inner ramp setting with episodic transitions to sand shoals.

The possible volcanic tuff beds might be related to a nearby volcanic eruption and deposited in a low energy environment, such as the deep inner ramp. The volcanic activity is a real possibility due to the extensional tectonics occurring in the Corumbá region through the Ediacaran. Moreover, volcanic tuff beds were reported within this interval of the Corcal section and dated by Babinski *et al.* (2008) and Parry *et al.* (2017) providing ages of 543 ±3 Ma and 541.85 ± 0.75 Ma respectively.

The $\delta^{13}C_{PDB}$ values have no clear correlation to $\delta^{18}O_{PDB,}$ which indicates a primary signal (Kaufman & Knoll, 1995; Derry *et al.*, 2010), even though there are some recrystallized samples. In addition, the isotopic values are not clustered according to the sedimentary facies. There is little point-to-point variation and a clear ascending trend is observed towards the upper part of the section, suggesting a transgression. The higher values probably indicate higher carbon recycling due to the more intense biotic activity in this part of the carbonate platform. Overall, Corcal carbon isotopic curve is consistent with previous studies of this section (Boggiani *et al.*, 2010) as well as with upper Ediacaran sections worldwide, such as in Northwester Canada (Macdonald *et al.*, 2013), South China (Tahata *et al.*, 2013), Namibia (Halverson *et al.*, 2005) and Oman (Fike *et al.*, 2006).

In summary, the Tamengo Formation in the Corcal section displays three shallowing-upward cycles (Figure 13), and can be attributed to a peritidal back-ramp and lagoon to inner

ramp depositional environment. The mudstones intervals represent transgressive episodes that pushed the coast line landward and temporarily stopped the carbonate deposition in this locality. Our observations improve the sedimentary model of Boggiani *et al.* (2010) and Oliveira *et al.* (2019), which proposed a mid to outer ramp environment, close to the storm wave base, for the Corcal section. This interpretation is based especially on the presence of hummocky cross stratification in the limestones of the upper part of the Tamengo Formation. This kind of feature appears only on slightly weathered surfaces that have the sedimentary structures enhanced. For this reason hummocky cross stratification was not observed in the Corcal section, which is exposed in an active quarry, however, the lithology is the same as that outcropping few kilometers away, along the Paraguay river, which clearly display this structure. Therefore, part of the Corcal section clearly represents a mid to outer ramp environment, though, the desiccation structures observed in thin sections and the mudstones intervals clearly indicate shifts towards shallower and deeper conditions.

According to litho- and biostratigraphic data from Adôrno *et al.* (2017) and Walde *et al.* (2015), Sobramil, another classic outcrop of the Tamengo Formation (Figures 1 and 3), is coeval and correlative to Corcal section, showing similar lithologies and even the three swallowing upward cycles.

3.6.2. Laginha

According to Boggiani (1998), the polymictic breccia in the Laginha section marks the base of Tamengo Formation, so the dolomitic grainstone, the sandstone, and the peloidal packstone occurring underneath should represent the top of the Bocaina Formation. The karstification surface above the dolomitic grainstone is evidence of exposition, indicating a shallow environment. Additionally, the very well rounded and sorted grains of the sandstone suggest great transportation of terrigenous sediments, possibly reworked by beach waves. Besides, the peloids are typical of shallow, low energy restricted marine conditions. Hence, these units can represent a peritidal environment, as suggested by Boggiani (1998) and Oliveira (2010).

The massive 15 m-thick breccia contains basement clasts, pointing to continental erosion occurring nearby. In addition, its large thickness and massive structure indicate rapid deposition. Considering that a rift was opening in this region at this time, this polymictic breccia might be related to a rapid graben infill, with material supplied in part by exposed

structural highs and in part by reworked carbonate coming from the platform along the surrounding margin (Figure 16). The dirty sandstone above the breccia is still evidence of continental erosion, but with finer sediment, maybe reflecting distal deposition after the sudden opening of accommodation space due to extensional tectonics.

The onset of carbonate deposition begins with calcimudstones, pointing to a low energy environment. However, these carbonate beds present many syn-sedimentary fractures and are occasionally brecciated, suggesting later seismic pulses of the opening of the rift. The presence of breccias, especially the mound-shaped body occurring between 5 m and 10 m, can represent another tectonic pulse that triggered a slide of carbonate debris, this time not strong enough to induce major basement erosion. However, the lithic sandstones with micritic matrix and the siliciclastic extraclasts occurring in the carbonates above the polymitic breccia reveal that terrigenous sediments were still supplied from the nearby land. Besides, the calcimudstones with birdseye structures above the polymitic breccia indicate a shift toward a shallower environment.

The middle section is composed of alternating marl and limestone, indicating alternating high and low energy periods, with variable terrigenous input. The rhythmicity is probably primary, due to the different fossil content of limestones and marls (Oliveira, 2010; Fazio *et al.*, 2019). The shifts between carbonate and siliciclastic deposition could have been driven by variation in sea level or by tectonically driven vertical movements – both possible for Laginha, in an inner to mid-ramp setting. The rhythmite grade to marly intraclastic packstones, representing the reestablishment of carbonate deposition and, consequently, a small regression.

Following, in the upper segment there are oolitic grainstones up until the contact with the mudstones of the Guaicurus Formation. The oolites are cemented by calcite and range in size from mid to coarse sand. They have nuclei covered by concentric laminae and are rather big, indicating a shallow, warm, high-energy environment (Sumner & Grotzinger, 1993). They probably represent oolitic sand shoals in an inner ramp.

Concerning the isotopic signal of Laginha samples there is no linear covariation between $\delta^{13}C_{PDB}$ and $\delta^{18}O_{PDB}$, demonstrating a primary signal (Kaufman & Knoll, 1995; Derry *et al.*, 2010). The petrographic study recognized dolomitization and recrystallization processes, but these are mild in most of the samples, supporting the primary $\delta^{13}C_{PDB}$ signal.

The great variability of $\delta^{13}C_{PDB}$ values in the lower and middle sections may be related to the high input of allochthonous material, as well as to other environmental, lithological and diagenetic factors. Even though $\delta^{13}C_{PDB}$ values are highly variable, there is no distinct relationship between them and sedimentary facies, nor lithology or diagenetic alteration. With this work's data, it is not possible to have a better interpretation of the Laginha isotopic curve, therefore future research should be done on behalf of this matter. Nevertheless, carbon isotopic data show a remarkable chemostratigraphic boundary between Bocaina and Tamengo formations, with a clear shift from growing positive values to decreasing negative ones. Overall, similar values were found by Boggiani *et al.* (2010) and Velásquez *et al.*, 2008 (in Boggiani *et al.*, 2010) for Tamengo Formation in Laginha.

Lastly, the basal portion of Laginha have highly diverse sedimentary facies, with considerable terrigenous input, indicating near-shore back-ramp to inner ramp settings. However, there is clear evidence of tectonic influence in this part of the basin, making Laginha very different from Corcal and other Tamengo sections. The middle and upper portions do not show much evidence of tectonic activity, but reflect a transgression for the rhythmite deposition, followed by a small regression towards the oolitic sand shoal.

Boggiani *et al.* (2010) propose that the basal polymictic breccia is related to a regression. However, since regression pushes the coastline basinward, it does not allow carbonate platforms to develop along the shore. Thus, a regression does not properly explain the high amount of micrite and carbonate grains that occur in the polymitic breccia together with the basement clasts. Such carbonate, indeed, must be supplied from a carbonate factory in the sourroundings. We propose, instead, that the polymitic breccia represents the fill of the opening of accommodation related to extensional tectonic, which created a steep topography and allowed the income of a big flux of reworked carbonate and basement material (Figure 16). Still, Bogianni *et al.* (2010) do not discard a purely tectonic origin for the breccia. Oliveira *et al.* (2019) admit a tectonic origin for the Tamengo Fm. breccias and support the interpretation of Laginha's upper section as an inner ramp setting, close to oolitic sand shoals.

3.6.3. Corcal *versus* Laginha

The Corcal and Laginha sections are the most studied outcrops of Tamengo Formation in the Corumbá region. Though, they are extremely different from each other, showing that the Ediacaran carbonate ramp in the Corumbá region was not homogeneous, and was

controlled, to different extents, by active extensional tectonic. Starting from the considerations presented in this work, we propose a new depositional model for the Tamengo Formation (Figure 16).

Warren *et al.* (2019) proposes a tectonic evolution model for the Itapucumi Group, in Paraguay, which outcrops circa 250 km to the south of Corumbá and is correlated to the Corumbá Group. According to this model, by the time of Tamengo's deposition (*ca* 555 to 542 Ma) the basin was in a thermal subsidence regime, during the post-rift stage, but still influenced by extensional tectonics. At this stage, the sea invaded the rift and allowed the deposition of shallow-water carbonates. In this context, the Corcal section corresponds to a stable portion of the ramp, located in a marginal setting, relatively far from the tectonic lineaments. On the other hand, the Laginha section probably sat close to or into a graben, facing a horst, which provided the terrigenous supply.

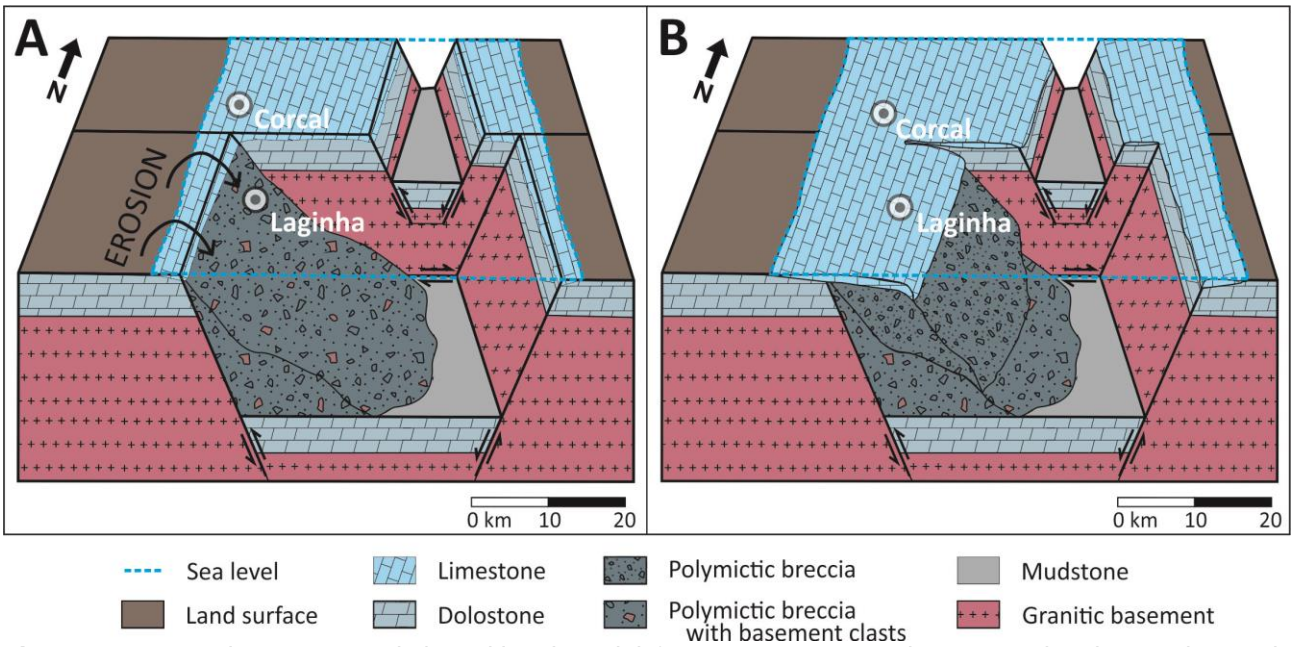

Figure 16: Tectonic context and depositional model for Tamengo Formation. Extensional tectonics at the Corumbá Graben System create accommodation space and steep topography near the normal faults. A) Laginha sits into the graben and is loaded with terrigenous input due to the steep topography near the fault. On the other hand, Corcal is located at a higher spot, more stable, at the carbonate ramp. B) In a later stage, with higher sea level, both sites sit at the carbonate ramp.

A vigorous debate exists in previous studies of the Tamengo Formation for explaining the difference in depositional setting between the Corcal and Laginha sections. While Boggiani *et al.* (2010) propose that the former represents a shallower setting; Oliveira *et al.* (2019) states the opposite. Here we propose that the difference is not simply due to the distance from the shore, but mainly to the topography, which was controlled by tectonics in a

rift context. The Corcal section was located on a shallow, gently dipping ramp, influenced by minor sea level fluctuations. This evidence also appear at other sections, such as Sobramil, also known as Itau-Saladeiro. The Laginha section, on the other hand, was possibly closer to the shoreline, thus receiving more detrital input, but with a steeper and tectonically controlled topography, with more variable depth than Corcal.

Boggiani (1998) proposes Laginha as a type-section of the Tamengo Formation, as it displays both the base and the top of this unit. However, we show here that the Laginha section is heterogeneous, both in terms of facies and isotopic composition, with highly discontinuous sedimentation. Therefore, the Corcal section, even not showing the complete Tamengo succession, would be a more suitable type-section, as it is more homogeneous lithologically and continuous stratigraphically. Besides, it yields an outstanding fossils record, as well as a more reliable chemostratigraphic record.

3.7. SUMMARY AND CONCLUSIONS

The Tamengo Formation, superior part of the Corumbá Group, comprises carbonate and siliciclastic sediments deposited on an upper Ediacaran ramp periodically and locally influenced by extensional tectonics related to the Corumbá Graben System. The studies sites, Corcal and Laginha quarries, show very different lithologic associations, as well as sedimentary facies when closely observed. Corcal section is homogeneous, continuous and show little facies variation. It comprises three coarsening upward cycles and depositional environments shallower than previously reported, due to evidence of peritidal, lagoon and inner ramp settings. It provides a $\delta^{13}C_{PDB}$ curve with high continuity and values on a clear ascending trend from ~3.5‰ to ~5‰, which together with facies association point to a transgression event. The Corcal carbon isotopic values are very similar to other renowned upper Ediacaran sections worldwide. Laginha section, on the other hand, is heterogeneous, have hiatus, and is clearly influenced by extensional tectonics. The analysis of all twenty sedimentary facies point to cyclic seismic influence and terrigenous input, producing breccias and impure carbonates. Contrarily than formerly proposed, we understand that the basal polymictic breccia and related facies are the filling of accommodation space created by extensional tectonics, in a steep topography site, with income of reworked carbonate and continental material. The upper section represents a steadier period, with progradation of facies on an inner ramp setting. Concerning Laginha carbon isotopic data values are highly variable, which may be related to environmental, lithological and diagenetic factors. The origin of this signal should be investigated in future research.

This work provided a detailed characterization of an upper Ediacaran ramp, on microfacies level, which must contribute to future stratigraphy and paleontological research. Nevertheless, we came across the limitations of the use of carbon chemostratigraphy as a correlation tool, therefore we endorse that the liable use of carbon isotopes must be evaluated together with a meticulous faciologic and petrographic study. In conclusion, the Corumbá Ediacaran Platform was heterogeneous, with sedimentation controlled, in various degrees, by extensional tectonics. Its mutable topography allowed the existence of distinct depositional environments side-by-side, as is the case of Laginha and Corcal. The first represents a shallow, gently dipping ramp, minimally affected by seismicity, while the former, even possibly closer to the shoreline, sits on a steep and tectonically controlled environment. Several authors use Laginha as the type-section of Tamengo Formation, however, due to its

high heterogeneity and puzzling isotopic signal, we suggest the Corcal is a more appropriate type-section, as it is lithologically homogenous, stratigraphically continuous, bears an outstanding fossil record and a more reliable chemostratigraphic record.

4. REFERENCES

Adôrno, R.R. (2019) Taxonomy, paleoecology and chronobiostratigraphy across the Ediacaran-Cambrian boundary: Tamengo and Guaicurus formations. Doctoral thesis, University of Brasília, 130 pp.

Adôrno, R.R., do Carmo, D.A., Germs, G., Walde, D.H.G., Denezine, M., Boggiani, P.C., Silva, S.C.S., Vasconcelos, J.R., Tobias, T.C., Guimarães, E.M., Vieira, L.C., Figueiredo, M.F., Moraes, R., Caminha, S.A., Suarez, P.A.Z., Rodrigues, C.V., Caixeta, G.M., Pinho, D., Schneider, G. and Muyamba, R. (2017) Cloudina lucianoi (Beurlen & Sommer, 1957), Tamengo Formation, ediacaran, Brazil: taxonomy, analysis of stratigraphic distribution and biostratigraphy. Precambrian Research, 301, 19–35.

Almeida, F.F.M. (1964) Geologia do sudoeste mato-grossense. Boletim da Divisão de Geologia e Mineralogia, DNPM, 116, 1–18.

Almeida, F.F.M. (1965) Geologia da Serra da Bodoquena (Mato Grosso), Brasil. Boletim de Geologia e Mineralogia, DNPM, 219, 1–96.

Almeida, F.F.M. (1984) Província Tocantins, setor sudoeste. In: de Almeida, F.F.M., Hasui, Y. (Eds.), O Pré-cambriano Do Brasil. Edgard Blücher, São Paulo, 265–281.

Alvarenga, C.J.S. and Trompette, R. (1992) Glacially influenced sedimentation in the later Proterozoic of the Paraguay Belt (Mato Grosso, Brazil). Palaeogeography, Palaeoclimatology, Palaeoecology, 92, 85-105.

Alvarenga, C.J.S., Boggiani, P.C., Babinski, M., Dardene, M.A., Figueiredo, M.F., San-tos, R.V. and Dantas, E.L. (2009). The Amazonian Palaeocontinet. In: Gaucher, C., Sial,A.N., Frimmel, H., Halverson, G.P. (Eds.), Neoproterozoic-Cambrian Tectonics,Global Changes and Evolution: A focus on Southwestern Gondwana. Elsevier, Amsterdam, 15–28.

Babinski, M., Boggiani, P.C., Fanning, M., Simon, C.M. and Sial, A.N. (2008) U–Pb shrimp geochronology and isotope chemostratigraphy (C, O, Sr) of the Tamengo Formation, southern Paraguay Belt, Brazil. 6th South American Symposium on Isotope Geology San Carlos de Bariloche, Proceedings, 160.

Babinski, M., Boggiani, P.C., Trindade, R.I.F. and Fanning, C.M. (2013). Detrital zircon ages and geochronological constraints on the Neoproterozoic Puga diamictites and associated BIFs in the southern Paraguay Belt, Brazil. Gondwana Research, 23, 988–997.

Barbosa, O. (1949) Contribuição à geologia da região Brasil-Bolívia. Mineracao Metal., 13, 271–278.

Becker-Kerber, B., Pacheco, M.L.A.F., Rudnitzki, I.D., Galante, D., Rodrigues, F., and Leme, J.d.M. (2017) Ecological interactions in Cloudina from the Ediacaran of Brazil: implications for the rise of animal biomineralization. Scientific Reports, 7, 5482.

Beurlen, K. and Sommer, F.W. (1957) Observações estratigráficas e paleontológicas sobre o calcário de Corumbá. Boletim de Geologia e Mineralogia – DNPM, 168, 1–35.

Boggiani, P.C. (1998) Análise Estratigráfica da Bacia Corumbá (Neoproterozoico) – Mato Grosso do Sul. Ph.D. Thesis, Universidade de São Paulo, Brasil, 1–181.

Boggiani, P.C., Fairchild, T.R. and Coimbra, A.M. (1993) O Grupo Corumbá (Neoproterozóico-Cambriano) na região central da Serra da Bodoquena (Faixa Paraguai), Mato Grosso do Sul. Revista Brasileira de Geociências, 23, 301–305.

Boggiani, P.C., Alvarenga, C.J.S. (2004) Faixa Paraguai. In: Mantesso- Neto, Bartorelli, A., Carneiro, C.D.R., Neves, B.B.B. (Eds.), Geologia do Continente Sul-Americano: Evolução da Obra de Fernando Flávio Marques de Almeida. Beca Produções Culturais Ltda, São Paulo, pp. 113–120.

Boggiani, P.C., Gaucher, C., Sial, A.N., Babinski, M., Simon, C.M., Riccomini, C., Ferreira, V.P. and Fairchild, T.R. (2010) Chemostratigraphy of the Tamengo Formation (Corumba group, Brasil): a contribution to the calibration of the ediacaran carbon-isotope curve. Precambrian Research, 182, 382–401.

Bristow, T.F. and Kennedy, M.J. (2008) Carbon isotope excursions and the oxidant budget of the Ediacaran atmosphere and ocean. Geology, 36, 863–866.

Burchette, T.P. and Wright, V.P. (1992): Carbonate ramp depositional systems. - Sedimentary Geology, 79, 3-57.

Campanha, G.A.C., Boggiani, P.C., Sallun FILHO, W., SÁ, F.R., Zuquim, M.P.S. and Piacentini, T. (2011). A Faixa de Dobramentos Paraguai na Serra da Bodoquena e Depressão do Rio Miranda, Mato Grosso do Sul. Geol. Usp. Série Científica, 11, 79–96.

Cortijo, I., Mus M. M., Jensen, S. and Palacios, T. (2010) A new species of Cloudina from the terminal Ediacaran of Spain. Precambrian Research, 176 , 1-10.

Cui, H., Kaufman, A.J., Peng, Y., Liu, X.M., Plummer, R.E. and Lee, E.I., (2018) The Neoproterozoic Hüttenberg δ13C anomaly: Genesis and global implications. Precambrian Research, 313, 242-262.

D'el-Rey Silva, L., Walde, D. and Saldanha, D. (2016). The Neoproterozoic–Cambrian Paraguay belt, Central Brazil: Part I— new structural data and a new approach on the regional implications. Tectonophysics, 676, 20–41.

Delgado, F. (1977) Primary textures in dolostones and recrystallized limestones: a technique for their microscopy study. Journal of Sedimentary Petrology, 47, 1339-1341.

Derry, L.A. (2010) A burial diagenesis origin for the Ediacaran Shuram–Wonoka carbon isotope anomaly. Earth and Planetary Science Letters, 294, 152–162.

Fairchild, T.R. (1978) Evidências paleontológicas de uma possível idade Ediacariana ou Cambriana Inferior, para a parte leste do Grupo Corumbá (Mato Grosso do Sul). In: 30º Congresso Brasileiro de Geologia, Resumo das Comunicações. Recife, pp. 181.

Falkowski, P. (2003) Biogeochemistry of Primary production in the Sea. Treatise on Geochemistry, 8,185-213.

Fazio, G., Guimarães, E.M.,Walde, D.G.H., Do Carmo, D.A., Adôrno, R.R., Vieira, L.C., Denezine, M., Silva, C.B., Godoy, H.V., Borges, P.C. and Pinho, D. (2019) Mineralogical and chemical composition of Ediacaran-Cambrian pelitic rocks of The Tamengo and Guaicurus formations, (Corumbá Group - MS, Brazil): Stratigraphic positioning and paleoenvironmental interpretations. Journal of South American Earth Sciences, 90, 487 – 503.

Fike, D.A., Grotzinger, J.P., Pratt, L.M., and Summons, R.E. (2006) Oxidation of the Ediacaran Ocean. Nature, 444, 744-747.

Flügel, E. (2004) Microfacies of Carbonate Rocks: Analysis, Interpretation and Application. Germany. Springer-Verlag Berlin Heidelberg. 976 p.

Fontanela, G.T. (2012) Dolomitização e Fosfogênese na Formação Bocaina, Grupo Corumbá (Ediacarano). 148p. Dissertação (Mestrado). Instituto de Geociências, Universidade de São Paulo, São Paulo.

Freitas, B.T., Warren, L.V., Boggiani, P.C., Almeida, R.P. and Piacentini, T., (2011). Tectono-sedimentary evolution of the Neoproterozoic BIF-bearing Jacadigo Group, SW-Brazil. Sedimentary Geology, 238, 48–70.

Frimmel, H.E. (2010) On the reliability of stable carbon isotopes for Neoproterozoic chemostratigraphic correlation. Precambrian Research, 182(4), 239-253.

Gaucher C., Boggiani P.C., Sprechmann P., Sial A.N. and Fairchild T.R. (2003) Integrated correlation of Vendian to Cambrian Arroyo del Soldado and Corumbá Groups Uruguay and Brazil): palaeogeographic, palaeoclimatic and palaeobiologic implications. Precambrian Research, 120, 241-278.

Gernon, T.M., Hincks, T.K., Tyrrell, T., Rohling, E.J. and Palmer, M.R. (2016) Snowball Earth ocean chemistry driven by extensive ridge volcanism during Rodinia breakup. Nature Geoscience, 9, 242–248.

Grant, S. (1990) Shell structure and distribution of Cloudina, a potential index fossil for the terminal Proterozoic. American Journal of Science, 290-A, 261–294.

Grotzinger, J.P. and James, N.P. (2000) Precambrian carbonates: evolution of understanding. In: Carbonate Sedimentation and Diagenesis in the Evolving Precambrian World. SEPM Special Publication, 67.

Grotzinger, J.P., Fike, D.A. and Fischer, W.W (2011) Enigmatic origin of the largest-known carbon isotope excursion in Earth's history. Nature Geoscience, 4, 285-292.

Hahn, G., Hahn, R., Leonardos, O.H., Pflug, H.D. and Walde, D.H.G. (1982) Korperlich erhaltene Scyphozoen-Reste aus dem Jungprakambrium Brasiliens. Geologica et Palaeontologica, 16, 1–18.

Halverson G.P., Hoffman P.F., Schrag D.P., Maloof A.C. and Rice A.H.N. (2005) Toward a Neoproterozoic composite carbon-isotope record. Geological Society of America Bulletin, 117, 1181-1207.

Halverson G.P., Wade B.P., Hurtgen M.T. and Barovich K.M. (2010) Neoproterozoic chemostratigraphy. Precambrian Research, 182, 337-350.

Hidalgo, R.L.L. (2002) Análise micropaleontológica das formações Tamengo e Guaicurus, Grupo Corumbá (MS), e Formação Araras (MT), transição do Neoproterozóico-Fanerozóico. Dissertação (Mestrado). Instituto de Geociências, Universidade de São Paulo, São Paulo.

Hoffman, P.F., Kaufman, A.J., Halverson, G.P. and Schrag, D.P. (1998) A Neoproterozoic snowball earth. Science, 281, 1342–1346.

Jones, J.P. (1985) The southern border of the Guaporé shield in Western Brazil and Bolivia: an interpretation of its geologic evolution. Precambrian Research, 28, 111—135.

Kaufman, A.J. and Knoll, A.H. (1995) Neoproterozoic variations in the C-isotopic composition of seawater: stratigraphic and biogeochemical implications. Precambrian Research, 73, 27-49.

Kerber, B.B., Rosa, A.L.Z., Gabas, S.G., Leme, J.M. and Pacheco, M.L.A.F. (2013) O registro fossilífero de metazoários ediacaranos na América do Sul e suas implicações nos estudos sobre origem e complexificação da vida animal. Geol. Usp. Série Científica, 13(3), 51–64.

Knauth, L.P. and Kennedy, M.J. (2009) The late Precambrian greening of the Earth. Nature, 460, 728–732.

Knoll, A.H. and Carroll, S.B. (1999) Early Animal Evolution: Emerging Views from Comparative Biology and Geology. Science 284, 2129-2137.

Knoll, A.H., Walter, M.R., Narbonne, G.M., and Christie-Blick, N. (2006) The Ediacaran Period: a new addition to the geologic time scale. Lethaia, 39, 13-30.

Laschet, C. (1984) On the origin of cherts. Facies, 10, 257-289

Li, Z., Evans, D.A.D. and Halverson, G.P. (2013) Neoproterozoic glaciations in a revised global palaeogeography from the breakup of Rodinia to the assembly of Gondwanaland. Sedimentary Geololy, 294, 219-232.

Macdonald, F.A., Strauss, J.V., Sperling, E.A., Halverson, G.P., Narbonne, G.M., Johnston, D.T., Kunzmann, M., Schrag, D.P., and Higgins, J.A. (2013) The stratigraphic relationship between the Shuram carbon isotope excursion, the oxygenation of

Neoproterozoic oceans, and the first appearance of the Ediacaran biota and bilaterian trace fossils in northwestern Canada. Chemical Geology, 362, 250-272.

Meira, F.V.E. (2011) Caracterização tafonômica e estratigráfica de Cloudina lucianoi (Beurlen e Sommer, 1957) Zaine e Fairchild, 1985, no Grupo Corumbá, Ediacarano do Brasil. Dissertação (Mestrado). Instituto de Geociências, Universidade de São Paulo, São Paulo.

Narbonne, G.M., Xiao, S., Shields, G.A. and Gehling, J.G. (2012) The Ediacaran Period. The geologic time scale, 1, 413-435.

Oliveira, R.S., Nogueira, A.C.R., Romero, G.R., Truckenbrodt, W. and da Silva Bandeira, J.C. (2019) Ediacaran ramp depositional model of the Tamengo Formation, Brazil. Journal of South American Earth Sciences. DOI: https://doi.org/10.1016/j.jsames.2019.102348.

Oliveira, R.S. (2010) Depósitos de rampa carbonática Ediacarana do Grupo Corumbá, região de Corumbá, Mato Grosso do Sul. Dissertação (Mestrado). Instituto de Geociências, Universidade Federal do Pará, Belém.

Parry, L., Boggiani, P.C., Condon, D., Garwood, R., Leme, J.M., Mcllroy, D., Brasier, M.D., Trindade, R., Campanha, G.A.C., Pacheco, M.L.A.F., Diniz, C., Q. C and Lui, A.G. (2017) Ichnological evidence for meiofaunal bilaterians from the terminal Ediacaran and earliest Cambrian of Brazil. Nature Ecology & Evolution 1, 1455–1464.

Piacentini, T., Vasconcelos, P.M. and Farley, K.A. (2013) $^{40}Ar/^{39}Ar$ constraints on the age and thermal history of the Urucum Neoproterozoic banded iron-formation. Brazil. Precambrian Research 228, 48–62.

Sial, A.N., Gaucher, C., Misi, A., Boggiani, P.C., Alvarenga, C.J.S., Ferreira, V.P., Pimentel, M.M., Pedreira, J.A., Warren, L.V., Fernández-Ramírez, R., Geraldes, M., Pereira, N.S., Chiglino, L. and Cezario, W.S. (2016) Correlations of some Neoproterozoic carbonate-dominated successions in South America based on high-resolution chemostratigraphy. Brazilian Journal of Geology, 46(3), 439–488.

Spangenberg, J.E., Bagnoud-Velasquez, M., Boggiani, P.C. and Gaucher, C. (2014) Redox variations and bioproductivity in the Ediacaran: evidence from inorganic and organic geochemistry of the Corumbá Group, Brazil. Gondwana Research, 26, 1186–1207.

Sumner, D.Y. and Grotzinger, J.P. (1993) Numerical modeling of ooid size and the problem of Neoproterozoic giant ooids. Journal of Sedimentary Petrology, 63(5), 974 – 982.

Sundquist, E.T. and Visser, K. (2004) The Geologic History of the Carbon Cycle. Treatise on Geochemistry, 8, 425:472.

Tahata, M., Sawaki, Y., Ueno, Y., Nishizawa, N., Yoshida, N.,Ebisuzaki, T., Komiya, T. and Maruyama, S. (2014) Three-step modernization of the ocean: Modeling of carbon cycles and the revolution of ecological systems in the Ediacaran/Cambrian periods. Geoscience Frontiers, 6, 121 – 136.

Tobias, T.C. (2014) Micropaleontologia da Formação Tamengo, Eco Parque Cacimba da Saúde, Ediacarano, Grupo Corumbá, Estado de Mato Grosso do Sul, Brasil. 88p. Dissertação (Mestrado). Instituto de Geociências, Universidade de Brasília, Brasília.

Trompette, R., Alvarenga, C.J.S. and Walde, D.H.G. (1998) Geological evolution of the Neoproterozoic Corumbá Graben System, Brazil: Depositional context of thestratified Fe and Mn ores of the Jacadigo Group. Journal of South American Earth Sciences, 11, 587–597.

Walde, D.H.G. (1988). Das Proterozoische Paraguay-Araguaia orogen in West-Brasilien, ausgehend von Untersuchungen im Raum Corumbá. Habil. Schrift. Albert-Ludwigs-Universitat, Freiburg, pp. 122p.

Walde, D.H.G., Leonardos, O.H., Hahn, G., Hahn, R. and Pflug, H. (1982) The first Precambrian megafossil from South America, Corumbella werneri. Anais da Academia Brasileira de Ciências, 54, 461.

Walde, D.H.G., Do Carmo, D.A., Guimarães, E.M., Vieira, L.C., Erdtmann, B.D., Sanchez, E.A.M., Adôrno, R.R. and Tobias, T.C. (2015) The Neoproterozoic-Cambrian transition in the Corumbá region. Ann. Palaontol., 101, 213–224.

Walde, D.G.H., Weber, B., Erdtmann, B.D. and Steiner, M. (2019) Taphonomy of Corumbella werneri from the Ediacaran of Brazil: sinotubulitid tube or conulariid test?. Alcheringa: An Australasian Journal of Palaeontology, DOI: 10.1080/03115518.2019.1615551

Walker, R.G. (1984) Shelf and Shallow Marine Sands. In: Walker, R.G. (Ed), Facies Models. Geological Association of Canada, Canada, pp. 141 – 170.

Warren, L.V., Freitas, B.T., Riccomini, C., Boggiani, P.C., Quaglio, F., Simões, M.G., Fairchild, T.R., Giorgioni, M., Gaucher, C., Poiré, D.G., Cáceres, A.A. and Sial A.N. (2019) Sedimentary evolution and tectonic setting of the Itapucumi Group, Ediacaran, northern Paraguay: From Rodinia break-up to West Gondwana Amalgamation. Precambrian Research, 322, 99 – 121.

Wentworth, C.K. (1922) A Scale of Grade and Class Terms for Clastic Sediments. The Journal of Geology, 30(5), 377-392.

Wright, V.P. (1992) A revised classification of limestones. Sedimentary Geology, 76, 177-186.

Xiao, S., Narbonne, G. M., Zhou, C., Laflamme, M. Grazhdankin, D. V., Moczydlowska-Vidal, M. and Cui, H. (2016) Toward an Ediacaran Time Scale: Problems, Protocols, and Prospects. Episodes, 39(4), 540-555.

Zaine, M.F. (1991). Análise dos fósseis de parte da Faixa Paraguai (MS, MT) e seu contexto temporal e paleoambiental. Ph.D. Thesis. University of São Paulo, Brazil, 218 p.

Zaine, M.F. and Fairchild, T.R. (1985) Comparison of Aulophycus lucianoi Beurlen & Sommer from Ladário (MS) and the genus Cloudina Germs, Ediacaran of Namibia. Anais Academia Brasileira de Ciências, 57, pp. 130.

5. SUPPLEMENTARY MATERIAL

The following pages contain supplementary information in four annexes: two tables containing samples information for Corcal and Laginha; and two photo compilations of the thin sections pictures for Corcal and Laginha.

Table A: Corcal samples data

Section	Sub-section	Sample	Level / m	Lithology	Sedimentary Facies	Thin section	SEM	$\delta^{13}C_{PDB}$ / ‰	$\delta^{18}O_{PDB}$ / ‰
Corcal	C1	108	0.90	Limestone	Massive calcimudstone			3.98	-9.09
Corcal	C1	109	0.95	Limestone	Massive calcimudstone			4.05	-9.00
Corcal	C1	128	1.28	Limestone	Massive calcimudstone			1.48	-8.90
Corcal	C1	163	1.63	Limestone	Massive calcimudstone			2.94	-8.71
Corcal	C1	171	1.71	Limestone	Massive calcimudstone				
Corcal	C1	207	2.07	Limestone	Massive calcimudstone				
Corcal	C1	232	2.32	Limestone	Massive calcimudstone			3.25	-8.41
Corcal	C1	262	2.62	Limestone	Massive calcimudstone	X		3.08	-8.42
Corcal	C1	279	2.79	Limestone	Massive calcimudstone				
Corcal	C1	290	2.90	Limestone	Massive calcimudstone			3.40	-8.16
Corcal	C1	310	3.10	Limestone	Massive calcimudstone			3.13	-8.12
Corcal	C1	335	3.35	Limestone	Massive calcimudstone				
Corcal	C1	380	3.80	Limestone	Massive calcimudstone				
Corcal	C1	400	4.00	Limestone	Massive calcimudstone				
Corcal	C1	460	4.60	Limestone	Massive calcimudstone			4.28	-8.07
Corcal	C1	480	4.80	Limestone	Massive calcimudstone			3.88	-8.00
Corcal	C1	510	5.10	Limestone	Massive calcimudstone			3.96	-7.92
Corcal	C1	540	5.40	Limestone	Massive calcimudstone			3.74	-9.01
Corcal	C1	560	5.60	Limestone	Massive calcimudstone			3.59	-8.16
Corcal	C1	580	5.80	Limestone	Massive calcimudstone			3.90	-7.62
Corcal	C1	630	6.30	Limestone	Calcimudstone with desiccation structures			3.81	-8.04

Corcal	C1	650	6.50	Limestone	Calcimudstone with desiccation structures	X	X		
Corcal	C1	665	6.65	Limestone	Calcimudstone with desiccation structures			3.10	-7.35
Corcal	C1	705	7.05	Limestone	Calcimudstone with desiccation structures			3.46	-7.37
Corcal	C1	725	7.25	Limestone	Calcimudstone with desiccation structures				
Corcal	C2	750	7.50	Limestone	Calcimudstone with desiccation structures			0.70	-8.56
Corcal	C1	755	7.55	Limestone	Calcimudstone with desiccation structures			3.96	-8.06
Corcal	MP	MP 2115	7.60	Marl	Marl	X			
Corcal	C2	770	7.70	Marl	Marl				
Corcal	C2	790	7.90	Limestone	Massive calcimudstone				
Corcal	MP	MP 2116	7.95	Limestone	Massive calcimudstone	X			
Corcal	C2	810	8.10	Mudstone	Mudstone				
Corcal	C2	860	8.60	Limestone	Massive calcimudstone			3.95	-7.63
Corcal	C2	890	8.90	Limestone	Massive calcimudstone			1.78	-10.47
Corcal	C2	908	9.08	Marl	Marl				
Corcal	C2	940	9.40	Limestone	Packstone	X			
Corcal	C2	970	9.70	Limestone	Massive calcimudstone			4.34	-7.60
Corcal	C2	990	9.90	Limestone	Massive calcimudstone			4.71	-7.65
Corcal	C2	1015	10.15	Limestone	Massive calcimudstone			5.33	-5.07
Corcal	C2	1040	10.40	Limestone	Massive calcimudstone	X	X	5.00	-6.66
Corcal	C2	1060	10.60	Limestone	Massive calcimudstone			4.77	-6.91
Corcal	C2	1100	11.00	Limestone	Massive calcimudstone			1.86	-6.09
Corcal	C2	1125	11.25	Limestone	Massive calcimudstone			4.45	-6.94

Corcal	C2	1140	11.40	Limestone	Massive calcimudstone				
Corcal	C2	1160	11.60	Limestone	Massive calcimudstone				
Corcal	MP	MP 2117	11.70	Limestone	Massive calcimudstone	X			
Corcal	C2	1185	11.85	Limestone	Massive calcimudstone			4.78	-6.85
Corcal	C2	1205	12.05	Limestone	Massive calcimudstone				
Corcal	C2	1235	12.35	Limestone	Massive calcimudstone			6.71	-6.75
Corcal	C2	1255	12.55	Limestone	Massive calcimudstone	X		5.24	-7.33
Corcal	C2	1275	12.75	Limestone	Calcimudstone with desiccation structures				
Corcal	MP	MP 2118	12.90	Limestone	Calcimudstone with desiccation structures	X			
Corcal	C2	1295	12.95	Limestone	Calcimudstone with desiccation structures			6.97	-5.31
Corcal	C2	1310	13.10	Limestone	Calcimudstone with desiccation structures				
Corcal	C2	1320	13.20	Limestone	Desiccation grainstone				
Corcal	MP	MP 2119	13.30	Limestone	Desiccation grainstone	X			
Corcal	C2	1350	13.50	Limestone	Calcimudstone with desiccation structures				
Corcal	C2	1370	13.70	Limestone	Calcimudstone with desiccation structures				
Corcal	C2	1390	13.90	Limestone	Calcimudstone with desiccation structures			5.91	-4.75
Corcal	MP	MP 1617	14.10	Limestone	Calcimudstone with desiccation structures	X		-2.17	-8.11
Corcal	C2	1415	14.15	Limestone	Calcimudstone with				

					desiccation structures				
Corcal	C2	1430	14.30	Limestone	Calcimudstone with desiccation structures			4.94	-7.20
Corcal	C2	1455	14.55	Limestone	Calcimudstone with desiccation structures			5.10	-6.99
Corcal	MP	MP 2120	14.60	Limestone	Desiccation grainstone	X			
Corcal	C2	1475	14.75	Limestone	Calcimudstone with desiccation structures				
Corcal	C2	1485	14.85	Limestone	Calcimudstone with desiccation structures			5.03	-7.74
Corcal	MP	MP 2121	15.05	Marl	Marl	X			
Corcal	C2	1510	15.10	Limestone	Calcimudstone with desiccation structures				
Corcal	C2	1530	15.30	Limestone	Calcimudstone with desiccation structures			4.77	-6.61
Corcal	C2	1550	15.50	Limestone	Calcimudstone with desiccation structures				
Corcal	C2	1560	15.60	Limestone	Calcimudstone with desiccation structures			5.00	-8.07
Corcal	C2	1568	15.68	Limestone	Calcimudstone with desiccation structures				
Corcal	MP	MP 2122	15.70	Mudstone	Mudstone	X			
Corcal	MP	MP 2123	15.95	Limestone	Calcimudstone with desiccation structures	X			
Corcal	C2	1595	15.95	Limestone	Calcimudstone with desiccation structures			5.75	-6.58
Corcal	C2	1625	16.25	Limestone	Calcimudstone with desiccation structures				

Corcal	C2	1645	16.45	Limestone	Massive calcimudstone			5.61	-7.00
Corcal	C2	1665	16.65	Limestone	Massive calcimudstone			5.11	-7.73
Corcal	C2	1690	16.90	Limestone	Massive calcimudstone			5.00	-7.80
Corcal	C2	1720	17.20	Limestone	Massive calcimudstone				
Corcal	C2	1740	17.40	Limestone	Massive calcimudstone			2.71	-7.11
Corcal	C2	1750	17.50	Limestone	Massive calcimudstone				
Corcal	MP	MP 2124	17.60	Mudstone	Mudstone	X			
Corcal	C2	1770	17.70	Limestone	Packstone				
Corcal	C2	1790	17.90	Limestone	Packstone			5.07	-8.94
Corcal	MP	MP 2125	18.02	Mudstone	Mudstone	X			
Corcal	MP	MP 1619	18.10	Limestone	Packstone	X		1.85	-7.06
Corcal	C2	1830	18.30	Limestone	Packstone			5.24	-8.87
Corcal	MP	MP 2126	18.60	Marl	Marl	X			
Corcal	MP	MP 2127	19.20	Mudstone	Mudstone	X			
Corcal	MP	MP 1623	23.28	Limestone	Massive calcimudstone	X		4.26	-7.15
Corcal	MP	MP 1625	23.71	Limestone	Massive calcimudstone	X		4.53	-6.78
Corcal	MP	MP 1626	24.08	Limestone	Massive calcimudstone	X		5.27	-6.88
Corcal	MP	MP 1627	24.46	Limestone	Grainstone	X		5.19	-7.17
Corcal	MP	MP 1628	24.83	Limestone	Packstone	X		5.16	-7.70
Corcal	MP	MP 1631	25.71	Limestone	Grainstone	X		4.74	-7.49
Corcal	C3	25	29.96	Limestone	Grainstone			5.30	-6.50
Corcal	MP	MP 2128	30.15	Limestone	Grainstone	X			
Corcal	C3	45	30.16	Limestone	Grainstone				
Corcal	C3	170	31.41	Limestone	Grainstone			4.94	-6.78
Corcal	C3	220	31.91	Limestone	Grainstone			5.08	-7.53
Corcal	C3	240	32.11	Limestone	Grainstone				
Corcal	C3	255	32.26	Limestone	Packstone	X	X	4.74	-7.34
Corcal	C3	270	32.41	Limestone	Packstone				
Corcal	C3	290	32.61	Limestone	Packstone				
Corcal	C3	315	32.86	Limestone	Packstone			4.16	-6.93
Corcal	C3	325	32.96	Limestone	Packstone				
Corcal	C3	340	33.11	Limestone	Packstone			4.59	-7.69
Corcal	MP	MP 1650	33.26	Limestone	Packstone	X		4.80	-6.37
Corcal	C3	370	33.41	Limestone	Packstone			5.17	-7.45
Corcal	C3	400	33.71	Limestone	Packstone				
Corcal	C3	420	33.91	Limestone	Packstone				
Corcal	C3	440	34.11	Limestone	Packstone			5.43	-8.14

Corcal	C3	490	34.61	Limestone	Packstone			5.23	-8.49
Corcal	MP	MP 2129	34.65	Limestone	Calcimudstone with desiccation structures	X			
Corcal	C3	520	34.91	Limestone	Massive calcimudstone				
Corcal	C3	555	35.26	Limestone	Massive calcimudstone			5.28	-7.43
Corcal	MP	MP 1651	35.51	Limestone	Massive calcimudstone	X		4.76	-9.60
Corcal	C3	583	35.54	Limestone	Massive calcimudstone				
Corcal	C3	600	35.71	Limestone	Massive calcimudstone				
Corcal	C3	615	35.86	Limestone	Massive calcimudstone			4.44	-8.23
Corcal	C3	630	36.01	Limestone	Massive calcimudstone				
Corcal	C3	660	36.31	Limestone	Massive calcimudstone			5.15	-7.49
Corcal	C3	695	36.66	Limestone	Massive calcimudstone			4.29	-7.98
Corcal	C3	712	36.83	Limestone	Massive calcimudstone				
Corcal	C3	750	37.21	Limestone	Massive calcimudstone			5.24	-7.27
Corcal	C3	814	37.85	Limestone	Massive calcimudstone			3.74	-7.32
Corcal	C3	864	38.35	Limestone	Massive calcimudstone	X		5.16	-6.92
Corcal	C3	894	38.65	Limestone	Massive calcimudstone			4.56	-7.78
Corcal	C3	916	38.87	Limestone	Massive calcimudstone				
Corcal	C3	926	38.97	Limestone	Massive calcimudstone			4.35	-7.24
Corcal	C3	1004	39.75	Limestone	Massive calcimudstone			5.16	-6.57
Corcal	C3	1024	39.95	Limestone	Massive calcimudstone				
Corcal	C3	1034	40.05	Limestone	Massive calcimudstone				
Corcal	C3	1054	40.25	Limestone	Massive calcimudstone			5.10	-5.87
Corcal	C3	1074	40.45	Limestone	Massive calcimudstone				
Corcal	C3	1090	40.61	Limestone	Massive calcimudstone			5.26	-6.93

Corcal	C3	1120	40.91	Limestone	Packstone			4.75	-6.66
Corcal	C3	1150	41.21	Limestone	Packstone			5.39	-6.78
Corcal	C3	1180	41.51	Limestone	Packstone				
Corcal	C3	1200	41.71	Limestone	Massive calcimudstone	X		5.05	-6.17
Corcal	C3	1210	41.81	Limestone	Massive calcimudstone				
Corcal	C3	1235	42.06	Limestone	Massive calcimudstone			5.30	-5.47
Corcal	C3	1263	42.34	Limestone	Massive calcimudstone			5.00	-6.82
Corcal	C3	1285	42.56	Limestone	Massive calcimudstone				
Corcal	C3	1305	42.76	Limestone	Massive calcimudstone			4.73	-7.47
Corcal	C3	1340	43.11	Limestone	Packstone			5.08	-5.25
Corcal	MP	MP 1652	43.41	Limestone	Packstone	X		4.91	-7.64
Corcal	C3	1375	43.46	Limestone	Packstone				
Corcal	C3	1405	43.76	Limestone	Packstone			4.98	-7.86
Corcal	C3	1435	44.06	Limestone	Packstone			5.68	-7.44
Corcal	C3	1460	44.31	Limestone	Packstone				
Corcal	C3	1480	44.51	Limestone	Packstone			5.49	-7.79
Corcal	C3	1512	44.83	Limestone	Massive calcimudstone			5.28	-9.08
Corcal	C3	1545	45.26	Limestone	Packstone			5.05	-7.96
Corcal	C3	1575	45.46	Limestone	Packstone				
Corcal	C3	1605	45.76	Limestone	Packstone			5.63	-7.09
Corcal	C3	1650	46.50	Limestone	Massive calcimudstone			4.94	-7.78
Corcal	C3	1685	46.56	Limestone	Massive calcimudstone				
Corcal	C3	1700	46.71	Limestone	Massive calcimudstone			5.37	-7.57
Corcal	C3	1715	46.86	Limestone	Massive calcimudstone				
Corcal	C3	1735	47.06	Limestone	Massive calcimudstone			5.67	-6.87
Corcal	MP	MP 2130	47.20	Limestone	Massive calcimudstone	X			
Corcal	C3	1755	47.26	Limestone	Massive calcimudstone				
Corcal	C3	1765	47.36	Limestone	Massive calcimudstone			5.09	-7.38
Corcal	C3	1795	47.66	Limestone	Packstone			5.43	-7.47
Corcal	C3	1815	47.86	Limestone	Packstone			5.07	-6.56
Corcal	C3	1830	48.01	Limestone	Packstone				

Corcal	C3	1838	48.09	Claystone	Volcanic tuff (?)				
Corcal	C3	1842	48.13	Limestone	Packstone	X	X	5.67	-7.54
Corcal	C3	1860	48.31	Limestone	Packstone			5.32	-6.86
Corcal	C3	1890	48.61	Limestone	Packstone			5.48	-6.68
Corcal	C3	1915	48.86	Limestone	Packstone				
Corcal	C3	1925	48.96	Limestone	Packstone			4.88	-8.06
Corcal	C3	1955	49.26	Limestone	Packstone				
Corcal	C3	1995	49.66	Limestone	Intraclastic breccia			5.00	-8.14
Corcal	MP	MP 1654	49.86	Limestone	Intraclastic packstone	X		4.12	-9.60
Corcal	C3	2021	49.92	Limestone	Packstone				
Corcal	C3	2030	50.01	Limestone	Packstone			4.87	-8.85
Corcal	C3	2035	50.06	Limestone	Packstone				
Corcal	C3	2045	50.16	Limestone	Packstone			5.25	-8.57
Corcal	C3	2060	50.31	Limestone	Packstone				
Corcal	C3	2080	50.51	Limestone	Packstone			4.92	-8.83
Corcal	C3	2087	50.58	Claystone	Volcanic tuff (?)				
Corcal	C3	2100	50.71	Limestone	Packstone			5.36	-8.39
Corcal	C3	2115	50.86	Limestone	Packstone				
Corcal	C3	2135	51.06	Limestone	Packstone			4.90	-8.93
Corcal	C3	2180	51.51	Limestone	Packstone			5.21	-8.74
Corcal	C3	2210	51.81	Limestone	Packstone			3.40	-9.08
Corcal	C3	2235	52.06	Limestone	Packstone			4.71	-9.85
Corcal	C3	2250	52.21	Limestone	Packstone			3.51	-9.00
Corcal	C3	2285	52.56	Limestone	Grainstone			4.48	-9.10
Corcal	MP	MP 2131	52.90	Limestone	Grainstone	X			
Corcal	C3	2325	52.96	Limestone	Grainstone			5.20	-9.02
Corcal	C3	2363	53.34	Limestone	Packstone			4.74	-9.19
Corcal	C3	2370	53.41	Limestone	Packstone			3.50	-10.47
Corcal	MP	MP 2132	53.90	Limestone	Packstone	X			
Corcal	C3	2460	54.31	Limestone	Grainstone	X		2.83	-9.79

Total Samples		198	
Total Samples from this study		168	
Total samples MP		30	
Total isotope samples			116
Total thin sections			40

Table B: Laginha samples data

Laginha	L1	-450	-4.50	Dolostone	Dolomitic grainstone			1.53	-9.66
Laginha	L1	-200	-2.00	Dolostone	Sandstone with dolomitic matrix			2.57	-7.70
Laginha	L1	0	-0.50	Dolostone	Peloidal packstone	X	X	3.14	-7.90
Laginha	L1	0	0.00	Breccia	Polymictic breccia with basement clasts				
Laginha	L2	15	4.90	Sandstone	Argillaceous sandstone				
Laginha	MP	MP 2151	15 to 20 m	Limestone	Calcimudstone microbreccia	X			
Laginha	MP	MP 2152	15 to 20 m	Limestone	Massive calcimudstone	X			
Laginha	MP	MP 2153	15 to 20 m	Limestone	Calcimudstone microbreccia	X			
Laginha	MP	MP 2154	15 to 20 m	Limestone	Massive calcimudstone	X			
Laginha	MP	MP 2155	15 to 20 m	Dolostone	Dolomitic sparstone	X			
Laginha	MP	MP 2156	15 to 20 m	Dolostone	Dolomitic sparstone	X			
Laginha	MP	MP 2157	15 to 20 m	Dolostone	Dolomitic sparstone	X			
Laginha	MP	MP 2158	15 to 20 m	Limestone	Calcimudstone desiccation breccia	X			
Laginha	MP	MP 2159	15 to 20 m	Dolostone	Dolomitic sparstone	X			
Laginha	MP	MP 2160	15 to 20 m	Dolostone	Dolomitic sparstone	X			
Laginha	MP	MP 2161	15 to 20 m	Limestone	Calcimudstone desiccation breccia	X			
Laginha	L2	100	16.20	Dolostone	Dolomitic calcimudstone			0.79	-7.51
Laginha	L2	350	17.70	Dolostone	Dolomitic sparstone			0.06	-8.86
Laginha	L2	250	18.70	Dolostone	Dolomitic sparstone	X		-0.13	-7.68
Laginha	L3	15	20.15	Dolostone	Extraclastic wackestone			-3.03	-2.12
Laginha	L3	39	20.39	Limestone	Grainstone			-1.64	-8.46
Laginha	L3	64	20.64	Dolostone	Dolomitic grainstone			-2.69	-4.12
Laginha	L3	81	20.81	Dolostone	Dolomitic grainstone				
Laginha	L3	85	20.85	Dolostone	Extraclastic wackestone	X		-0.03	-9.38

Laginha	L3	110	21.10	Dolostone	Dolomitic grainstone				
Laginha	L3	150	21.50	Dolostone	Extraclastic wackestone			-3.01	-3.17
Laginha	L3	235	22.35	Dolostone	Dolomitic grainstone			-2.14	-10.09
Laginha	L3	235.9	22.36	Dolostone	Dolomitic calcimudstone			-2.23	-8.48
Laginha	L3	245	22.45	Dolostone	Dolomitic calcimudstone				
Laginha	L3	260	22.60	Dolostone	Dolomitic grainstone			-1.73	-7.86
Laginha	L3	275	22.75	Brecha	Intraclastic breccia	X			
Laginha	L3	285	22.85	Limestone	Grainstone			-2.28	-9.06
Laginha	L3	310	23.10	Dol/Limestone	Laminated carbonate	X	X	-2.25	-5.52
Laginha	L3	326	23.26	Dolostone	Dolomitic grainstone				
Laginha	L3	350	23.50	Dolostone	Dolomitic grainstone			-1.99	-5.18
Laginha	L3	370	23.70	Dolostone	Dolomitic grainstone				
Laginha	L3	395	23.95	Limestone	Grainstone				
Laginha	L3	420	24.20	Limestone	Grainstone			-1.64	-3.67
Laginha	L3	460	24.60	Limestone	Grainstone			-1.10	-5.70
Laginha	L3	460.9	24.61	Dolostone	Dolomitic grainstone			-1.66	-3.60
Laginha	L3	490	24.90	Limestone	Grainstone			-0.62	-4.71
Laginha	L3	500	25.00	Marl	Dolomitic marl			-2.97	-6.63
Laginha	L3	515	25.15	Limestone	Grainstone			-1.29	-6.43
Laginha	L3	530	25.30	Marl	Dolomitic marl			-1.25	-4.10
Laginha	L3	555	25.55	Limestone	Grainstone			-1.14	-4.14
Laginha	L3	574	25.74	Marl	Dolomitic marl				
Laginha	L3	590	26.10	Limestone	Grainstone			0.17	-8.82
Laginha	L3	645	26.45	Breccia	Polymictic breccia	X	X		
Laginha	L3	735	27.35	Limestone	Calcimudstone with desiccation structures	X		0.13	-6.17
Laginha	L3	1075	30.75	Limestone	Calcimudstone with desiccation structures	X	X	1.92	-5.69
Laginha	L3	1150	31.50	Limestone	Grainstone			-2.74	-6.25
Laginha	L3	1250	32.50	Limestone	Grainstone			-0.72	-9.28
Laginha	L3	1320	33.15	Limestone	Grainstone			-0.79	-6.27
Laginha	L3	1380	33.60	Limestone	Packstone	X	X	-1.27	-6.21
Laginha	L3	1440	34.30	Limestone	Grainstone			-1.51	-7.87
Laginha	L3	1490	34.80	Limestone	Grainstone			-2.14	-5.74
Laginha	L3	1540	35.15	Limestone	Grainstone			-1.34	-9.72

Laginha	L3	1590	35.60	Limestone	Grainstone			-0.85	-6.80
Laginha	L3	1640	36.05	Limestone	Grainstone			-0.61	-4.95
Laginha	L3	1690	36.55	Limestone	Grainstone			-0.33	-4.85
Laginha	L3	1715	36.85	Limestone	Grainstone				
Laginha	L3	1750	37.20	Limestone	Grainstone			-0.39	-6.68
Laginha	L3	1780	37.45	Limestone	Grainstone				
Laginha	L3	1805	37.65	Limestone	Grainstone			-3.11	-9.50
Laginha	L3	1840	38.10	Limestone	Grainstone			-0.55	-7.74
Laginha	L3	1875	38.45	Limestone	Grainstone				
Laginha	L3	1905	38.65	Limestone	Extraclastic wackestone	X		-2.33	-9.26
Laginha	L3	1925	38.95	Limestone	Grainstone				
Laginha	L3	1945	39.20	Limestone	Grainstone			-0.76	-7.45
Laginha	L3	1970	39.45	Limestone	Grainstone				
Laginha	L3	2000	39.85	Limestone	Grainstone			-0.72	-7.37
Laginha	MP	MP 1663	Lower section	Marl	Marl	X		4.21	-6.78
Laginha	MP	MP 1664	Lower section	Marl	Marl	X		3.81	-7.00
Laginha	MP	MP 1665	Lower section	Limestone	Marly packstone	X		3.86	-6.59
Laginha	MP	MP 1666	Lower section	Mudstone	Mudstone	X			
Laginha	MP	MP 1674	Upper section	Marl	Marl	X		4.92	-6.82
Laginha	MP	MP 1675	Upper section	Limestone	Marly packstone	X		4.59	-7.02
Laginha	MP	MP 1676	Upper section	Limestone	Marly packstone	X		2.06	-7.63
Laginha	MP	MP 1677	Upper section	Limestone	Grainstone	X			
Laginha	MP	MP1681	Upper section	Limestone	Grainstone			2.26	-7.09
Laginha	MP	MP 1682	Upper section	Limestone	Grainstone	X		2.36	-6.02
Laginha	MP	MP 1684	Upper section	Marl	Marl	X		2.48	-7.83
Laginha	MP	MP 1685	Upper section	Limestone	Grainstone	X		2.39	-8.36
Laginha	MP	MP 1686	Upper section	Marl	Marl	X			
Laginha	MP	MP 2162	Upper section	Limestone	Grainstone	X			
Laginha	MP	MP 2163	Upper section	Limestone	Grainstone	X			
Laginha	MP	MP 2164	Upper section	Limestone	Grainstone	X			

Total Samples	87		Total isotope samples	54
Total Samples from this study	60		Total thin sections	36
Total samples MP	27			

Corcal Thin Sections

C1 2.62

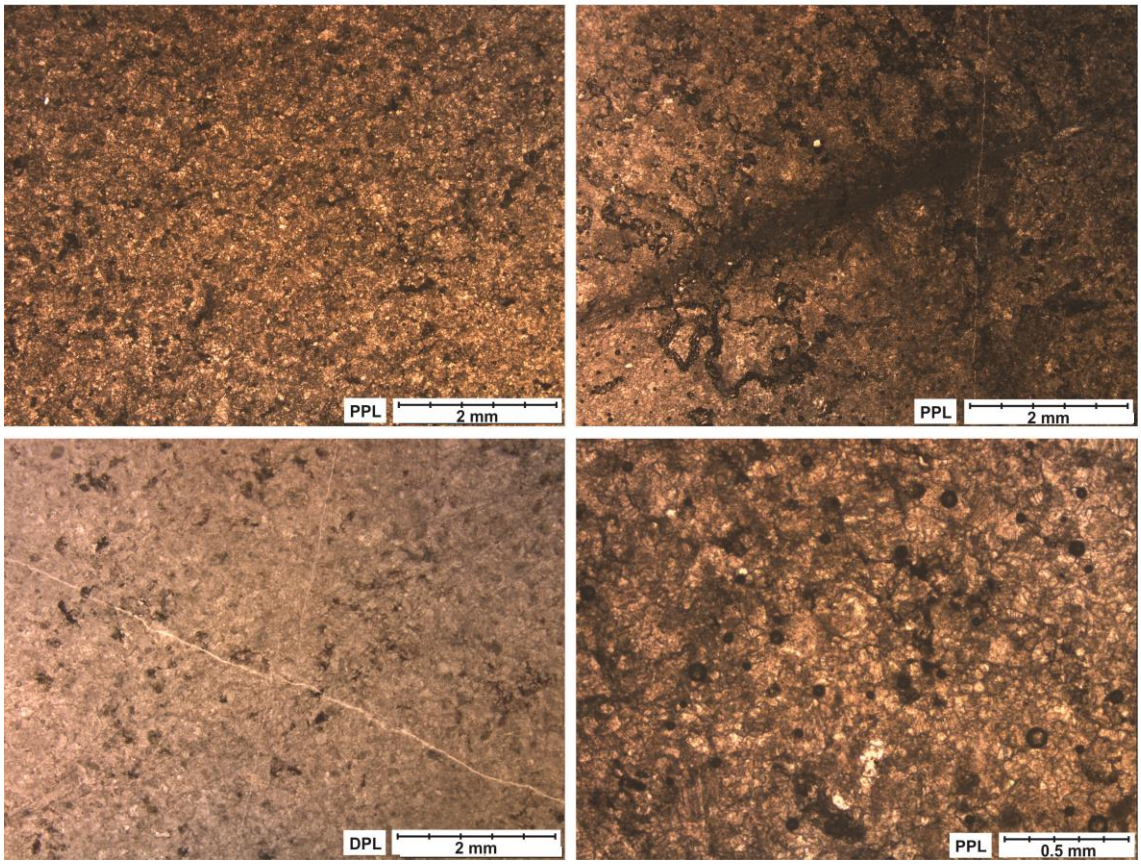

C1 6.50

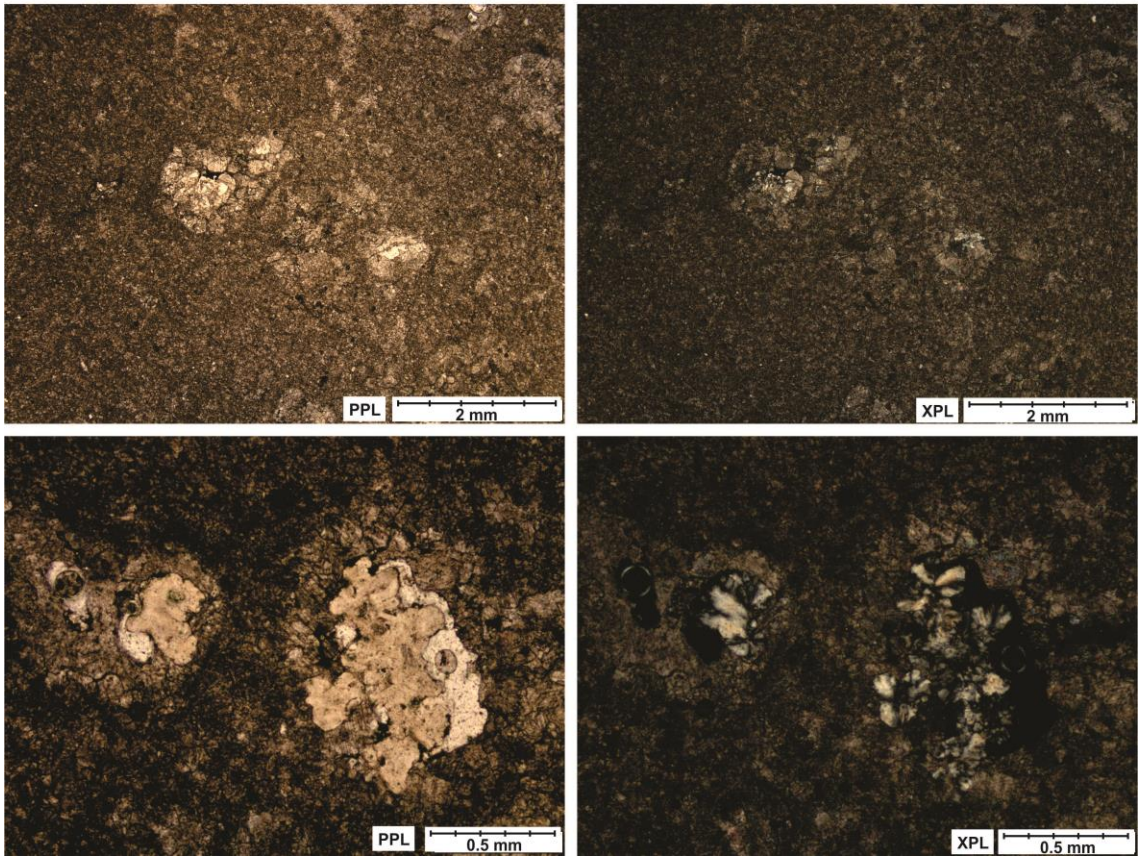

C2 9.40

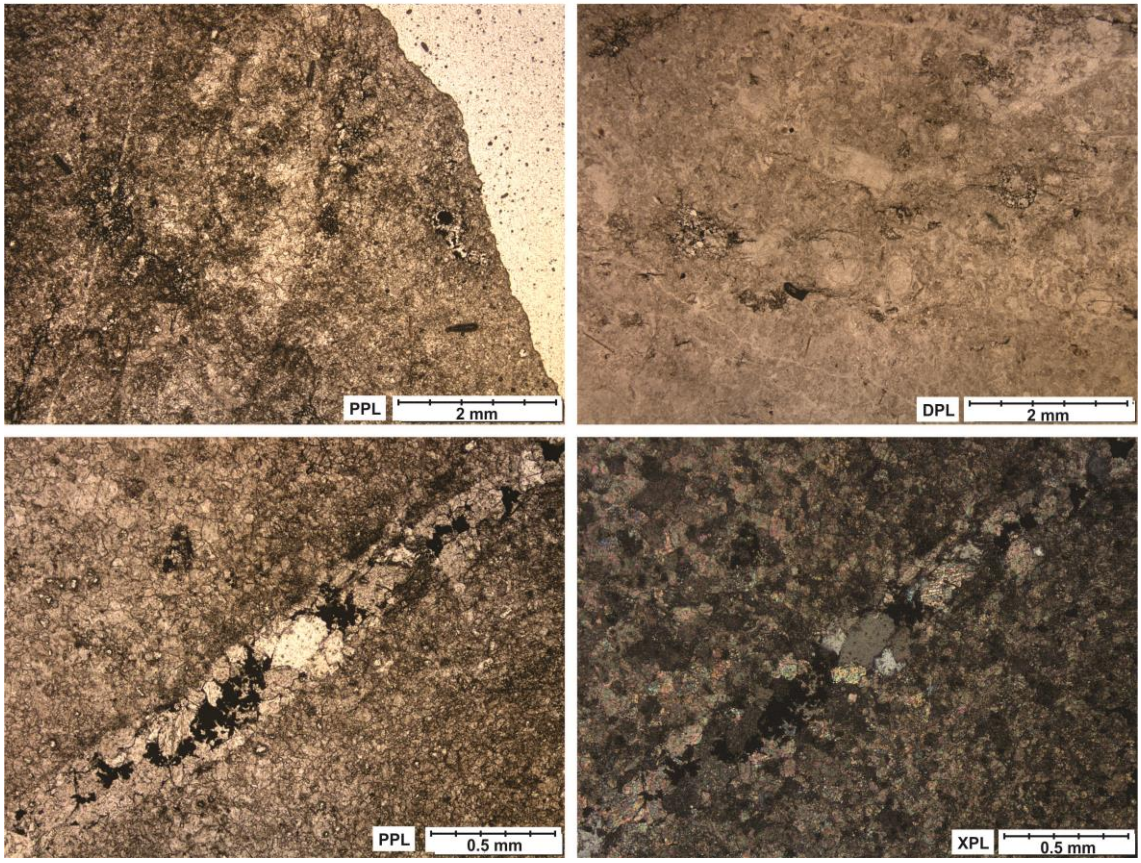

C2 10.40

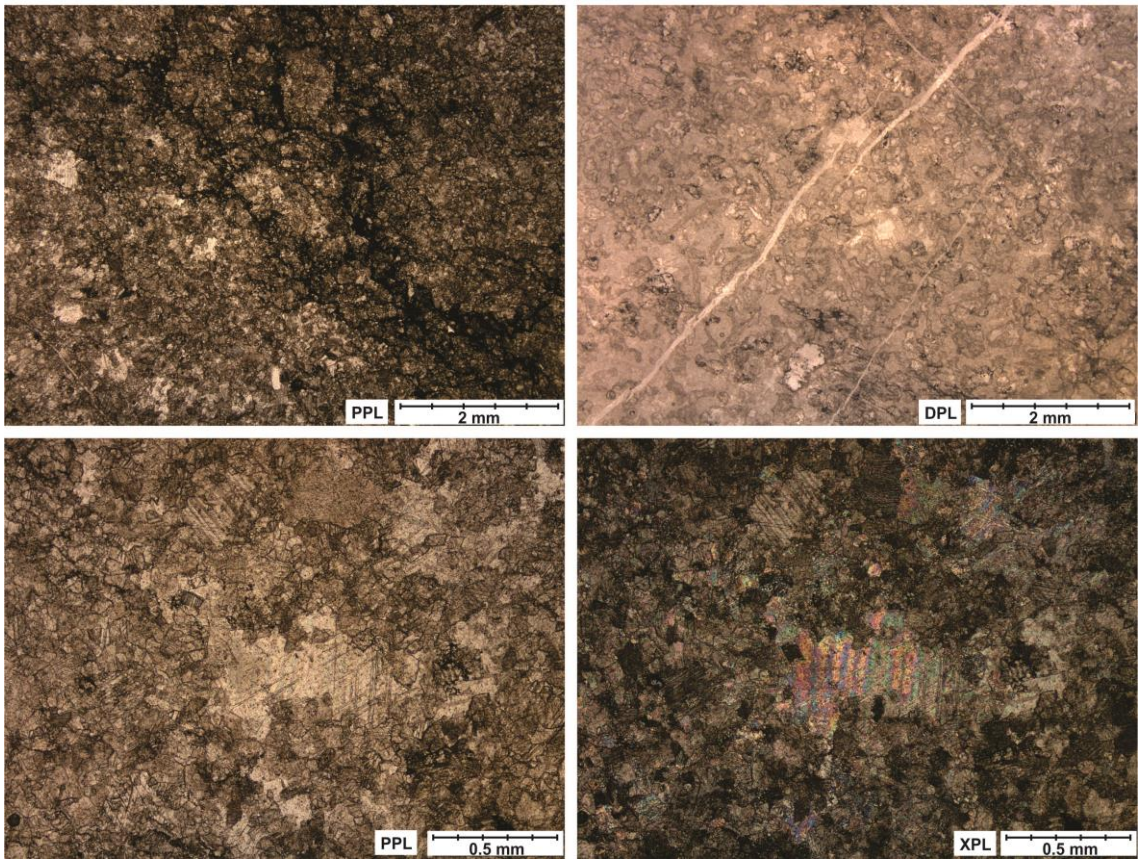

C2 12.55

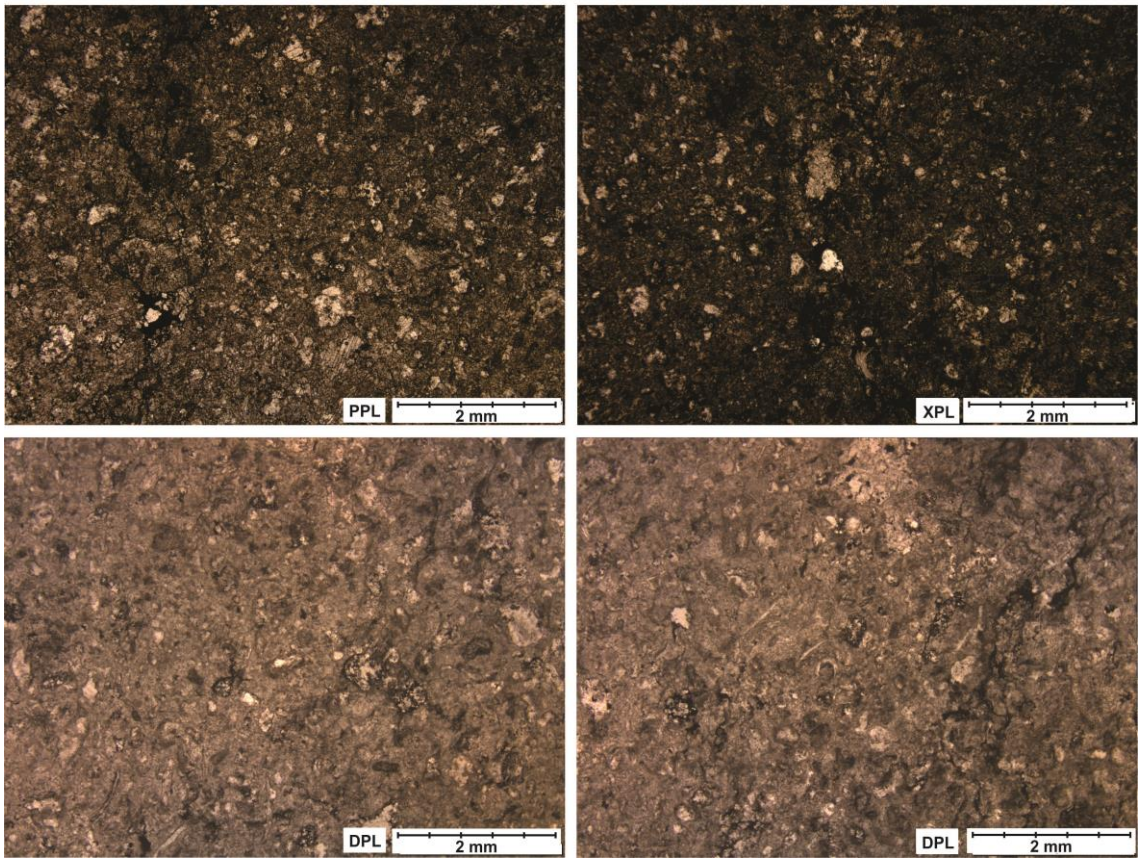

C3 2.55

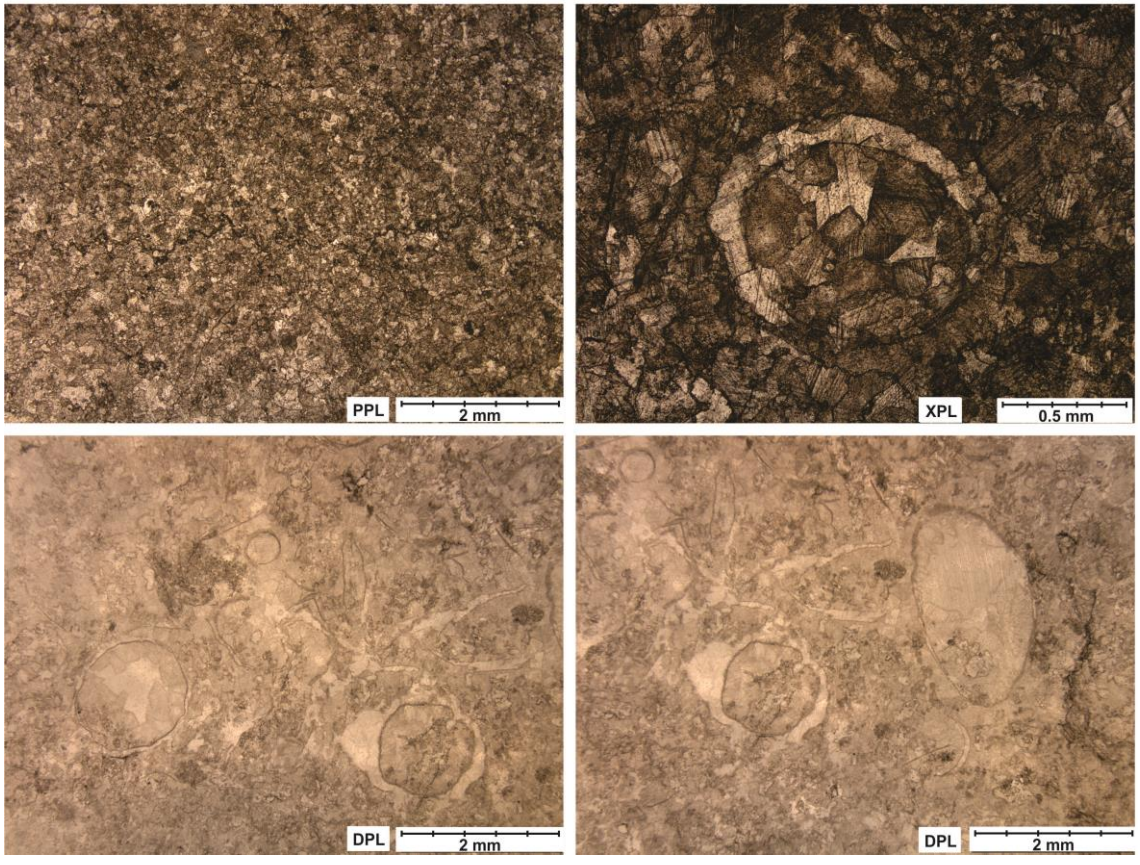

C3 8.64

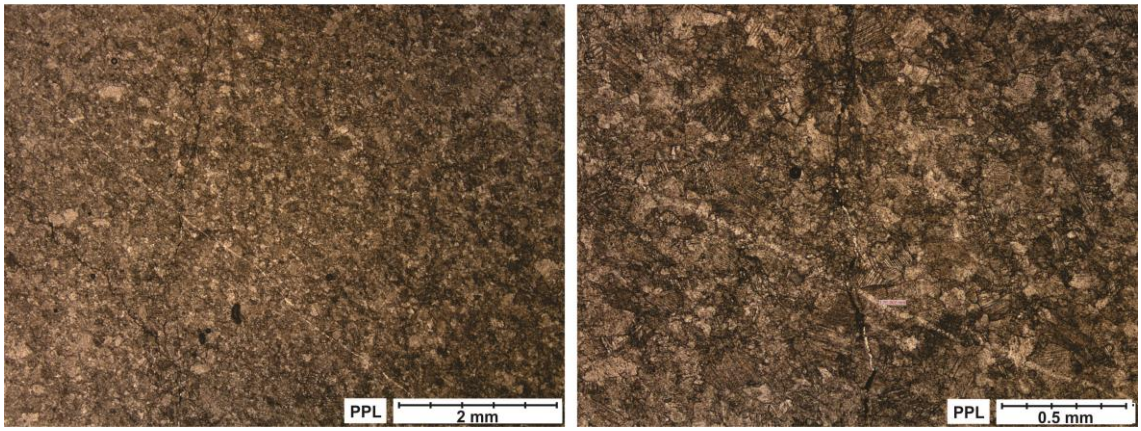

C3 12.00

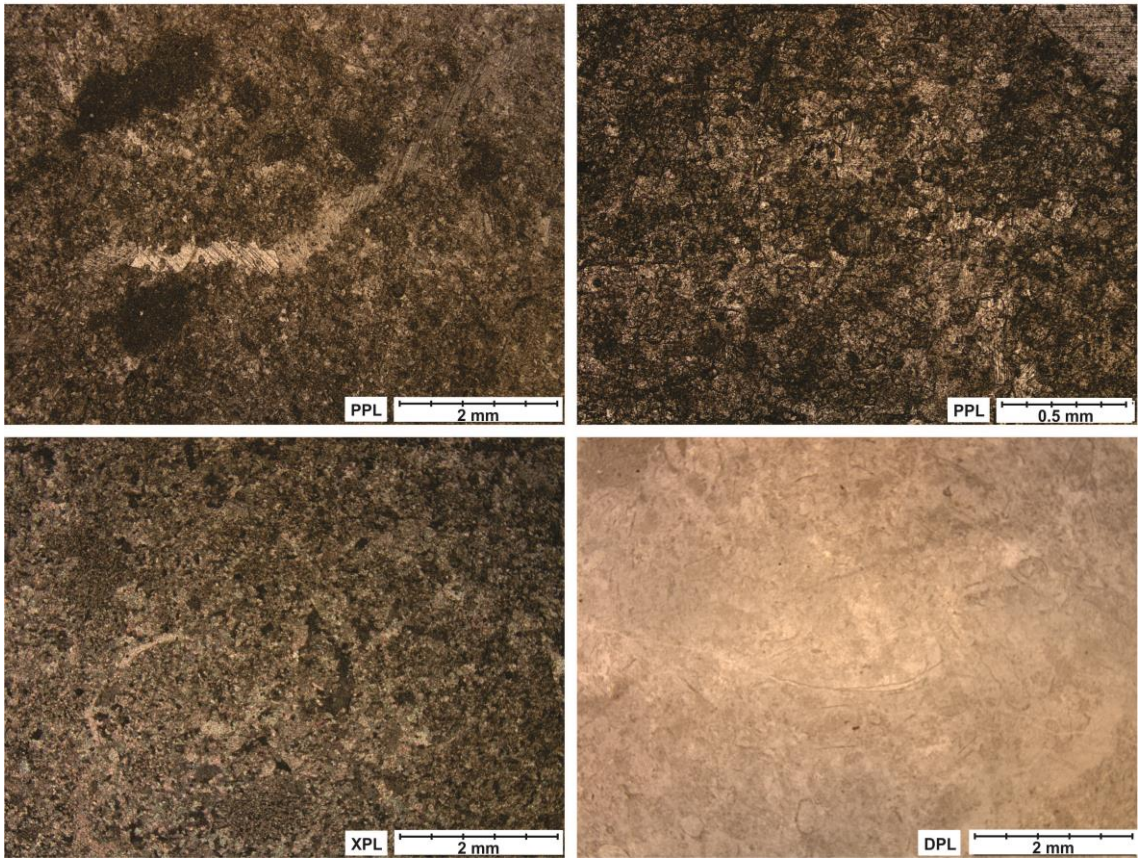

C3 18.42

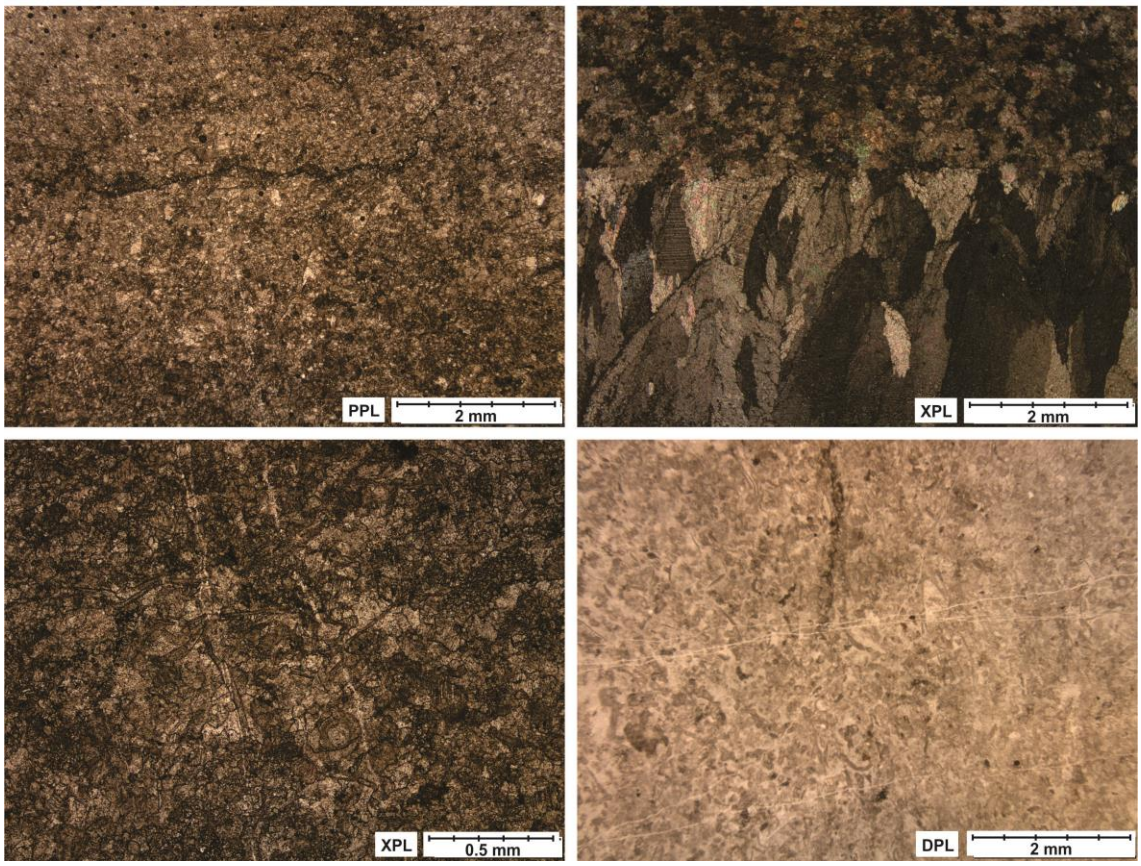

C3 24.60

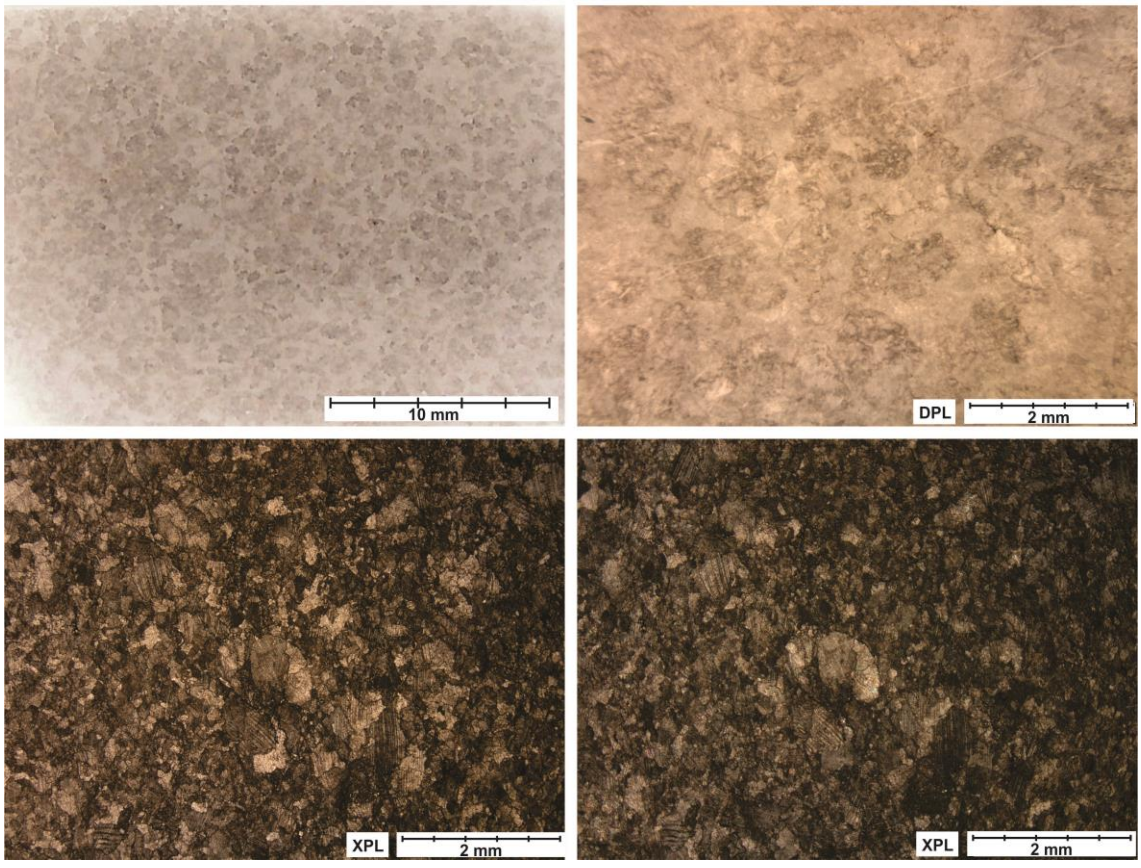

MP 2115

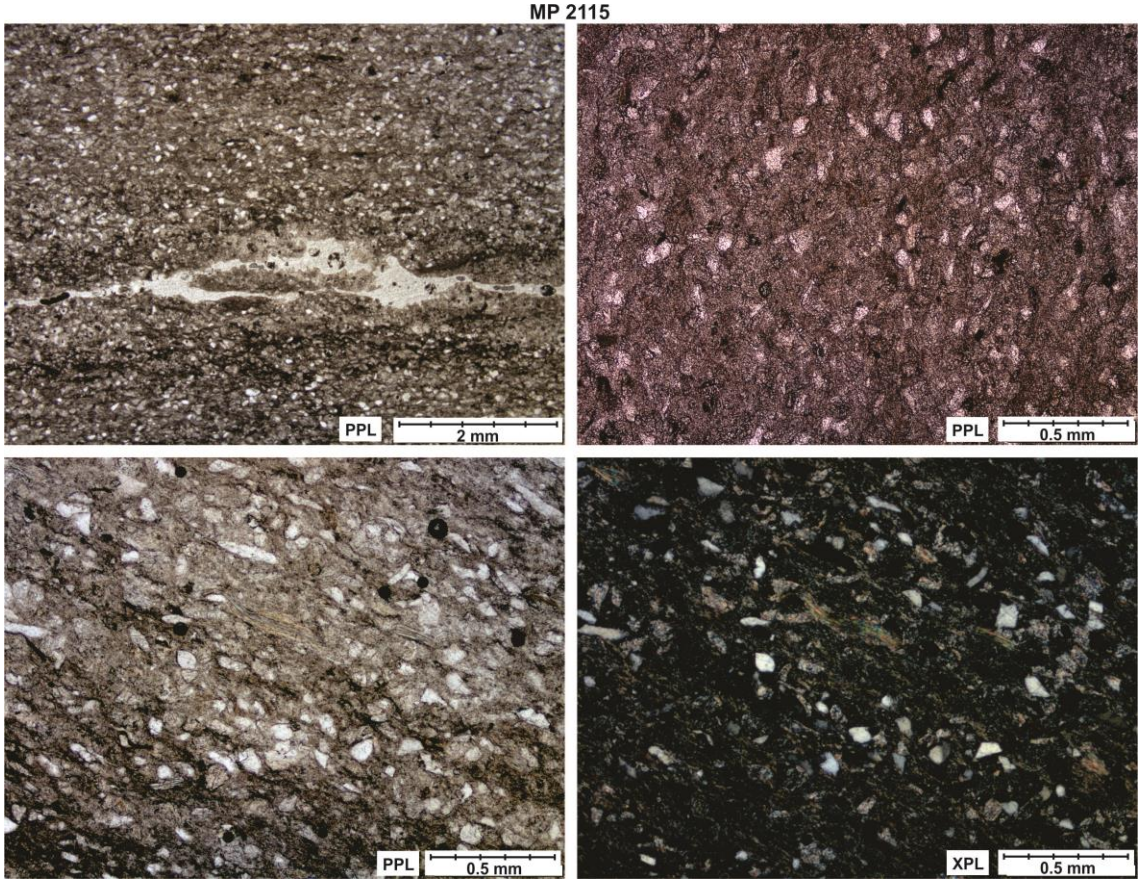

MP 2116

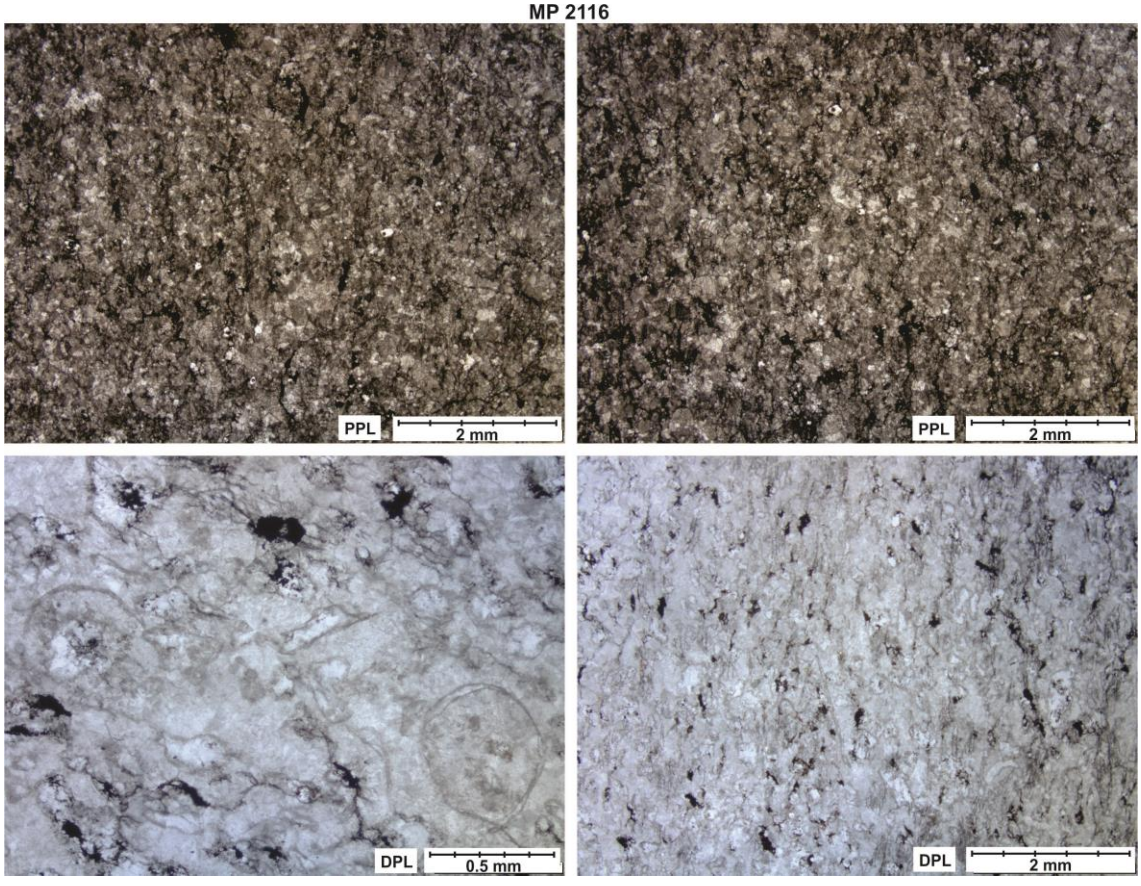

MP 2117

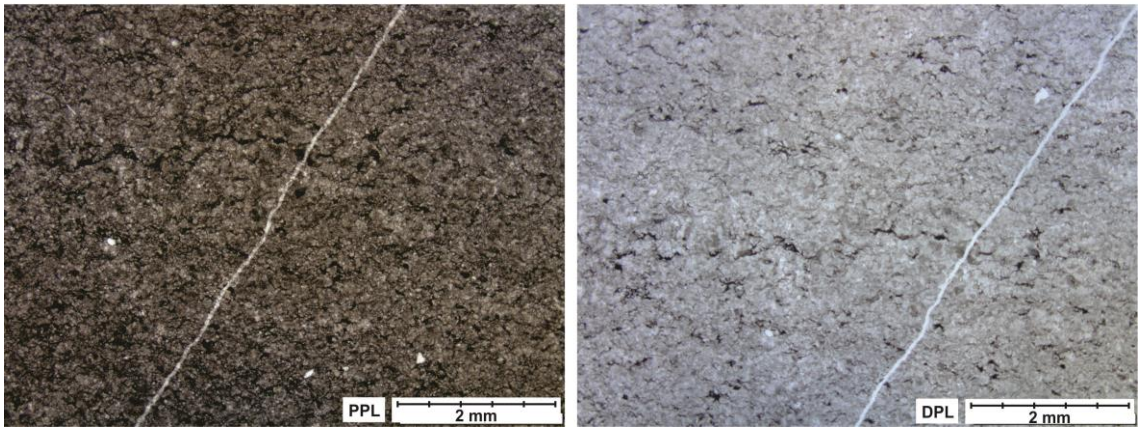

MP 2118

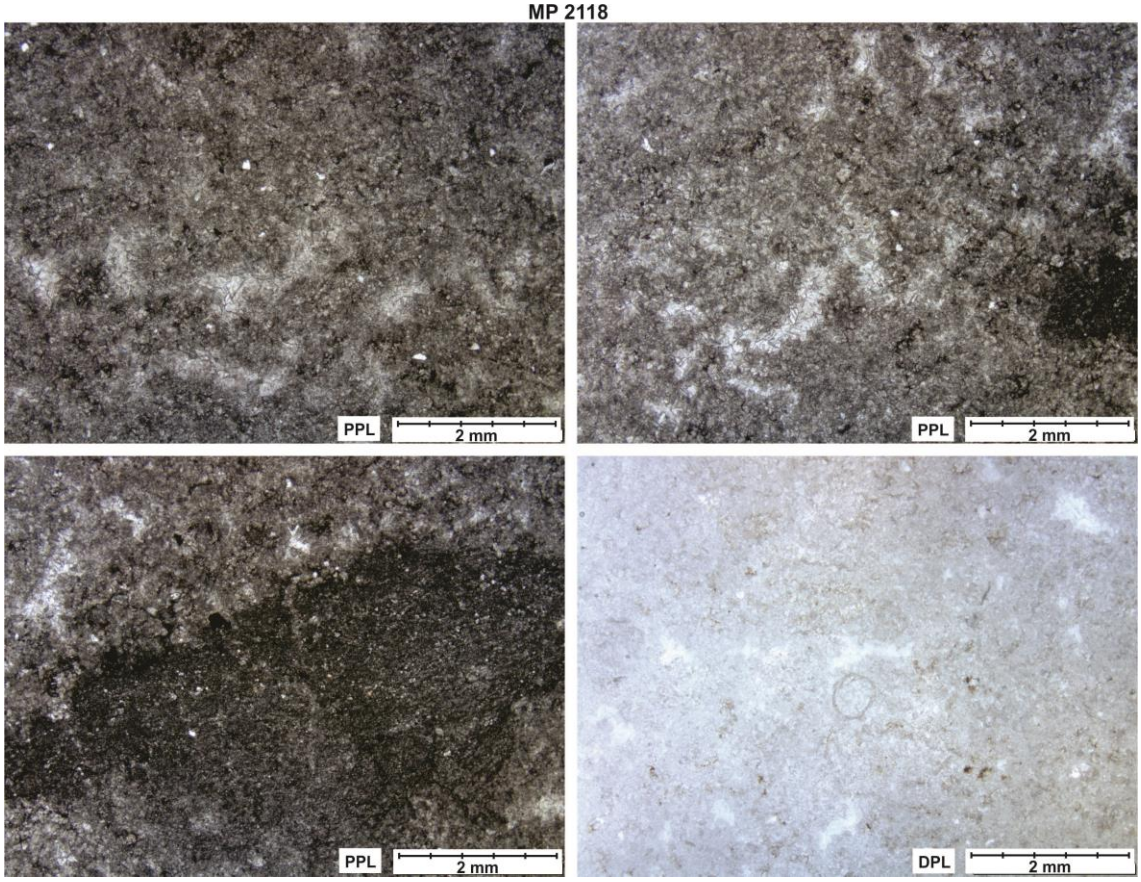

MP 2119

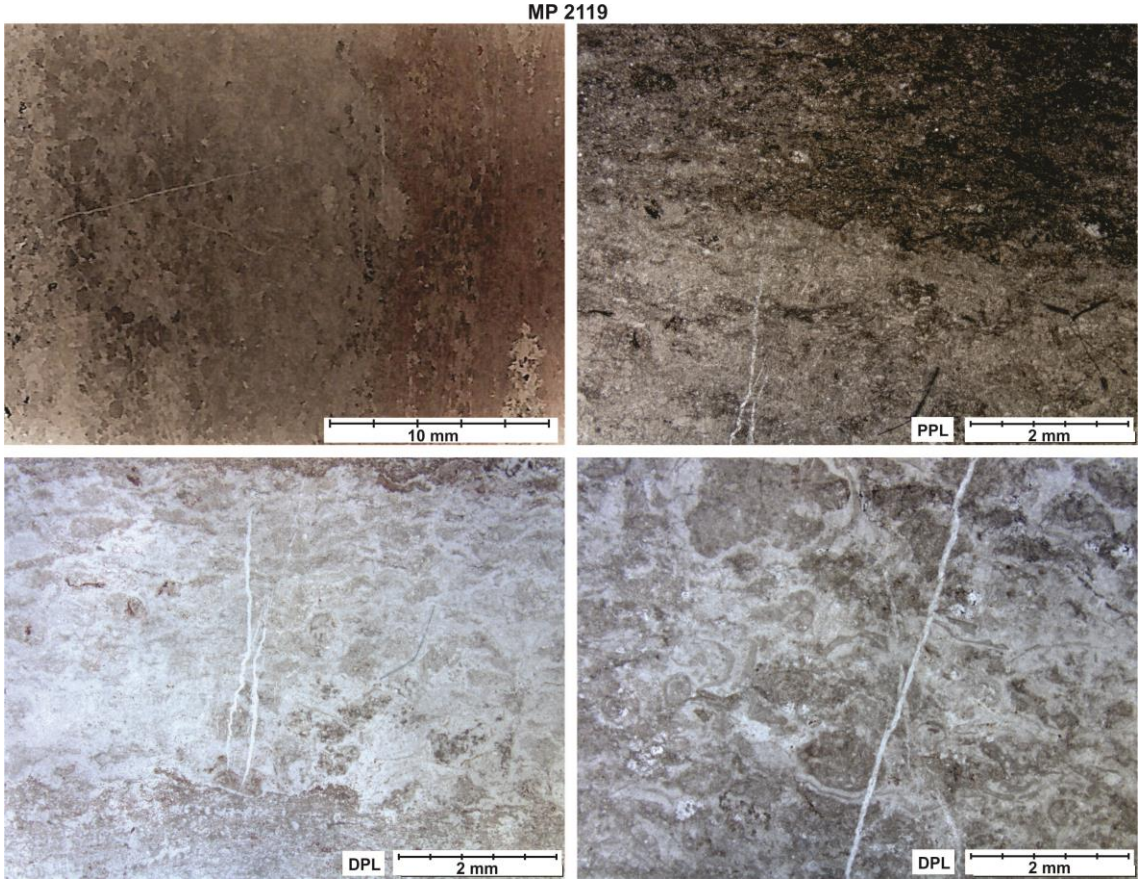

MP 2120

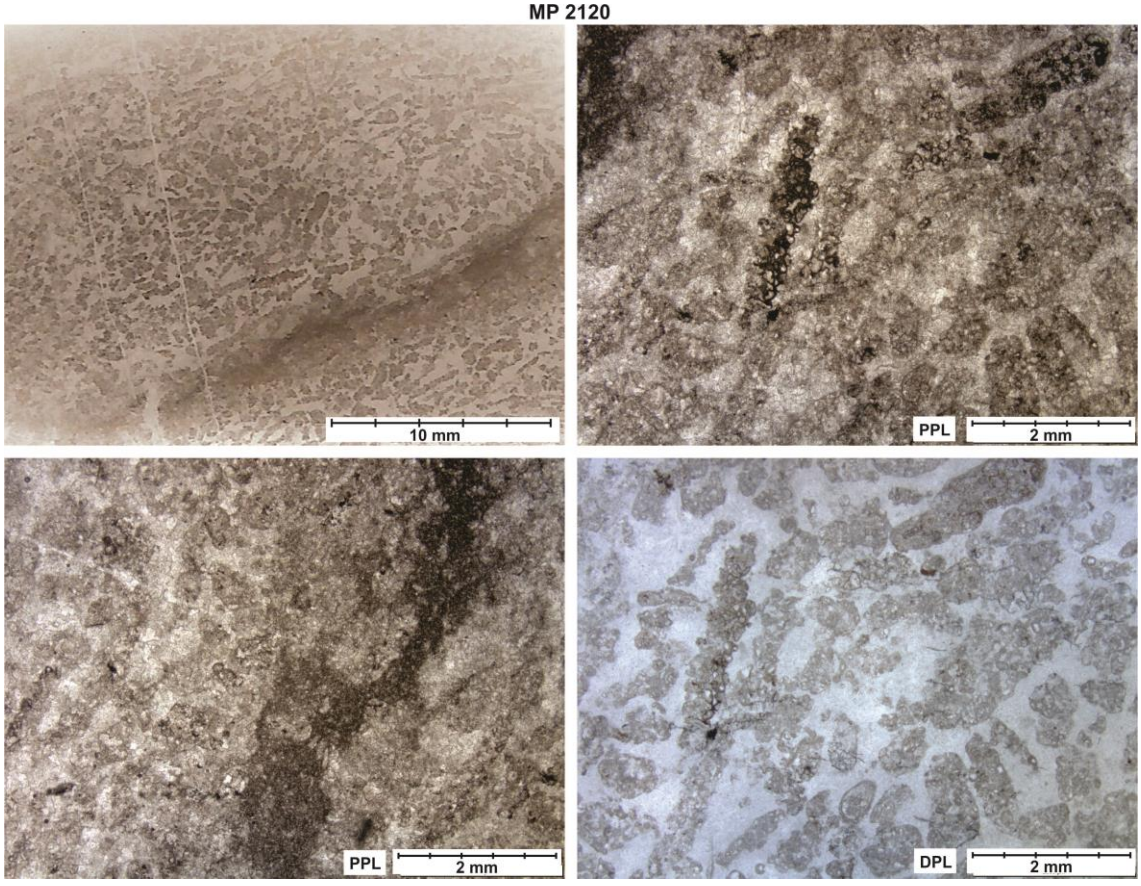

MP 2121

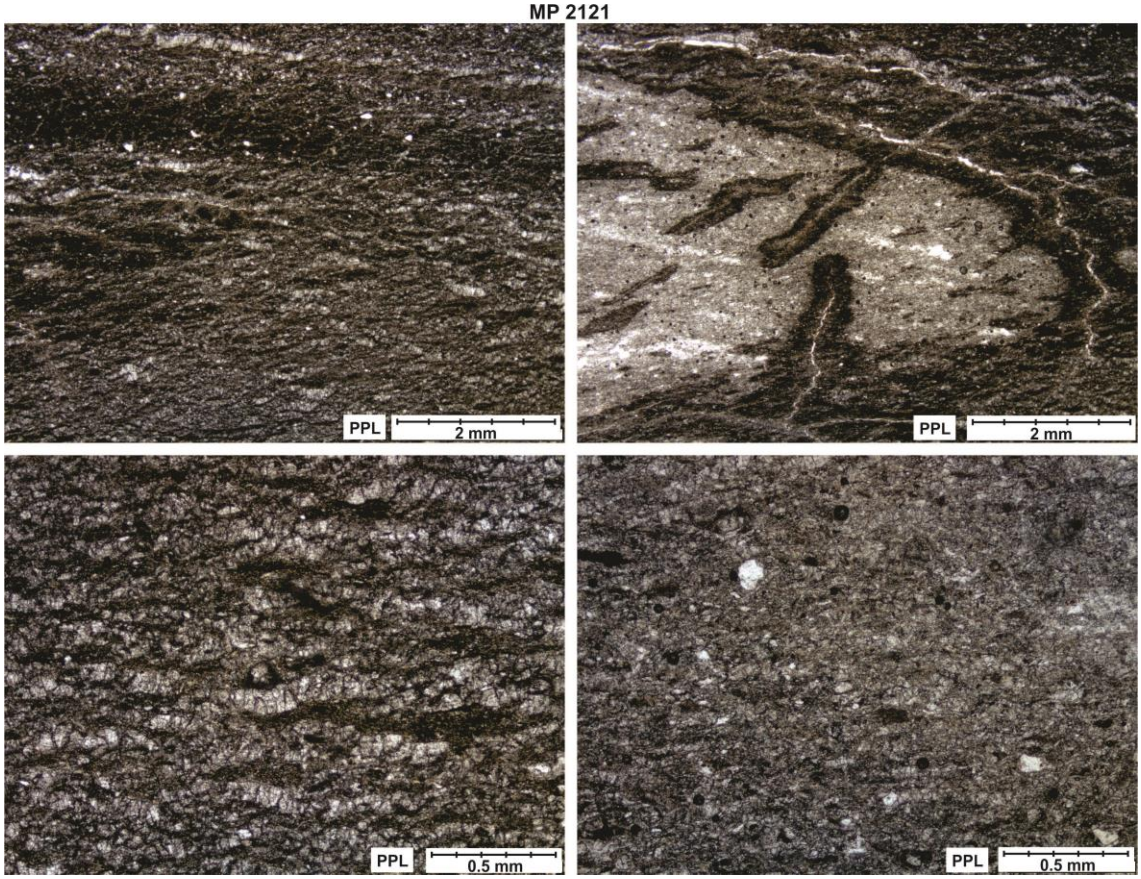

MP 2122

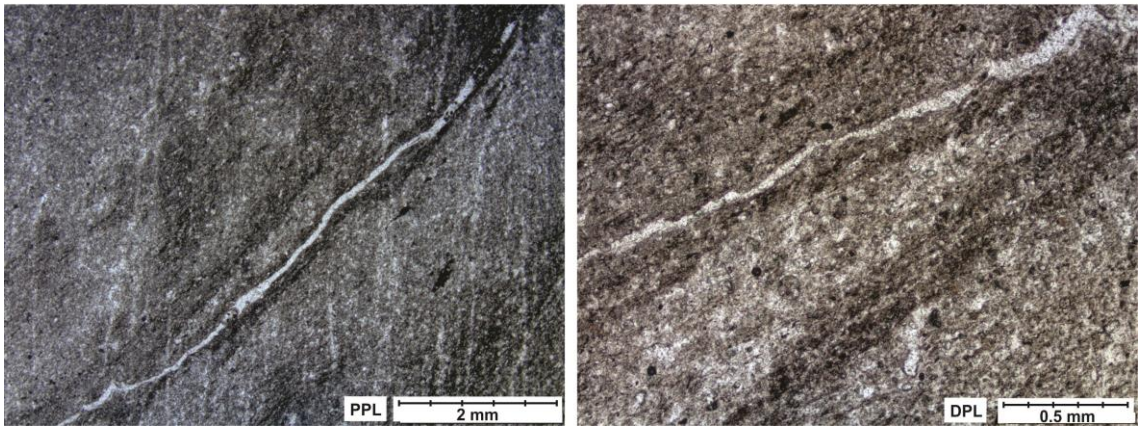

MP 2123

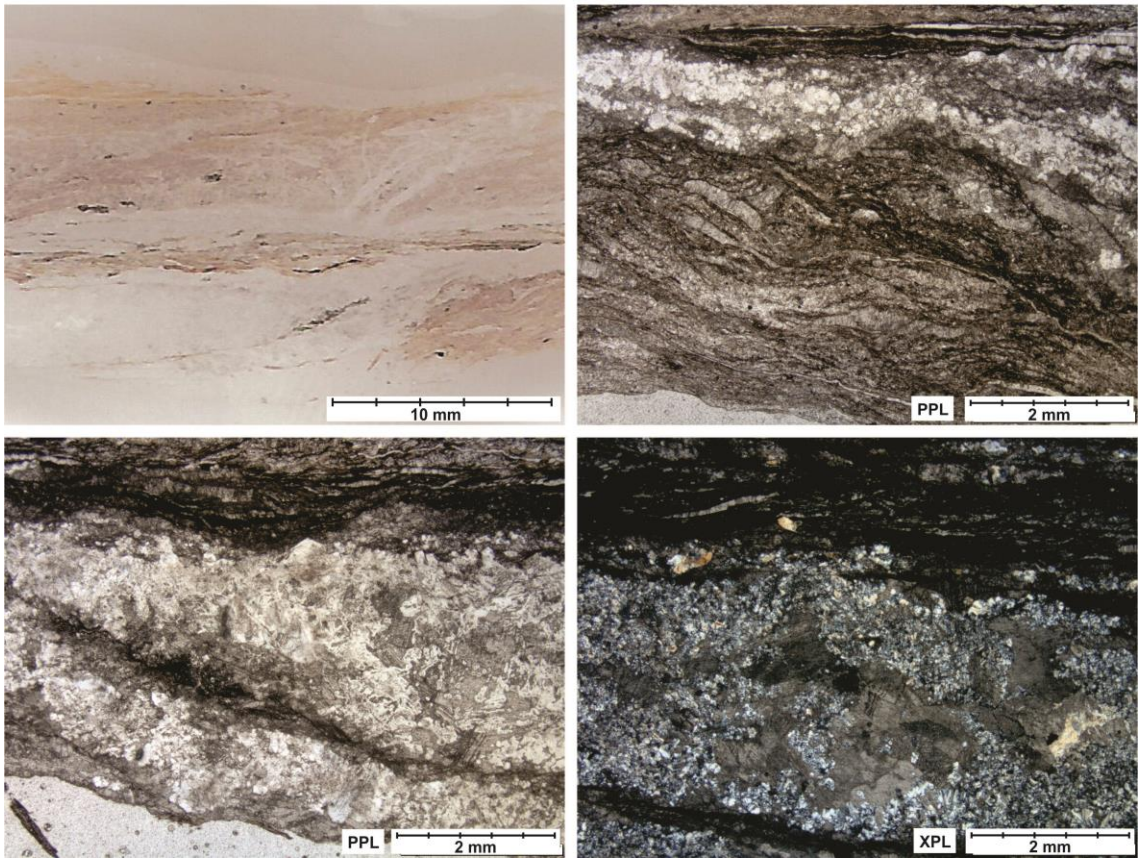

MP 2124

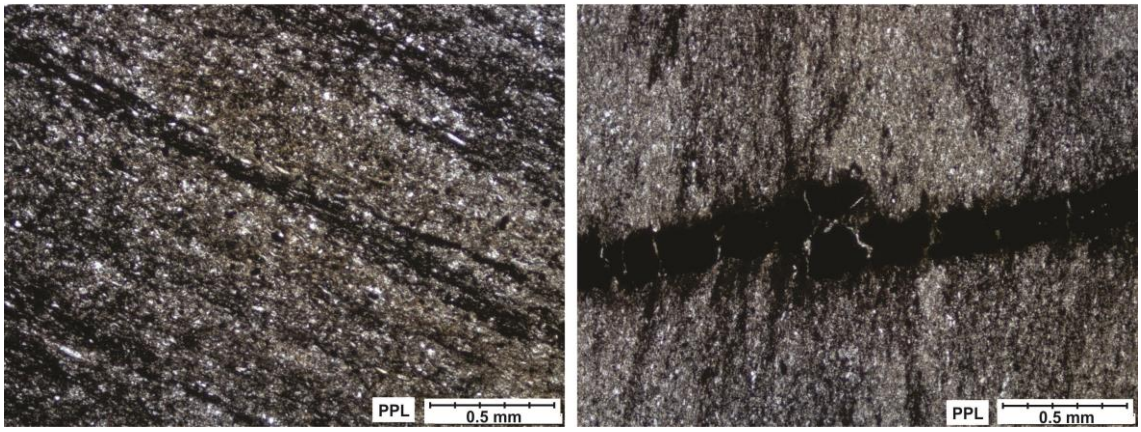

MP 2125

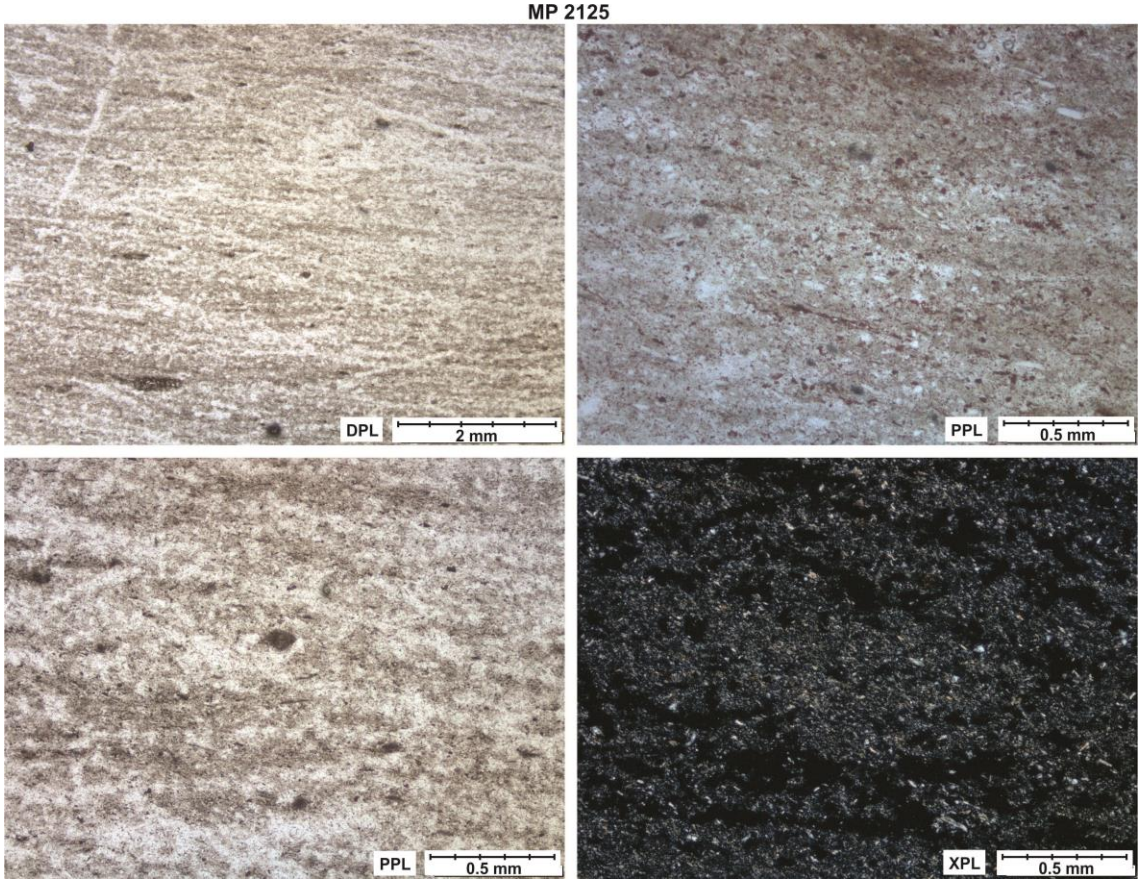

MP 2126

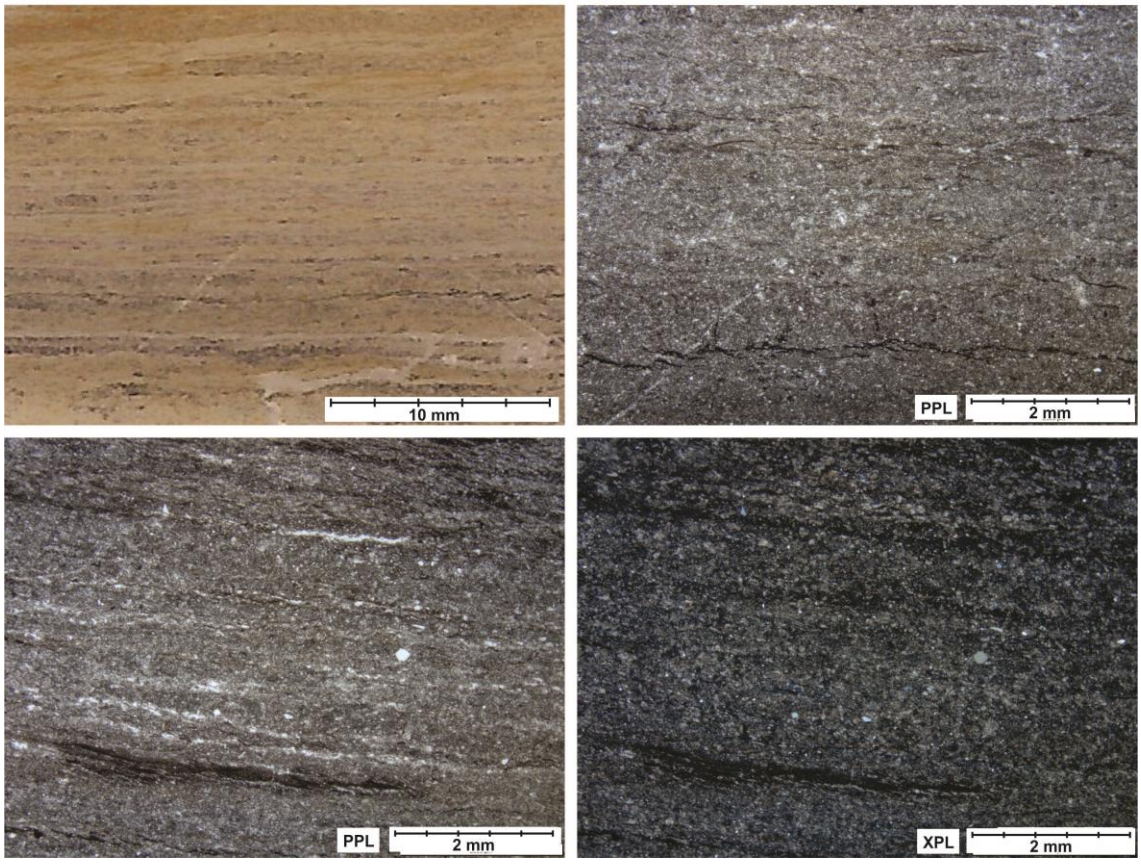

MP 2127

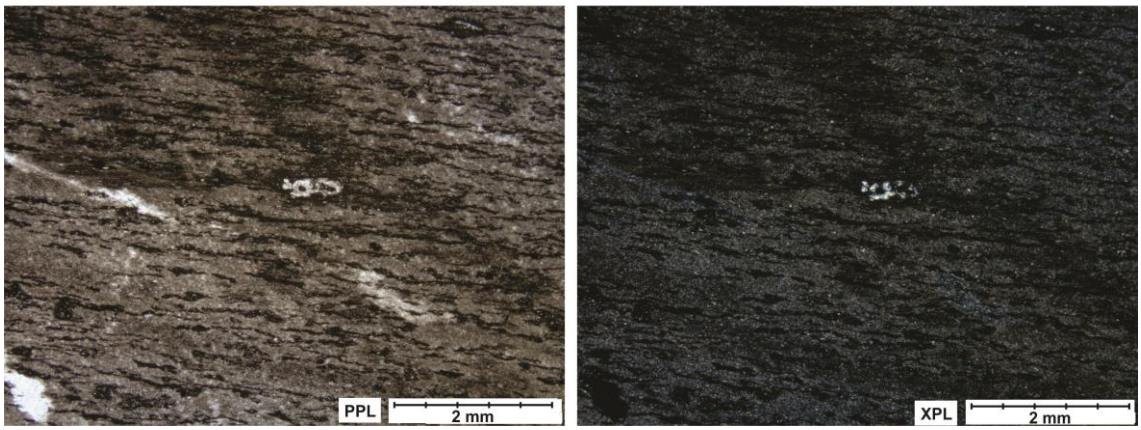

MP 2128

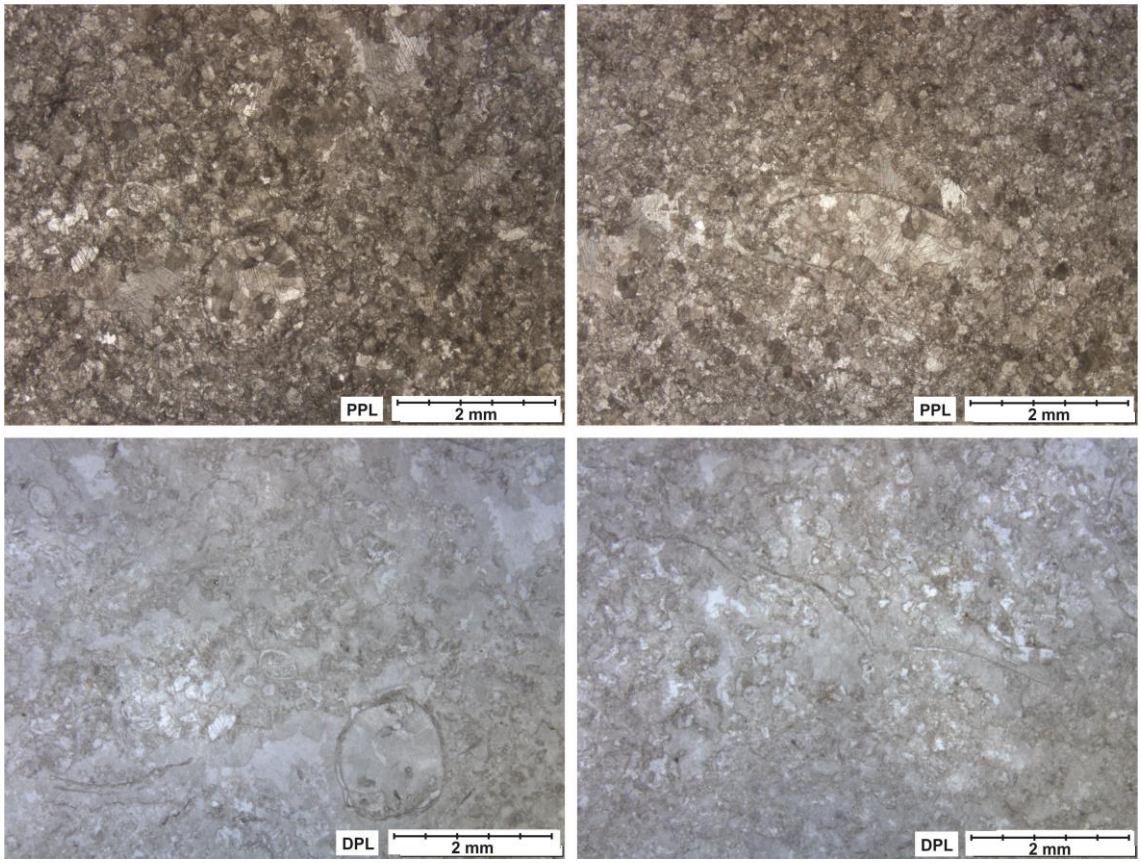

MP 2129

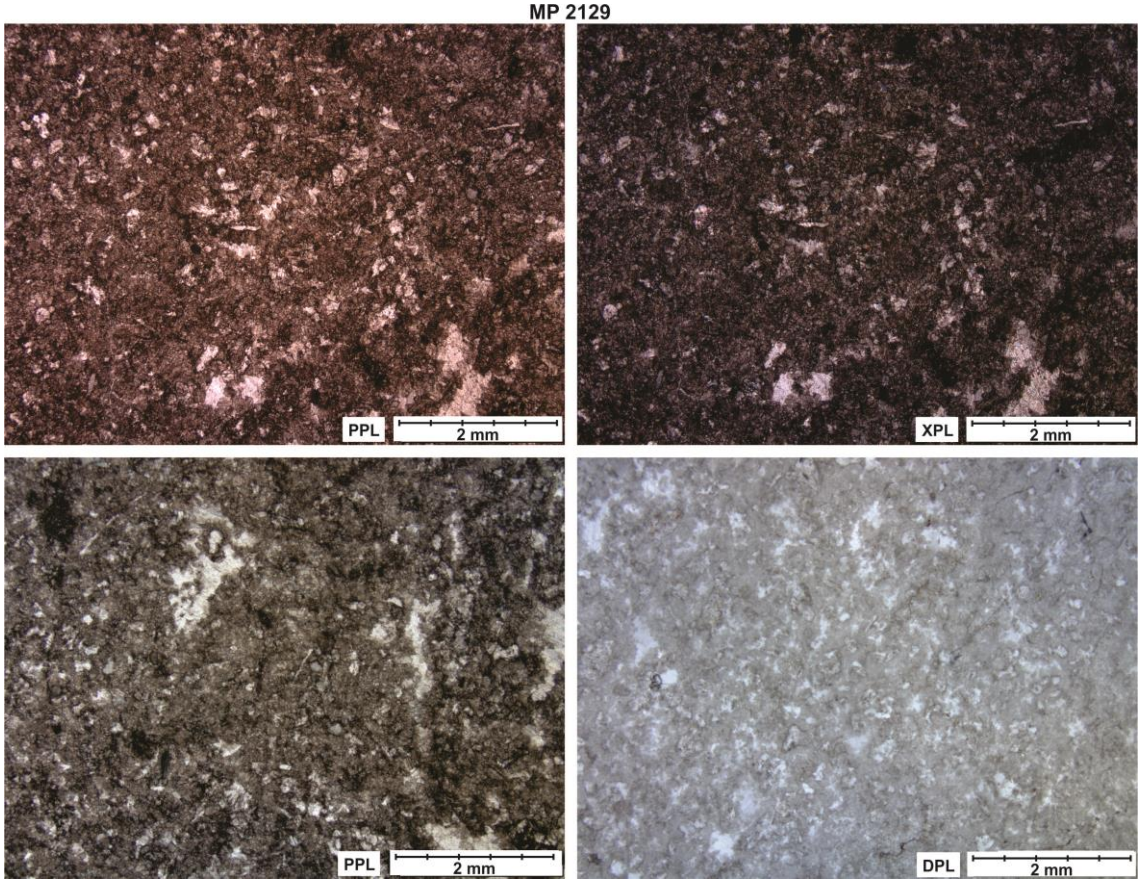

MP 2130

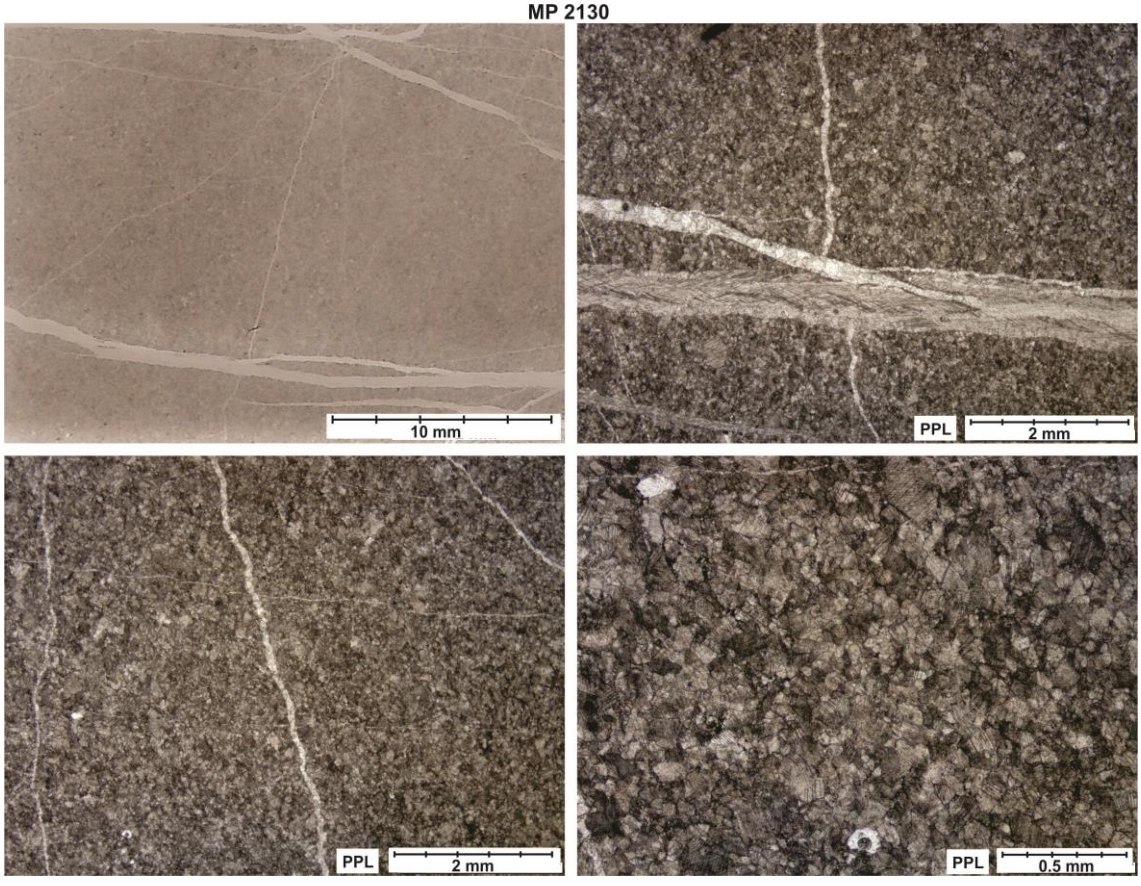

MP 2131

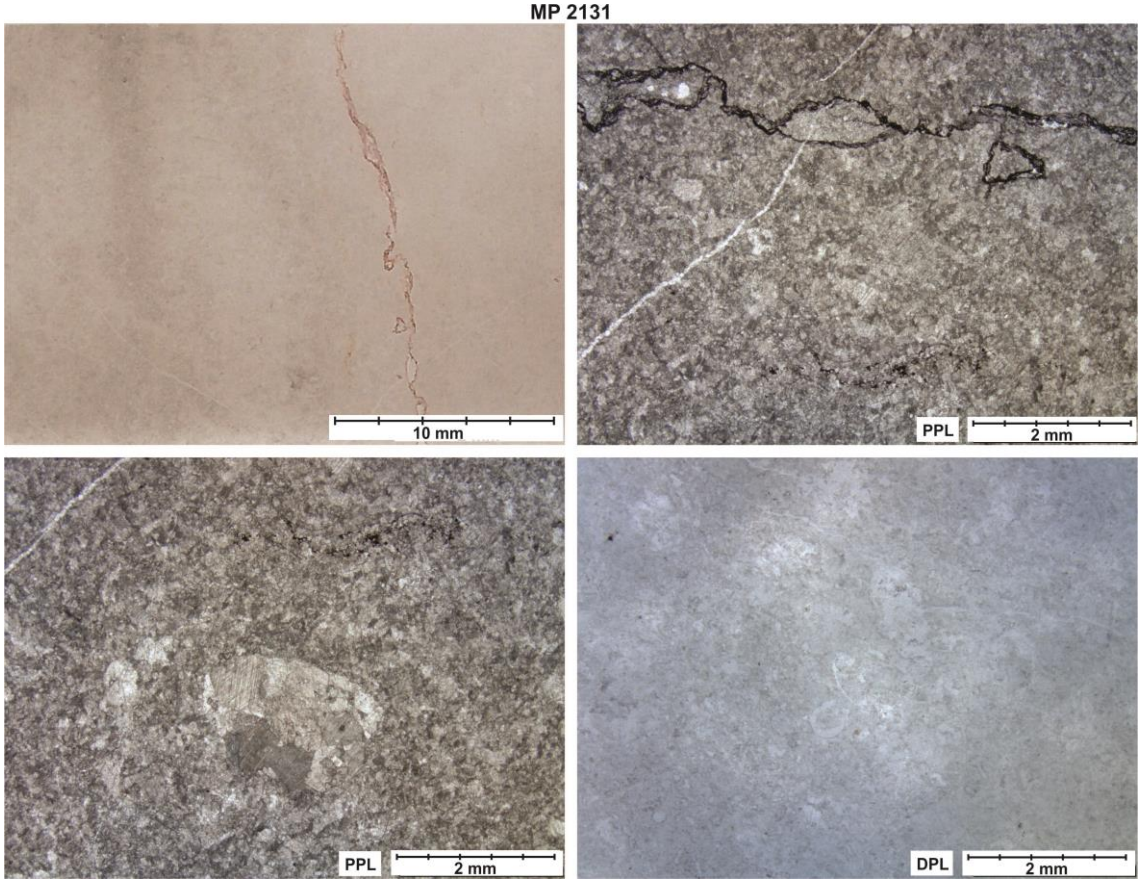

MP 2132

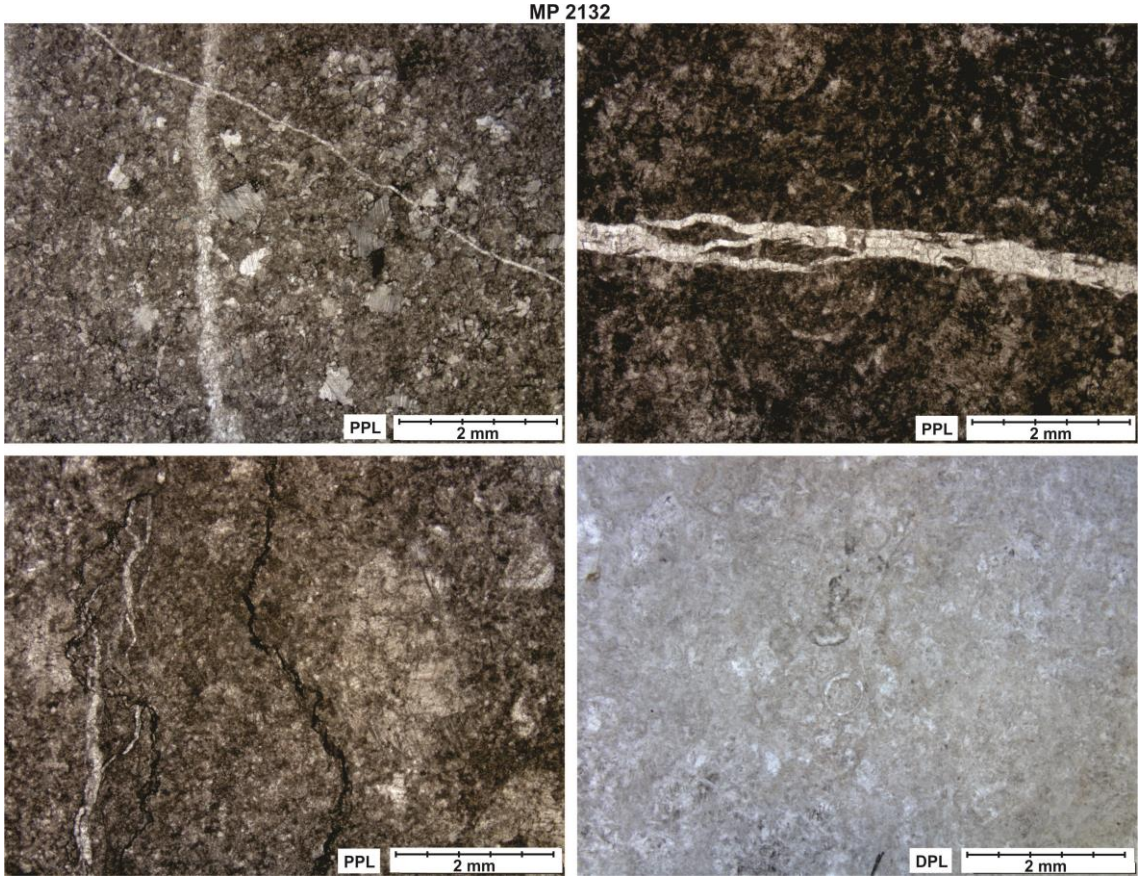

MP 1617

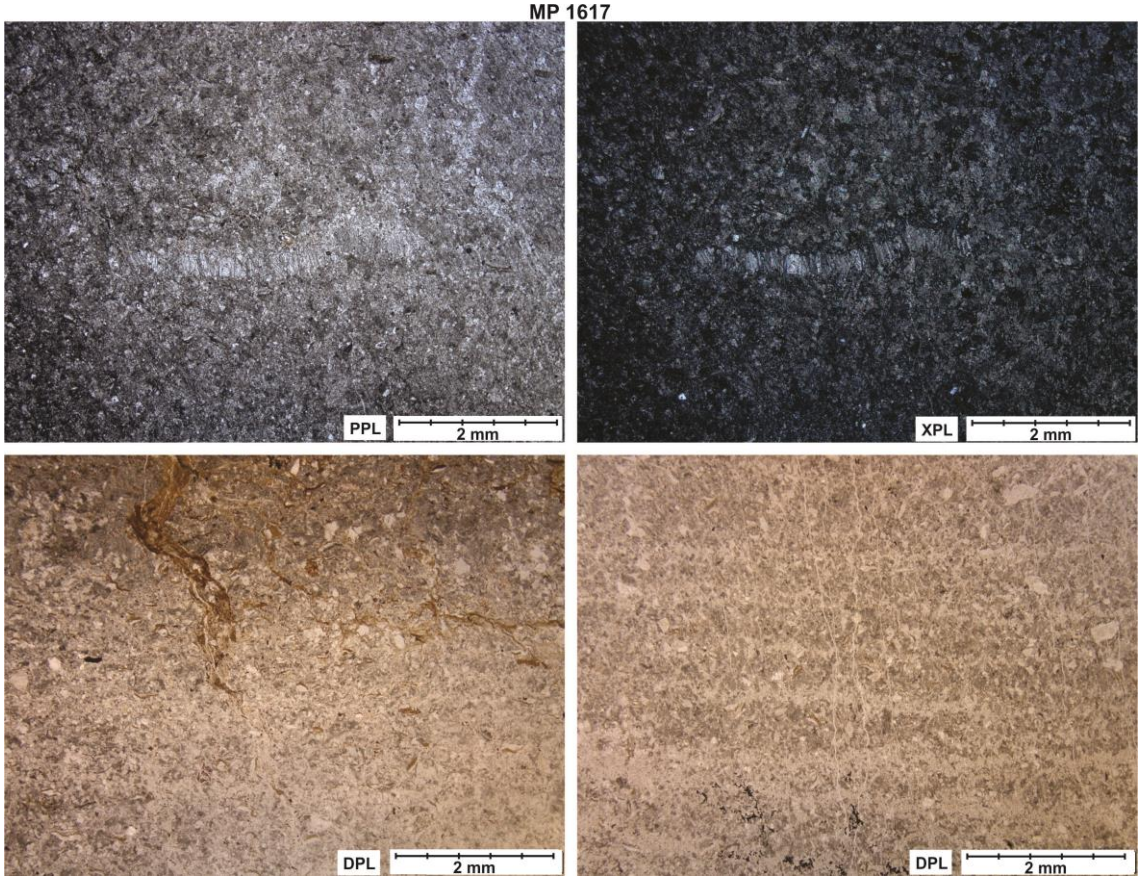

MP 1619

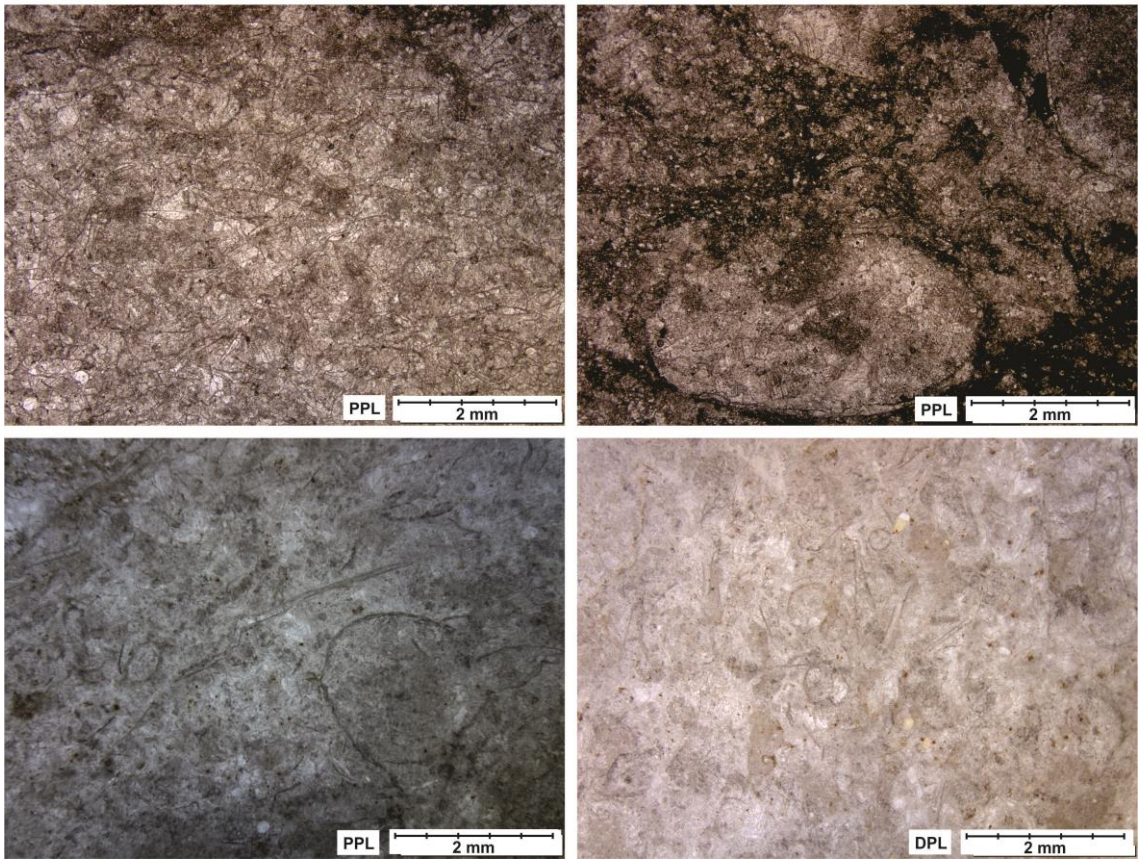

MP 1623

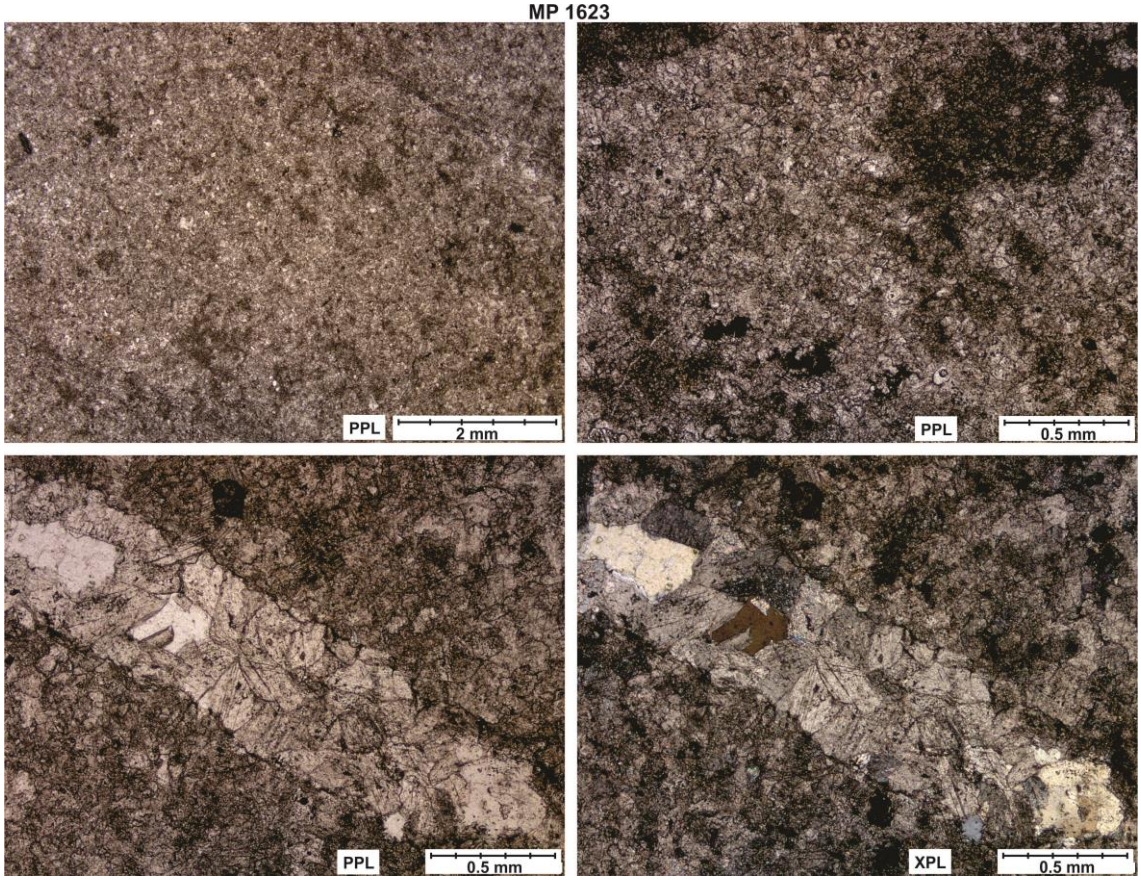

MP 1625

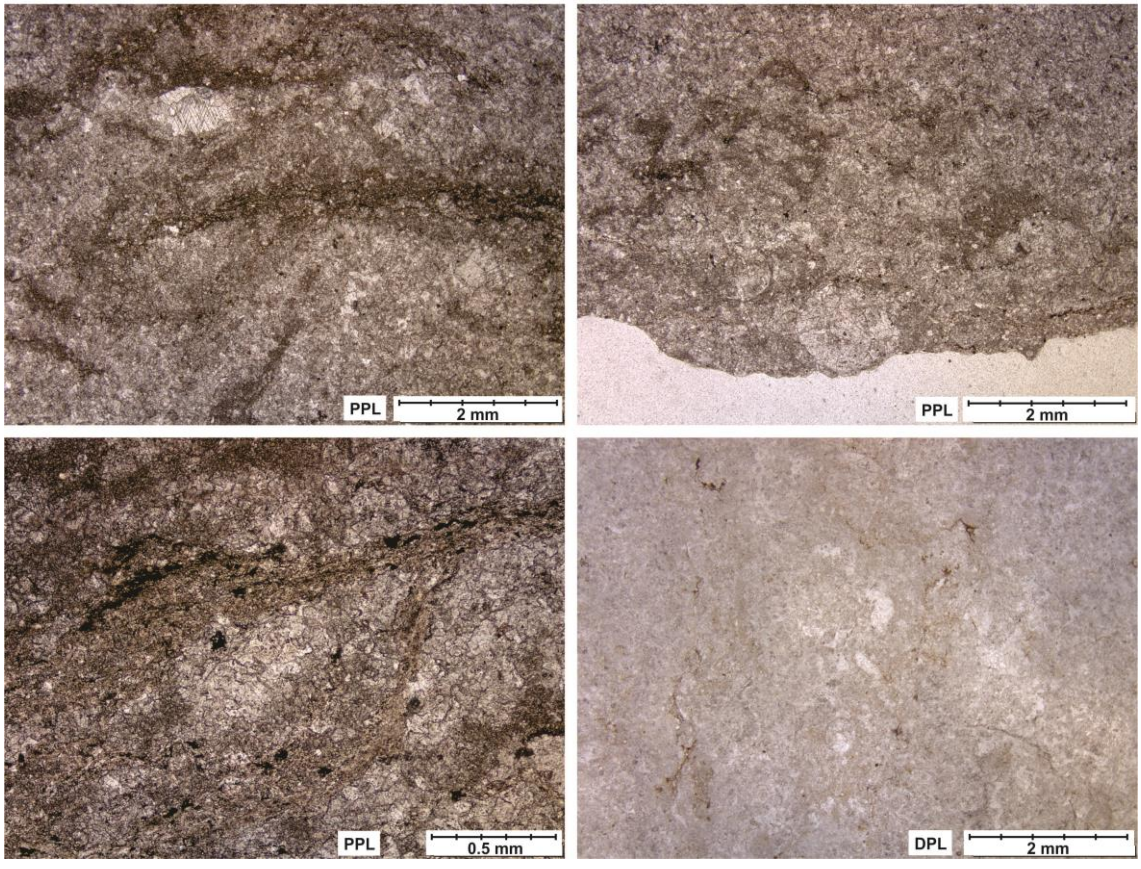

MP 1626

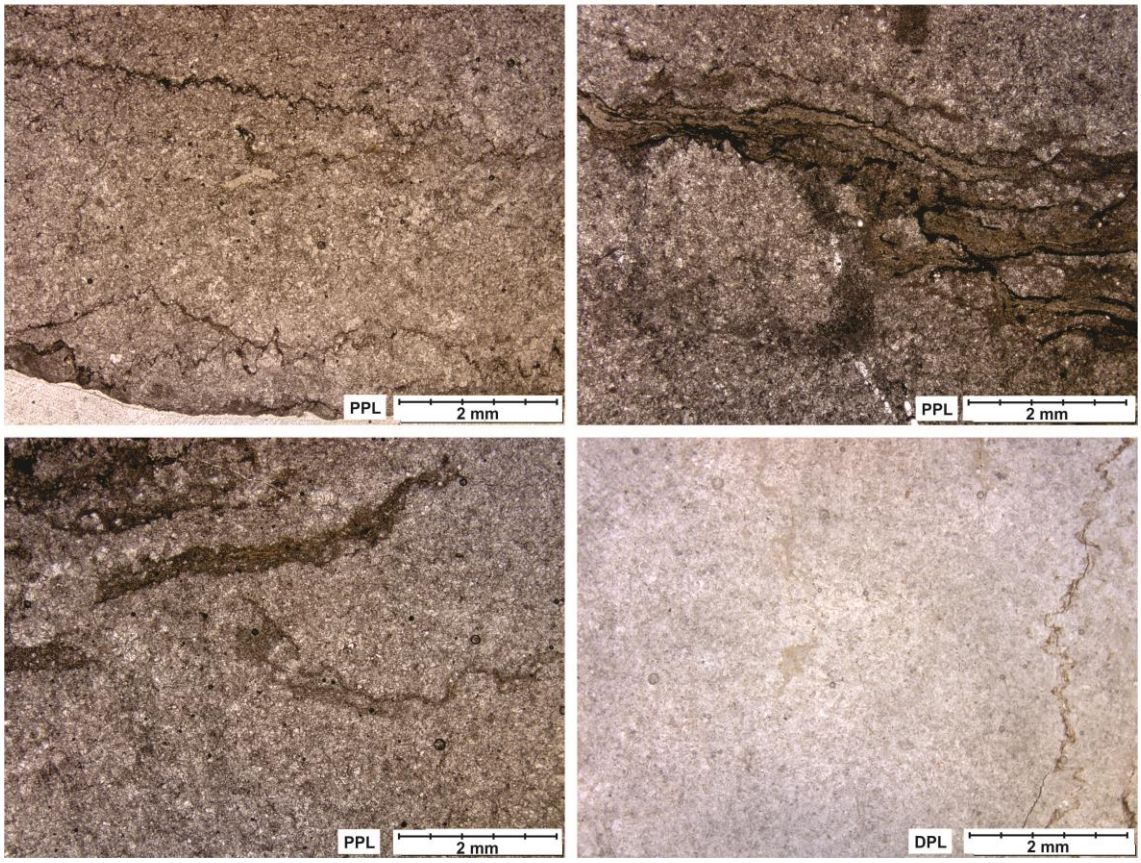

MP 1627

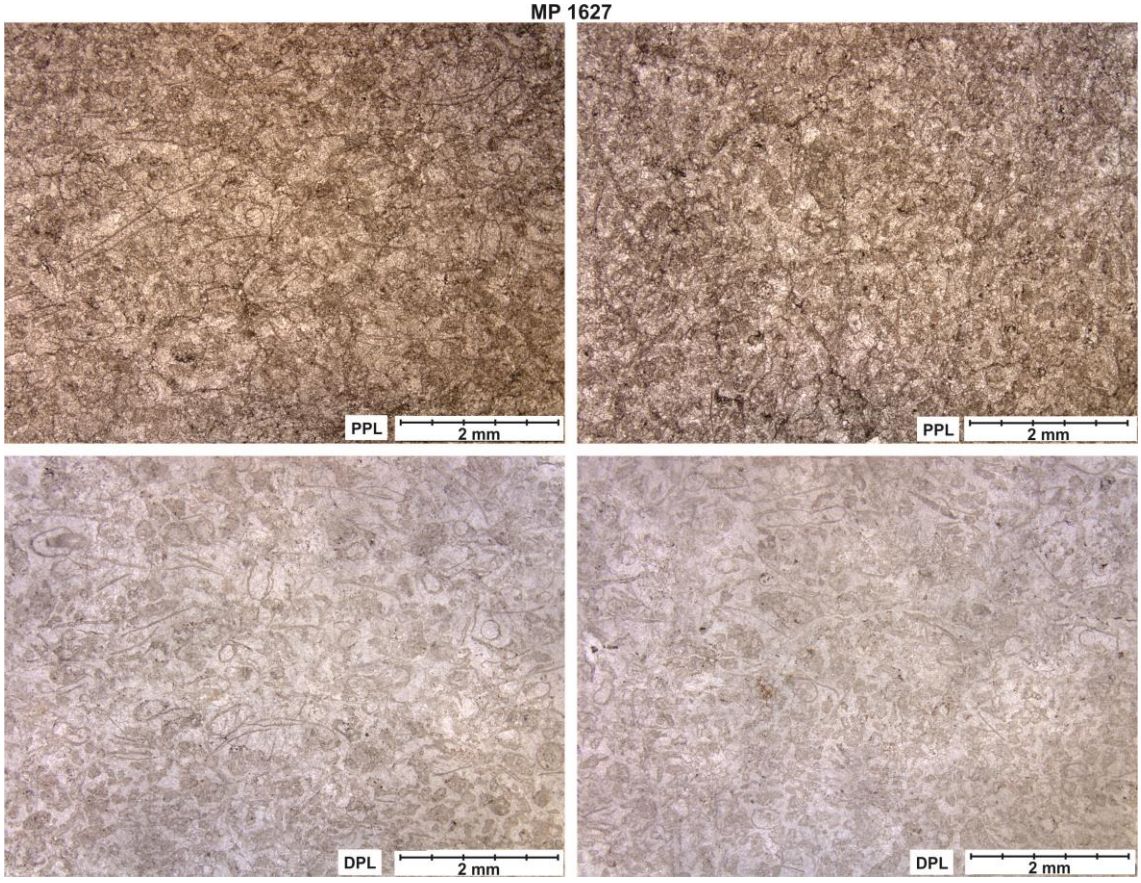

MP 1628

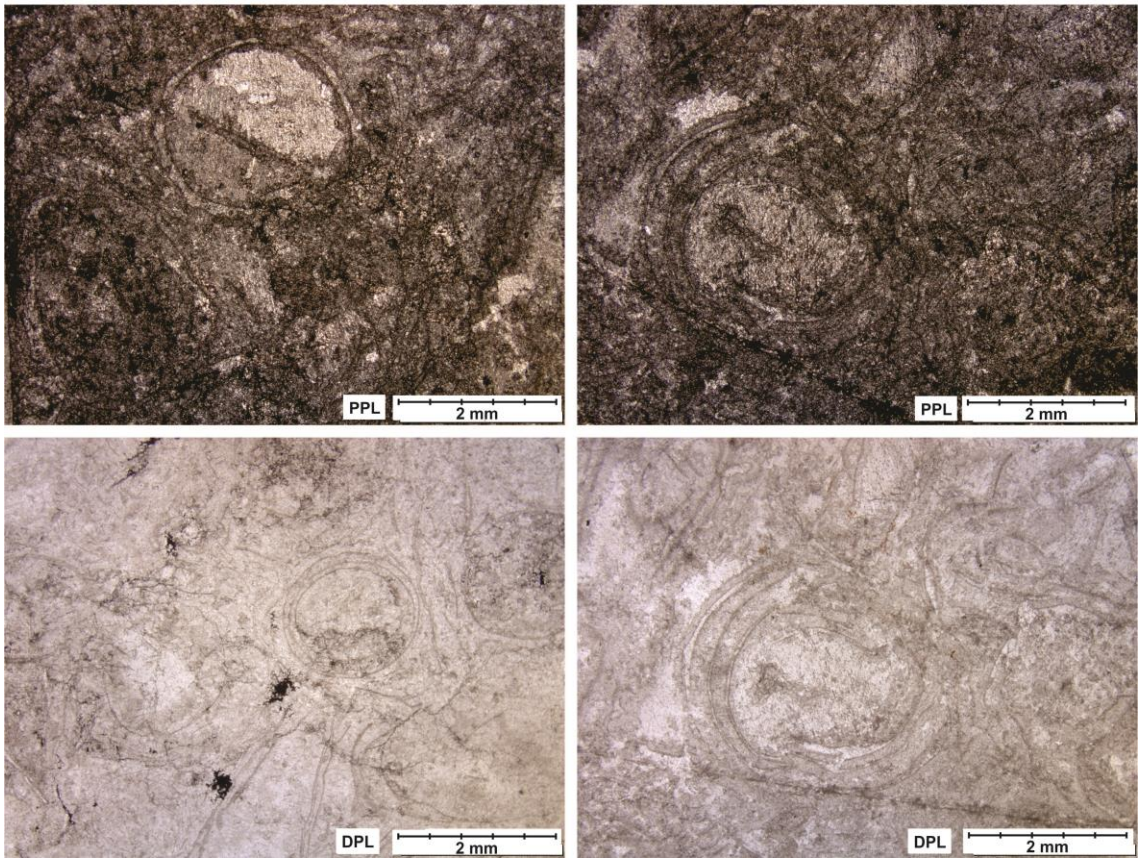

MP 1631

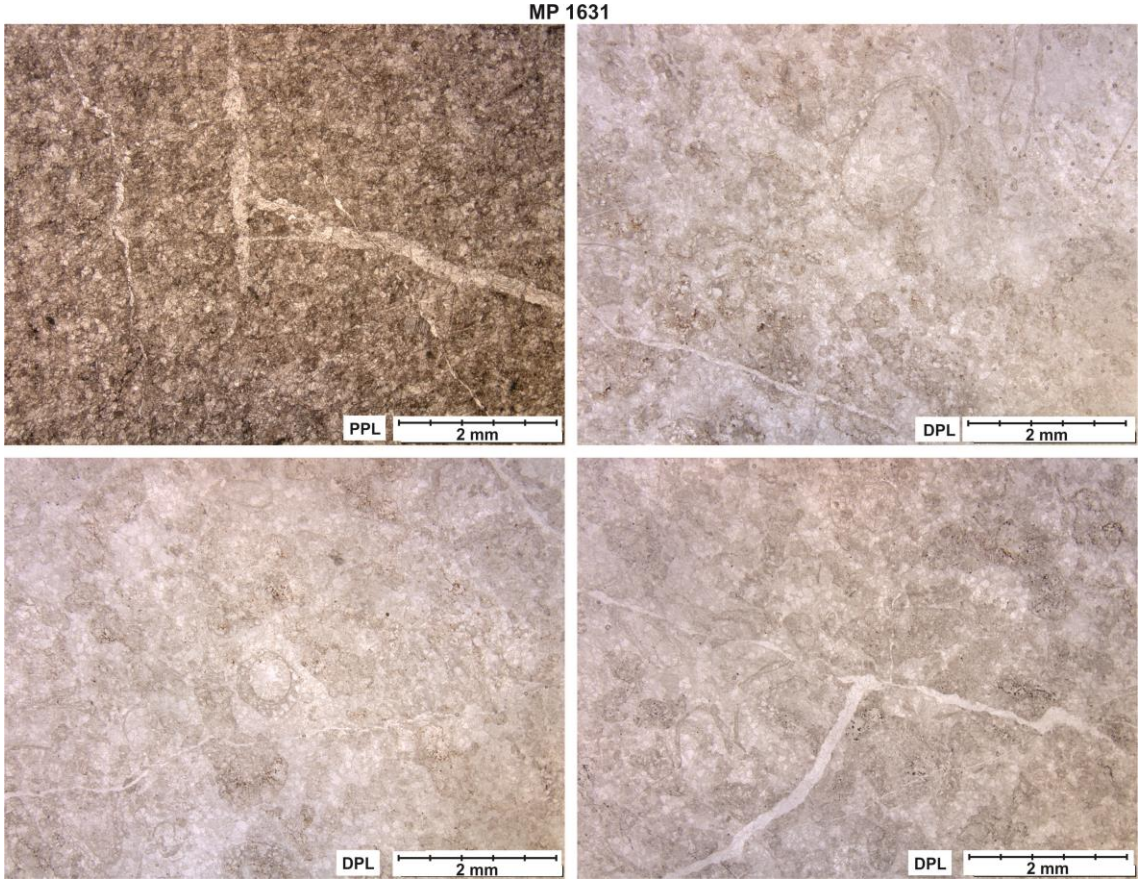

MP 1650

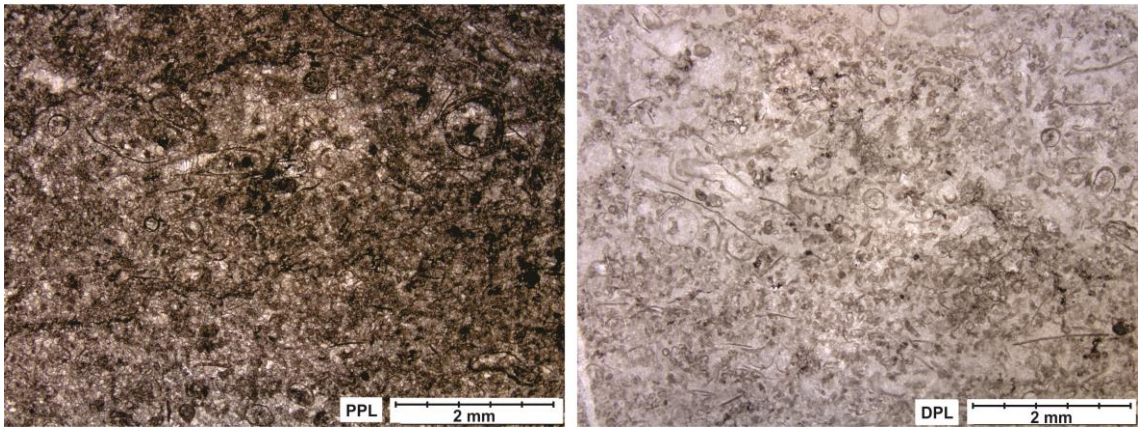

MP 1651

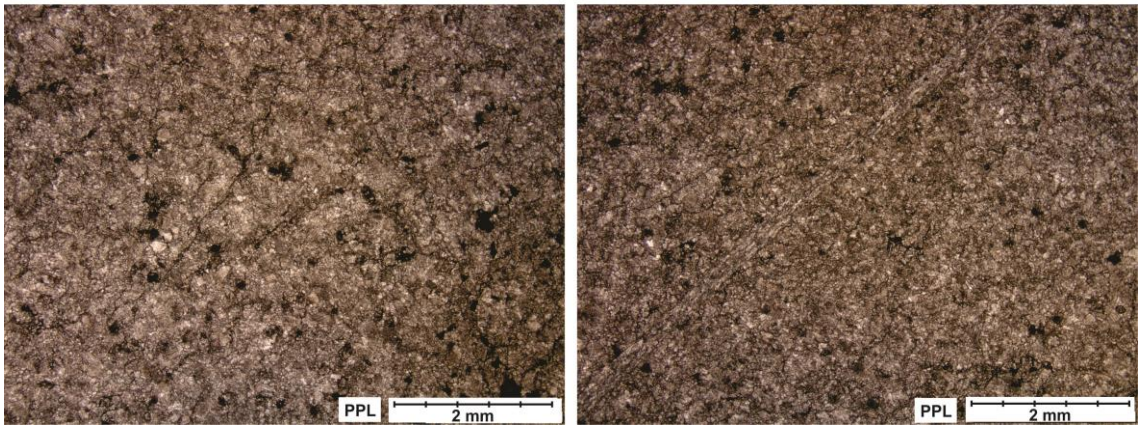

MP 1652

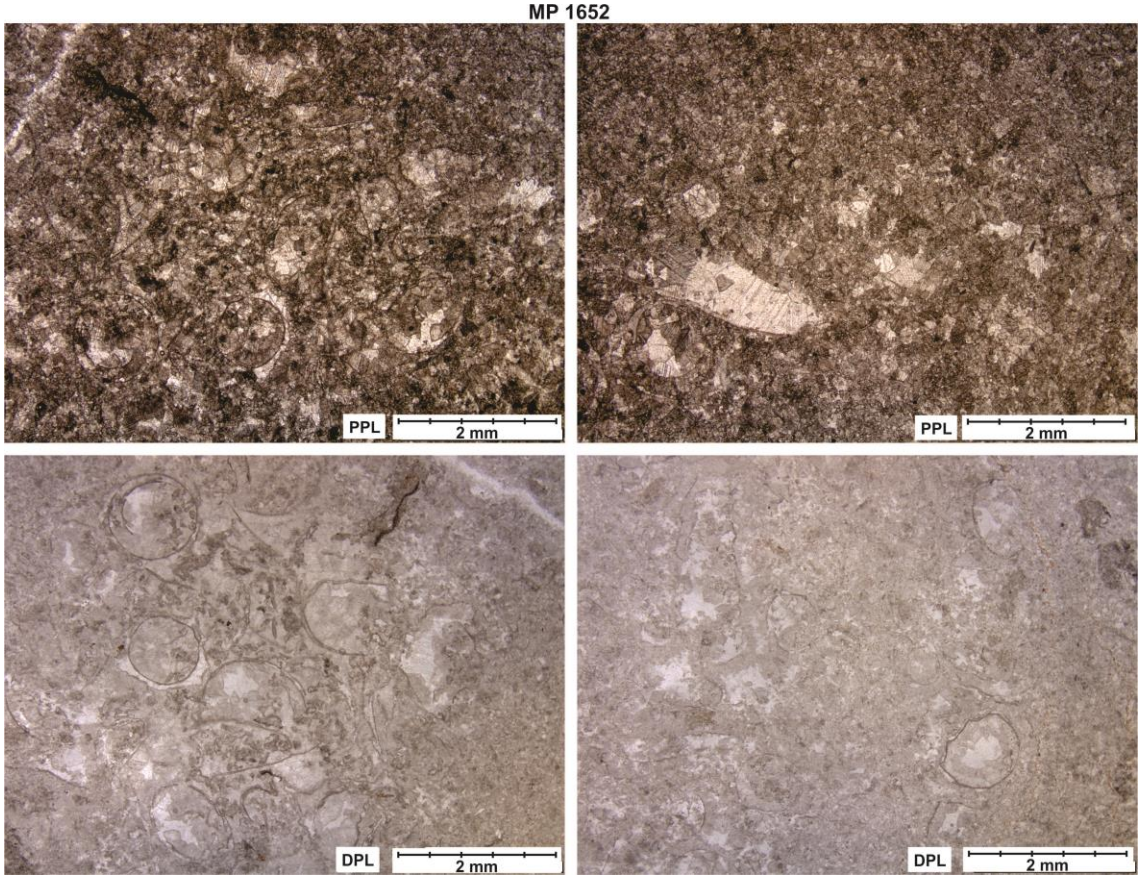

MP 1654

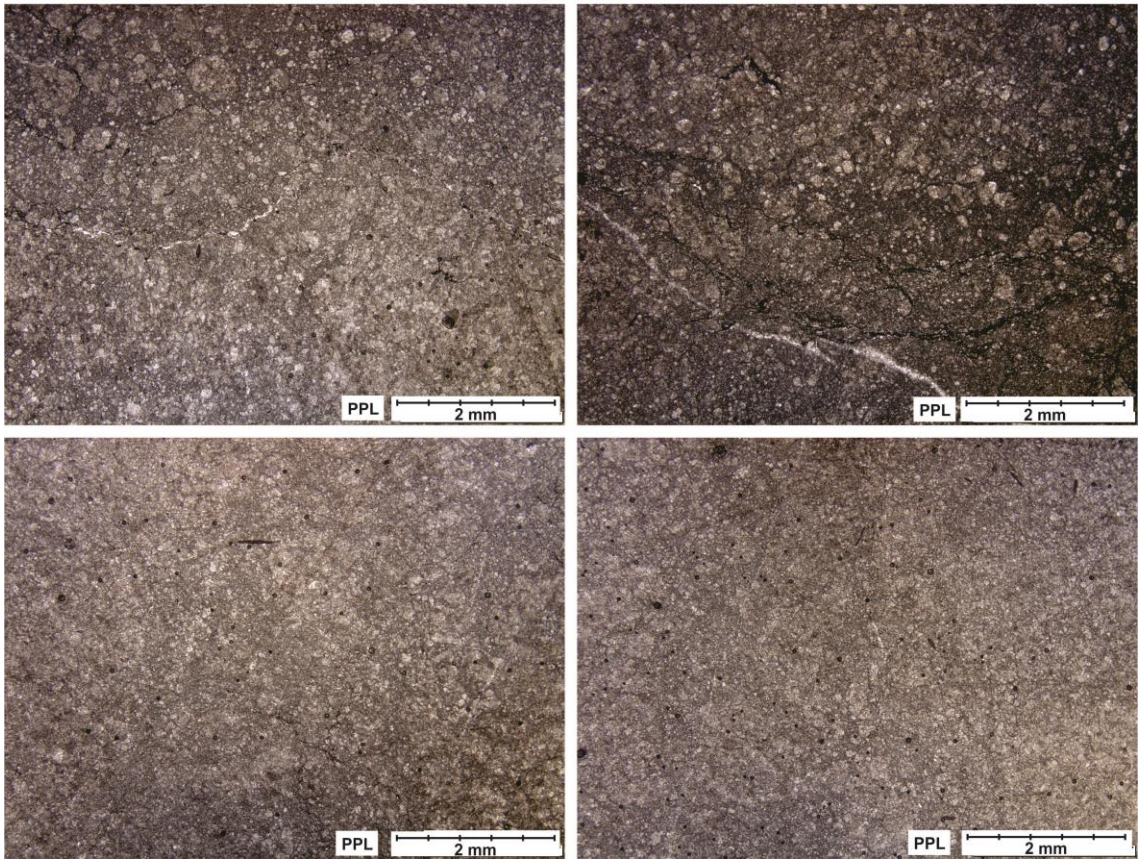

Laginha Thin Sections

L1 CONT BT

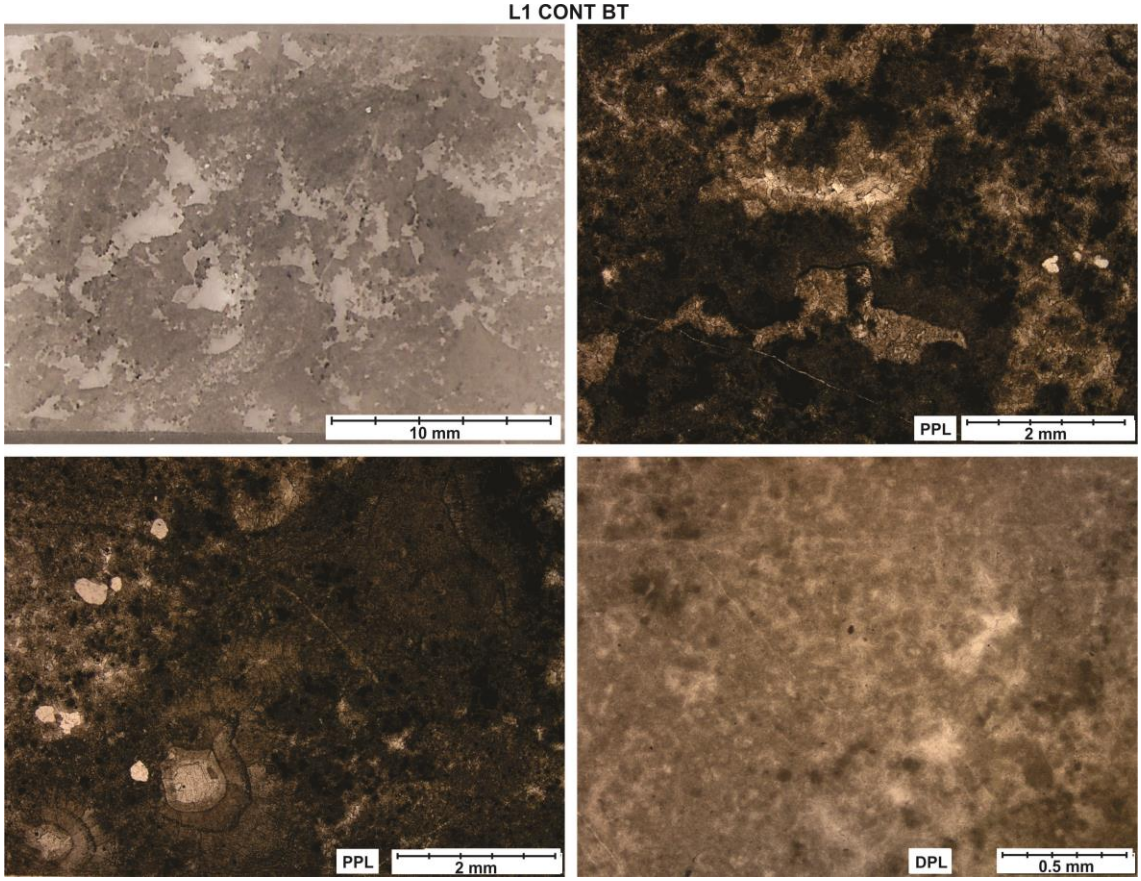

L2 2.50

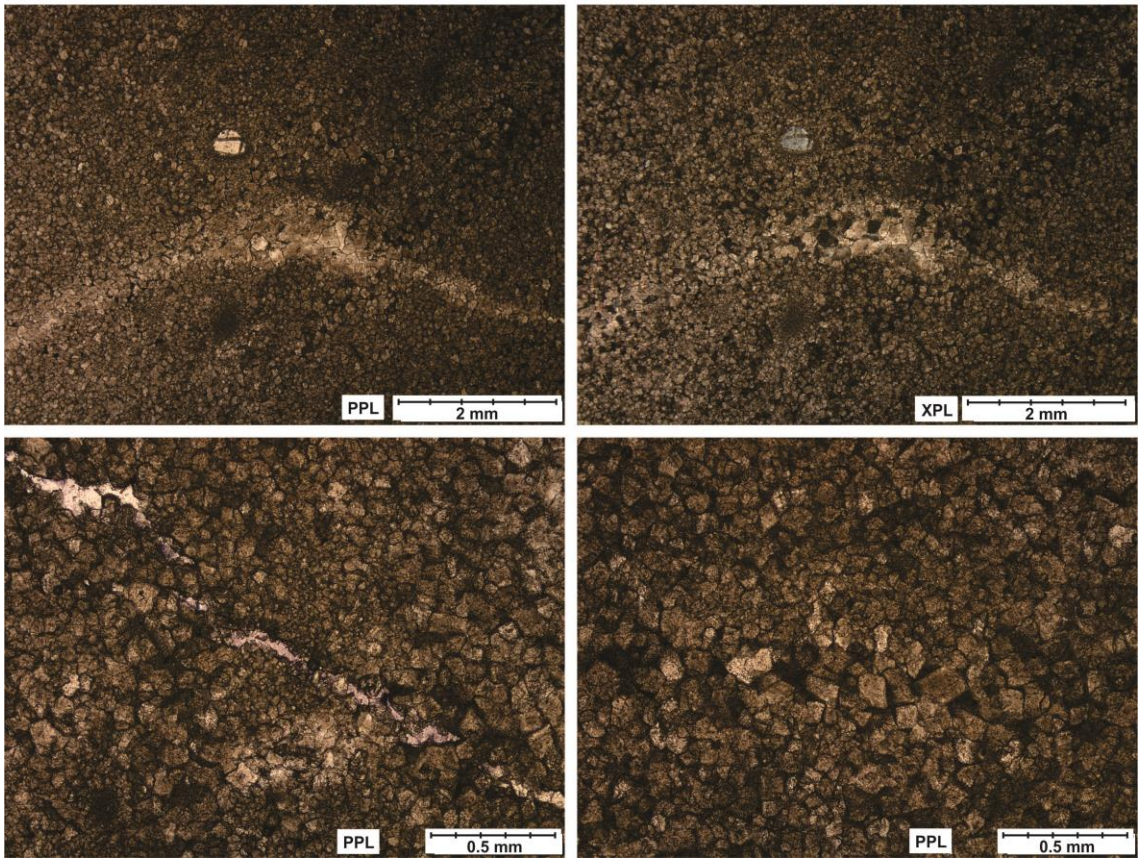

L3 0.85

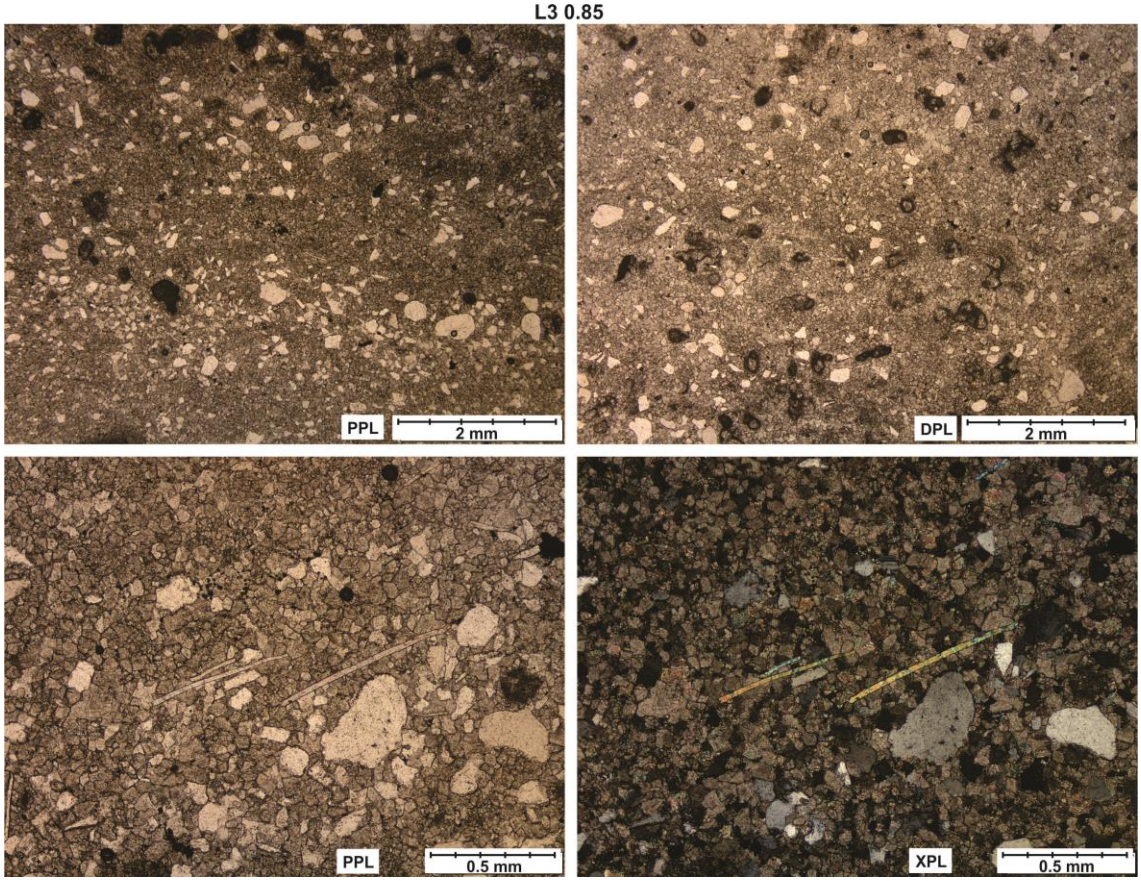

L3 2.75

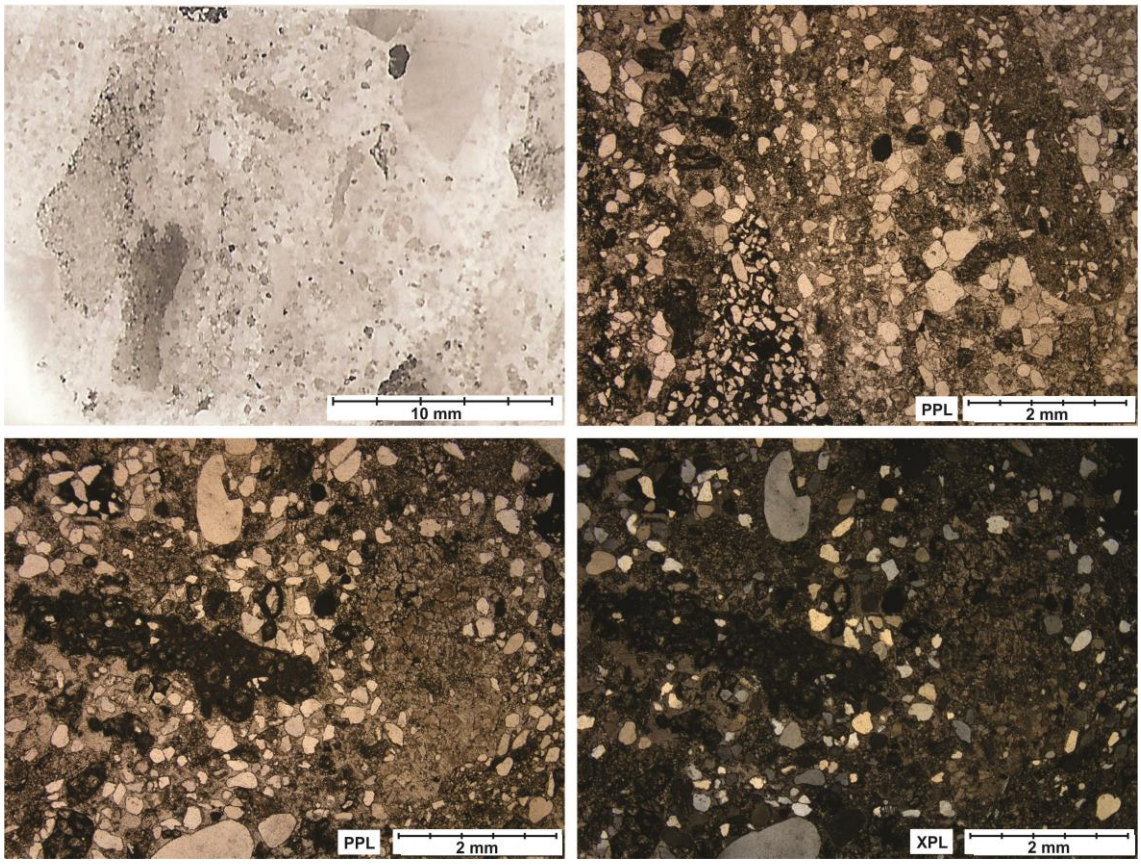

L3 3.10

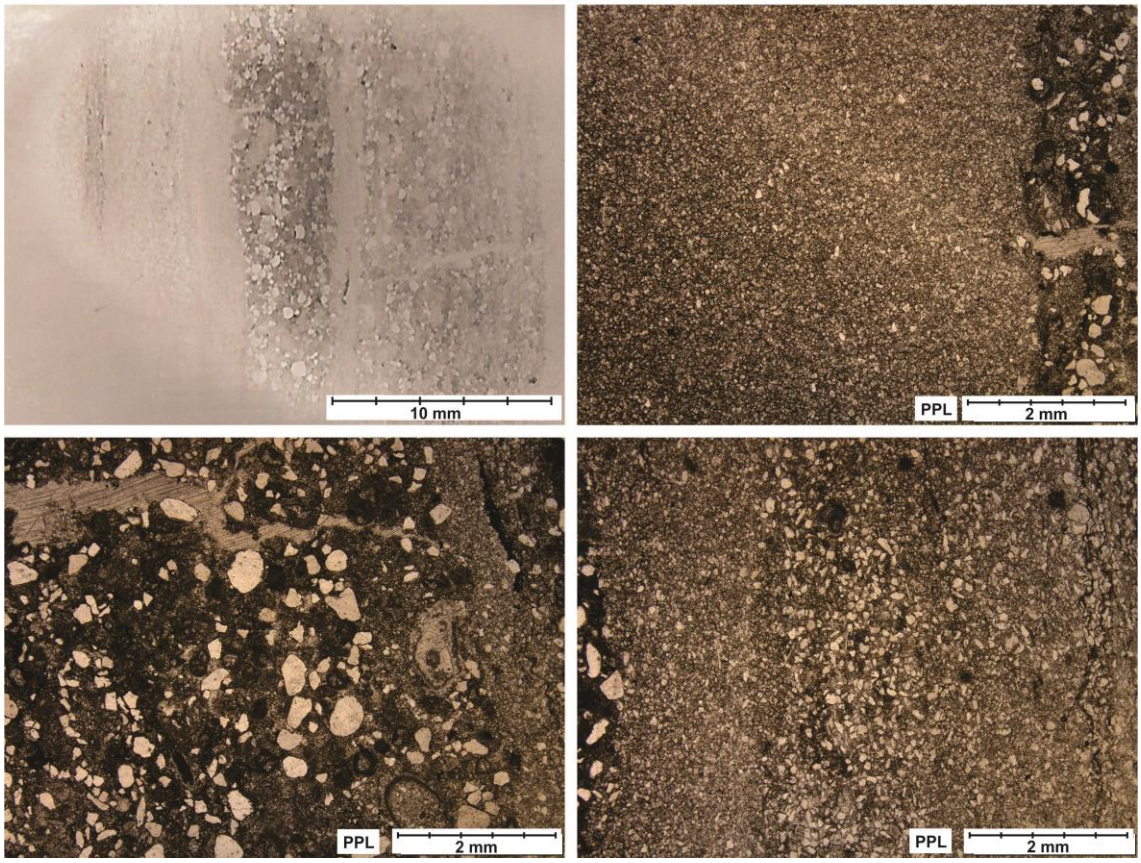

L3 6.45

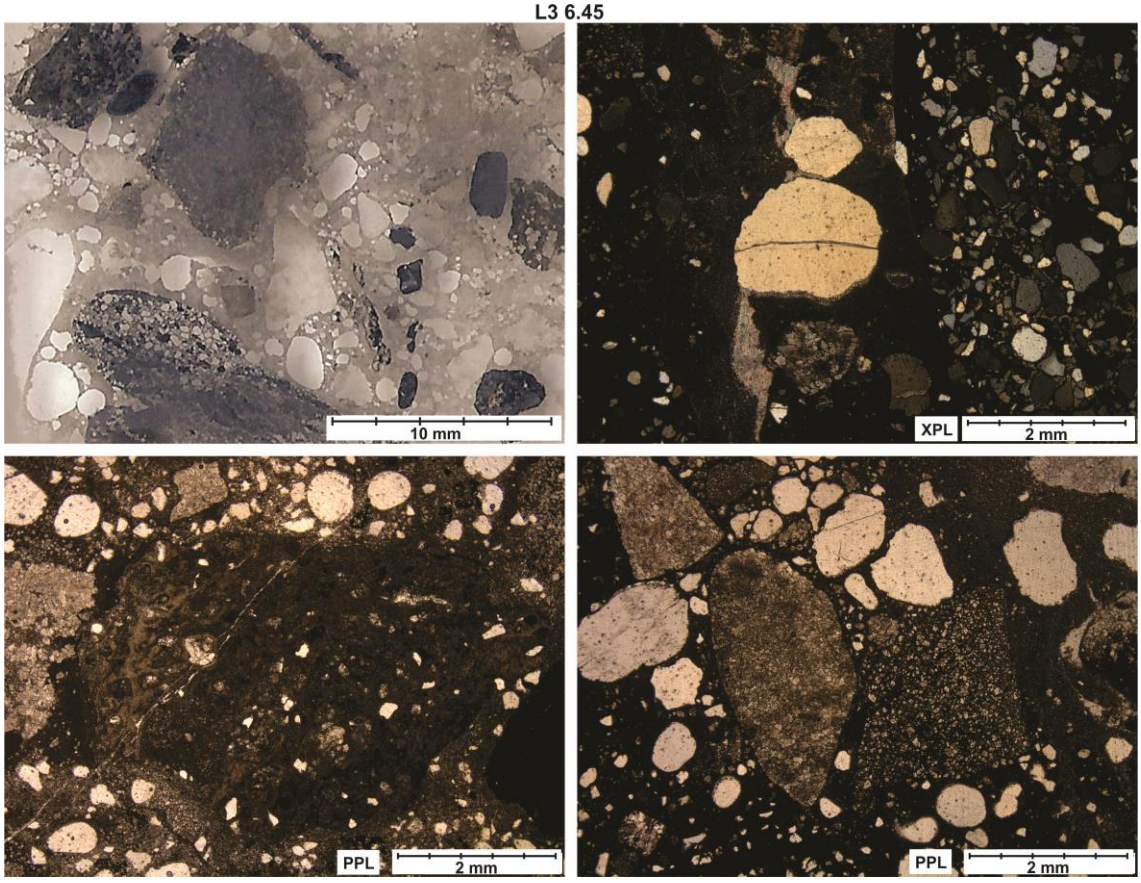

L3 7.35

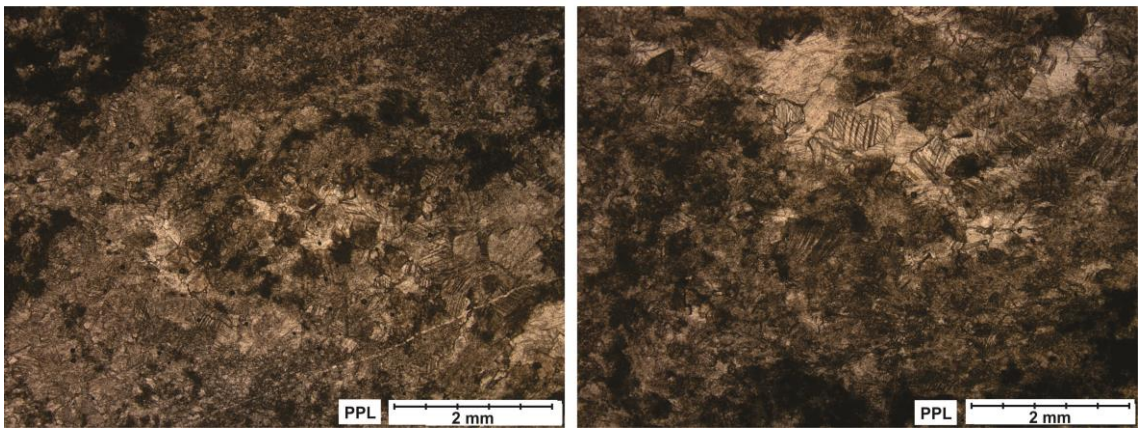

L3 10.75

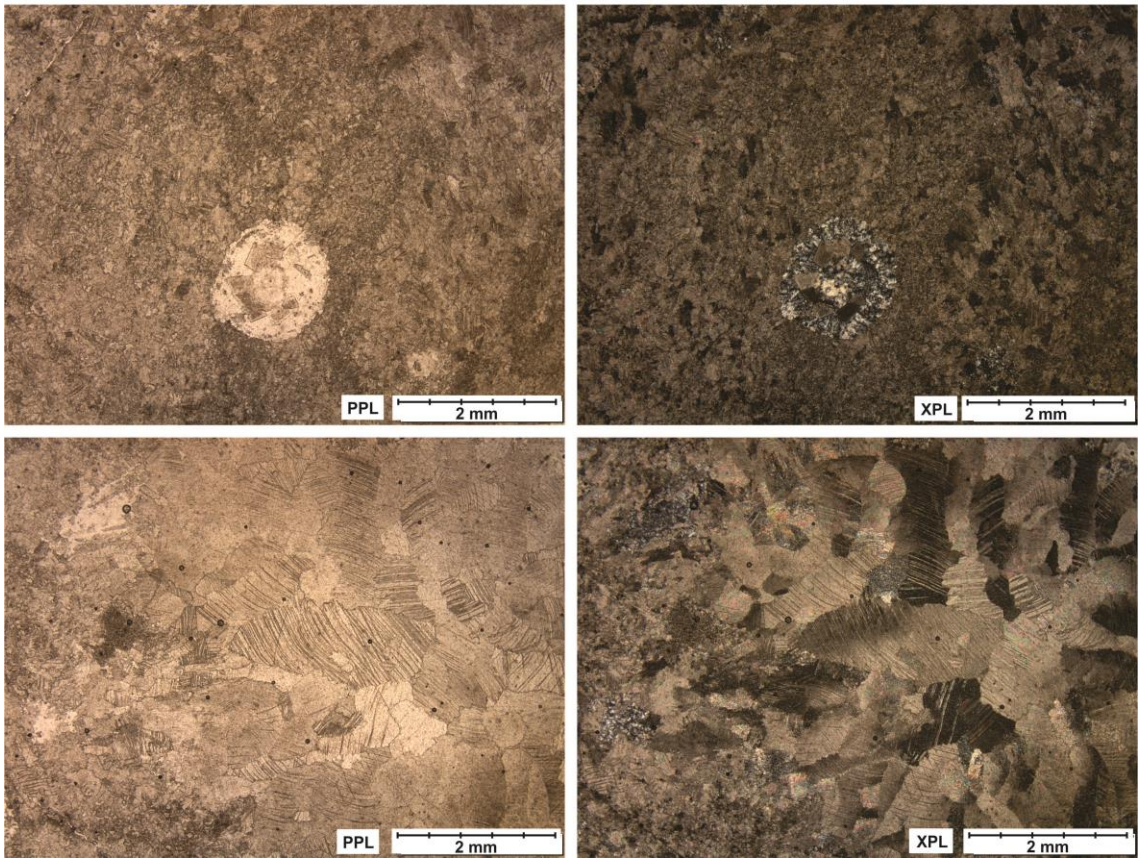

L3 13.80

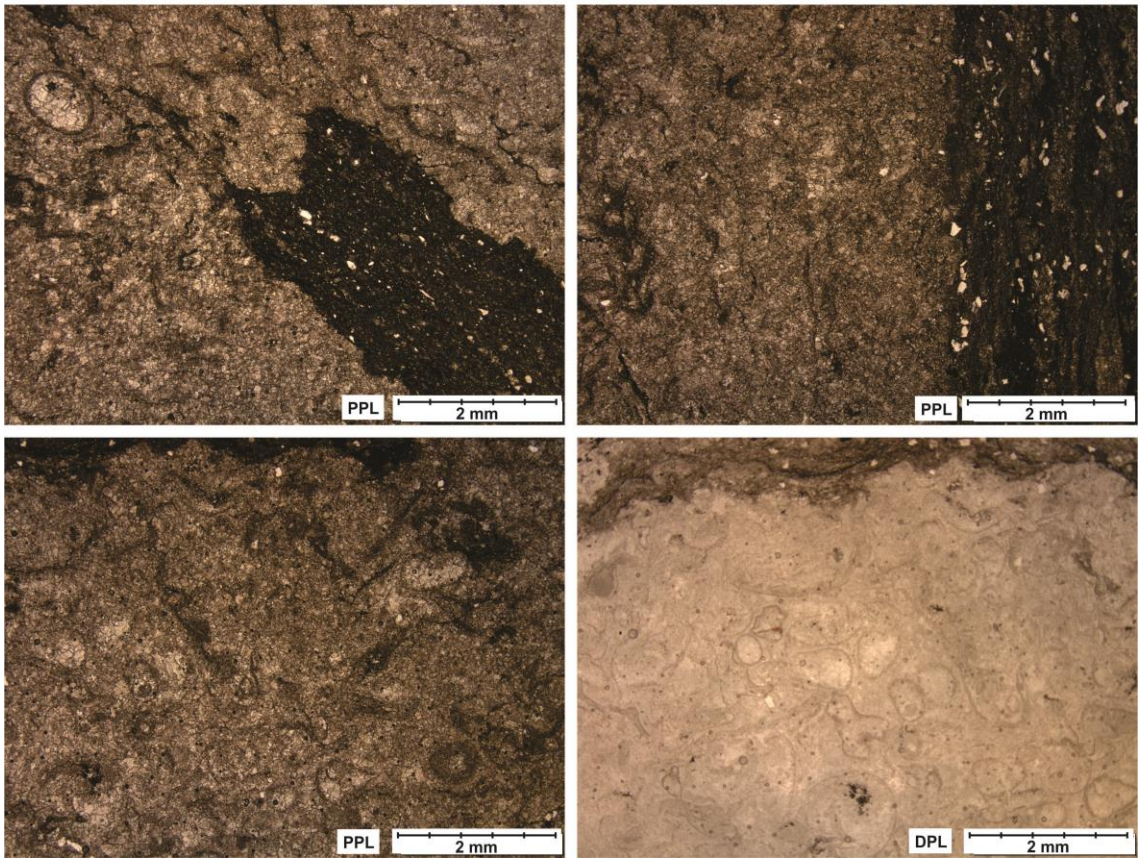

L3 19.05

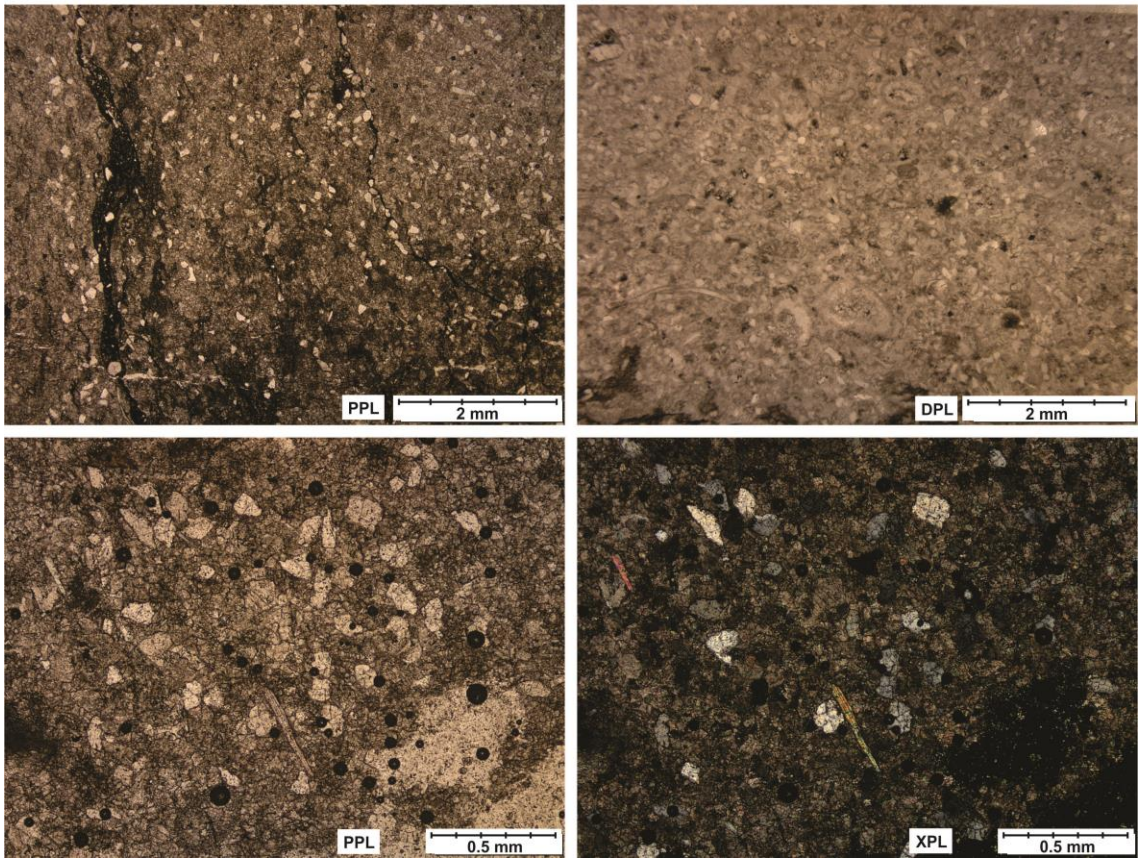

MP 2151

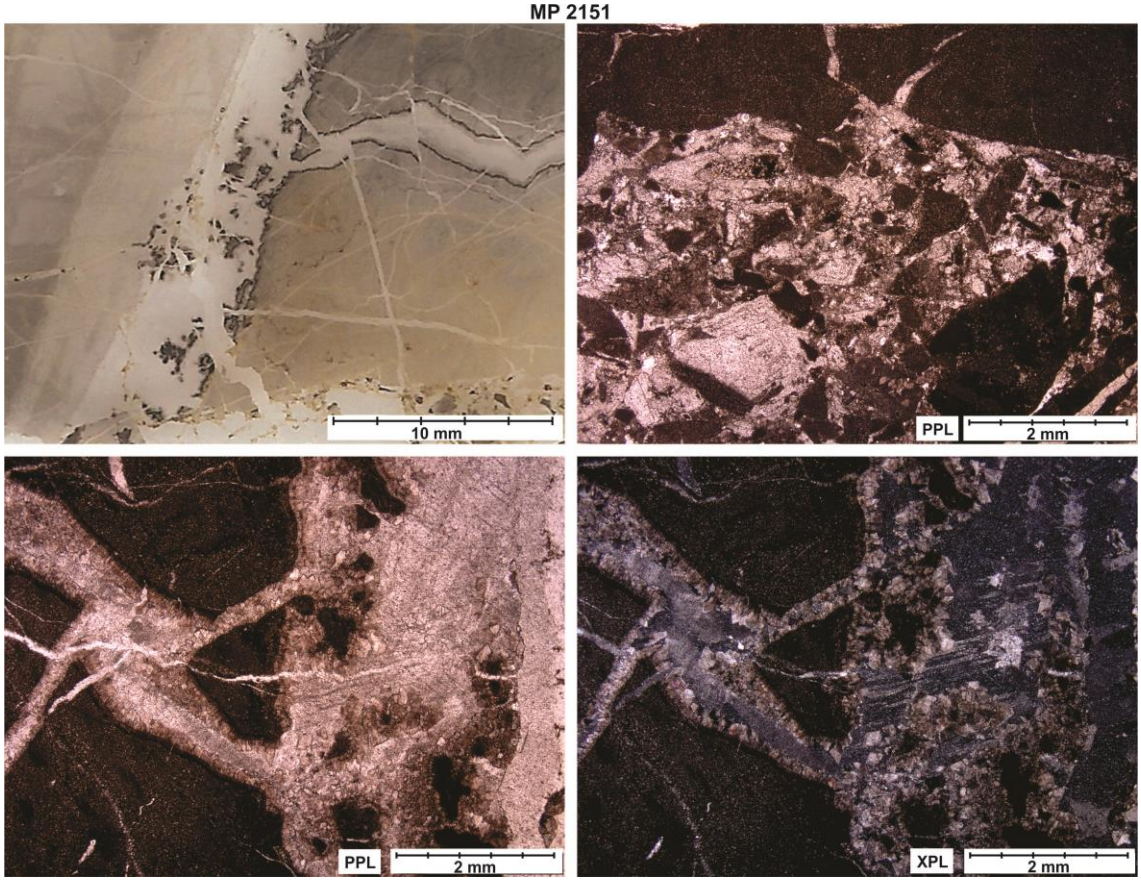

MP 2152

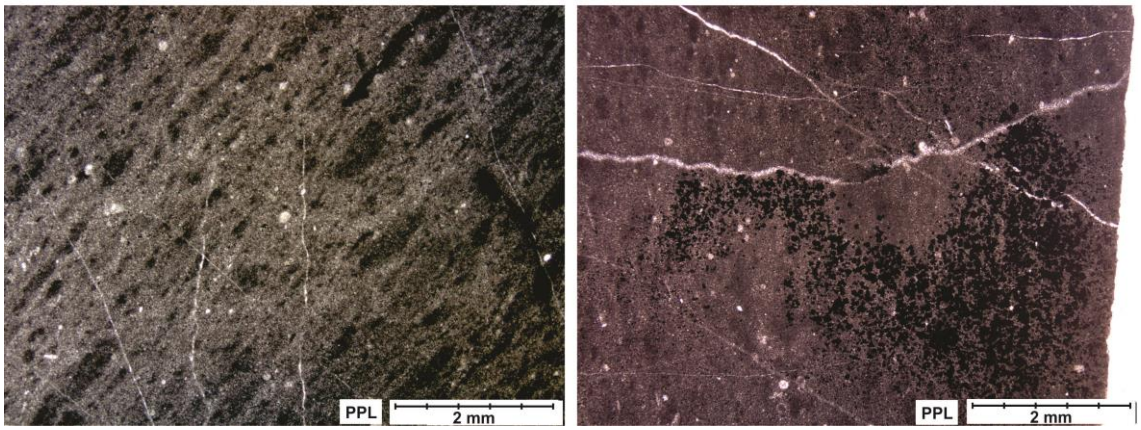

MP 2153

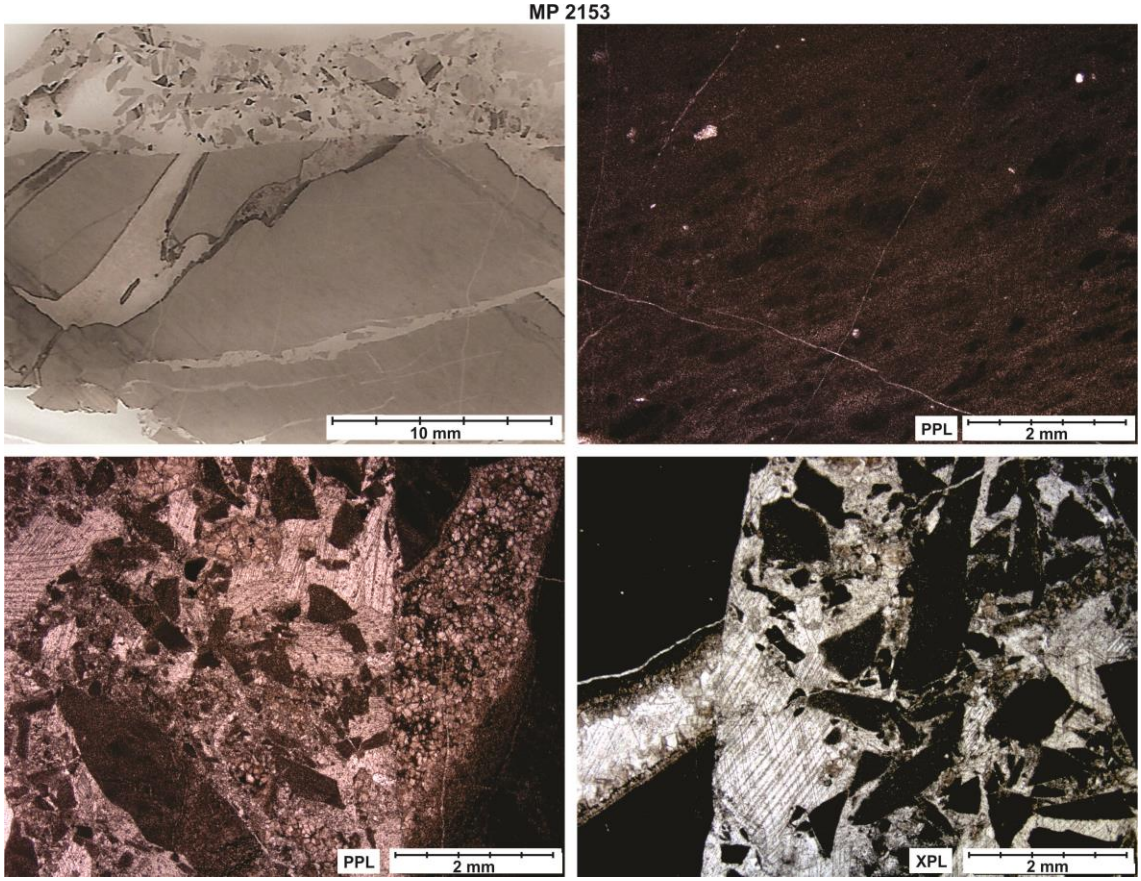

MP 2154

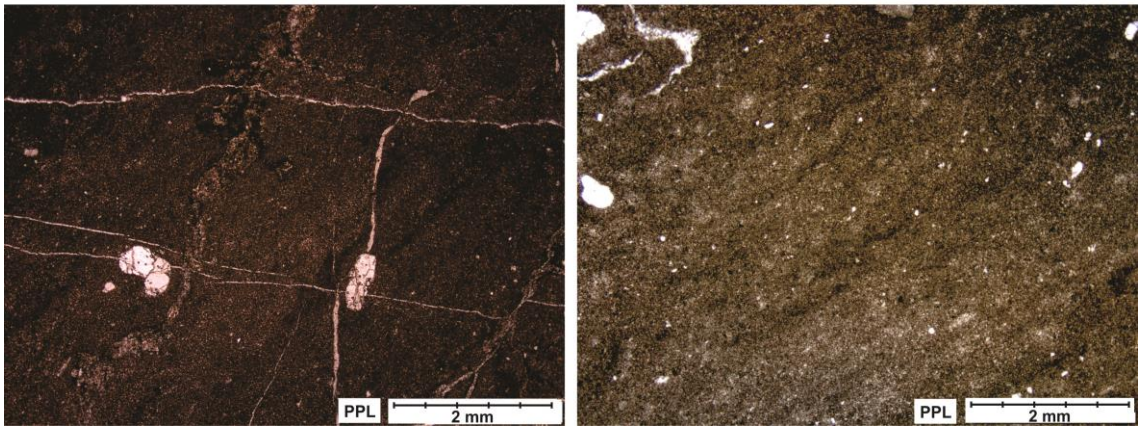

MP 2155

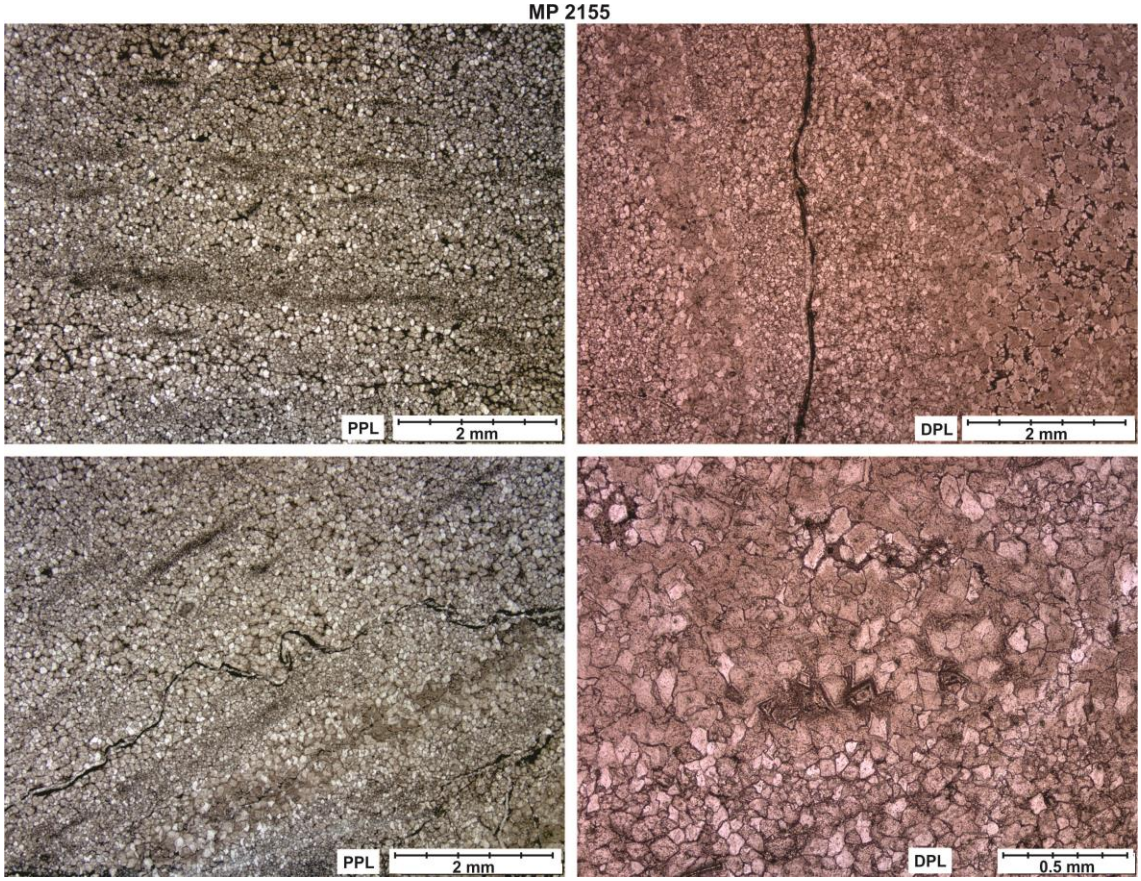

MP 2156

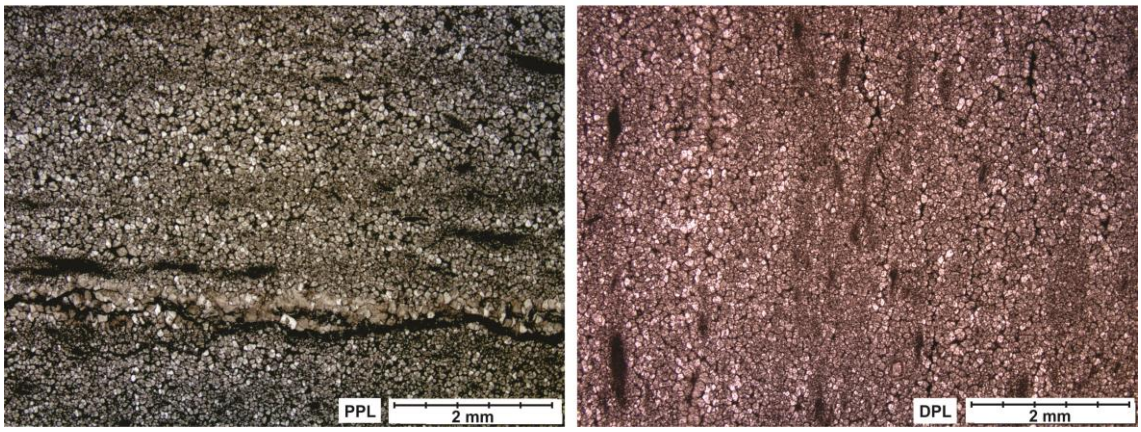

MP 2157

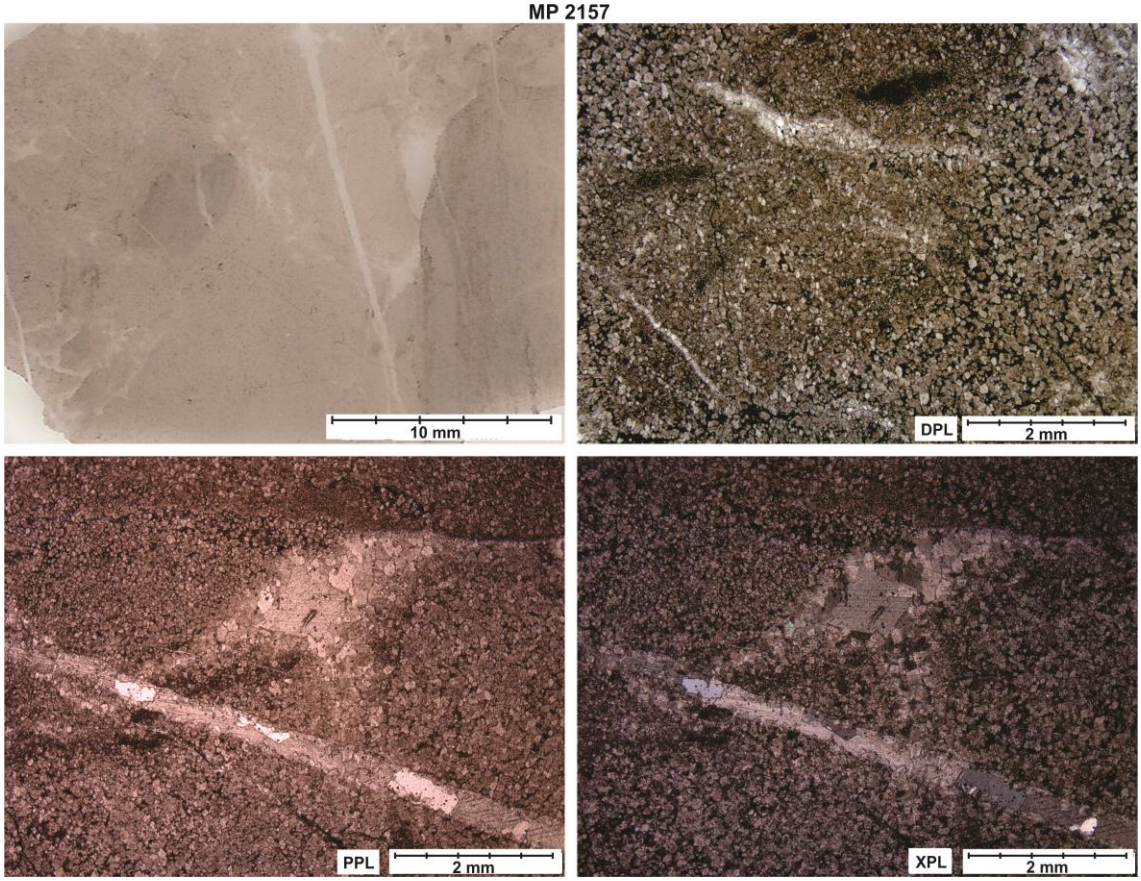

MP 2158

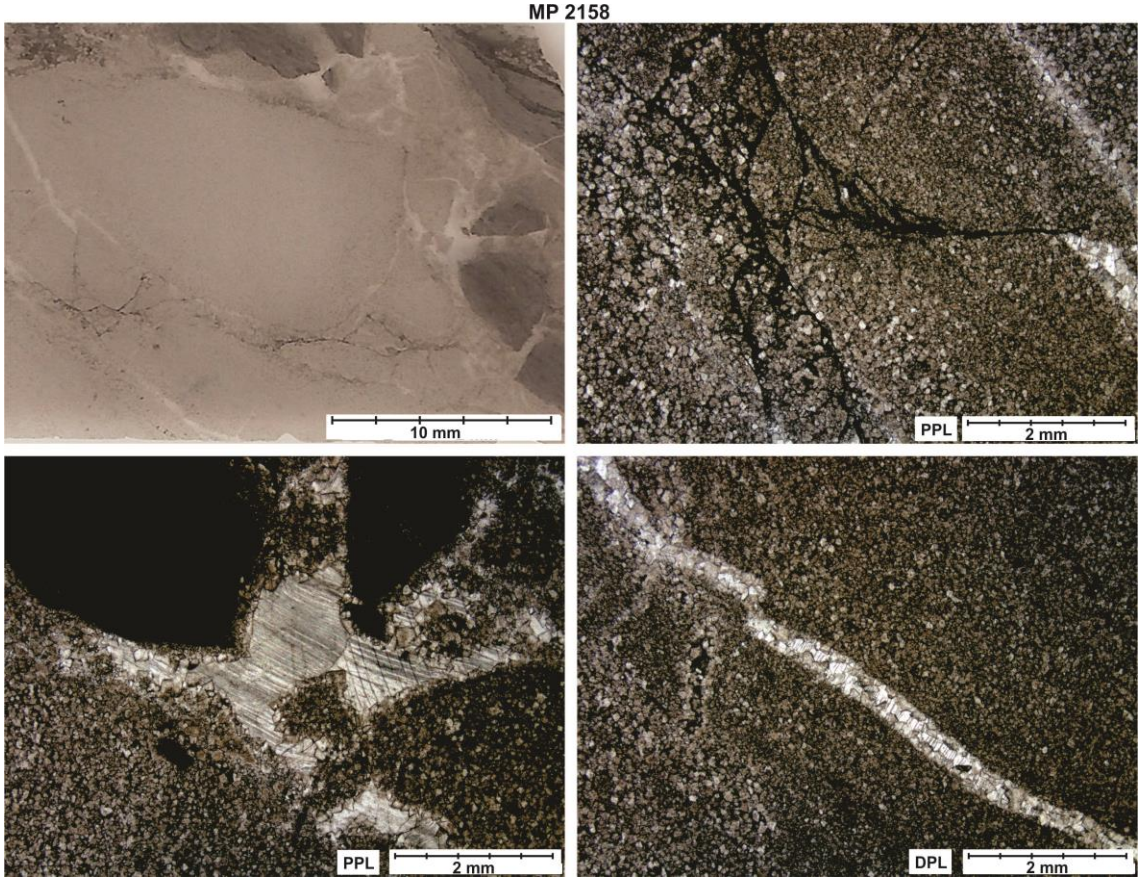

MP 2159

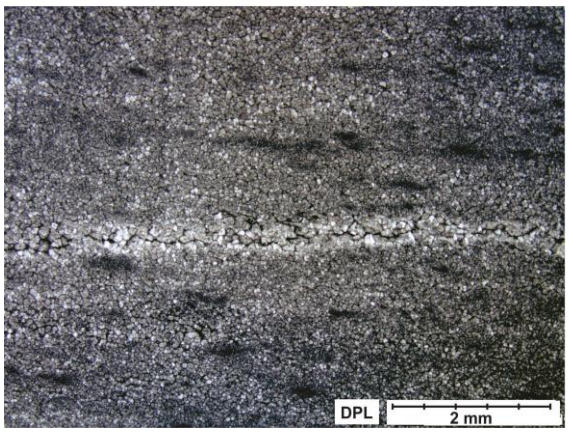

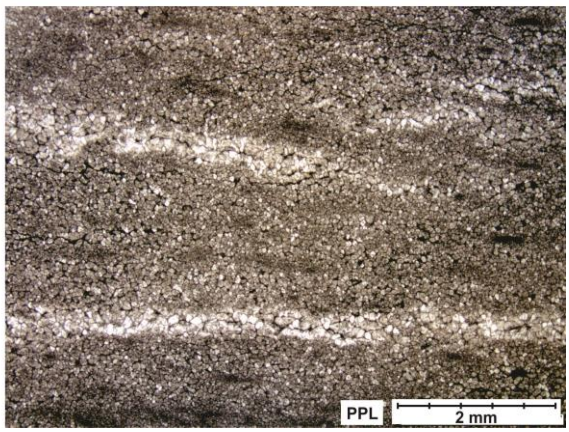

MP 2160

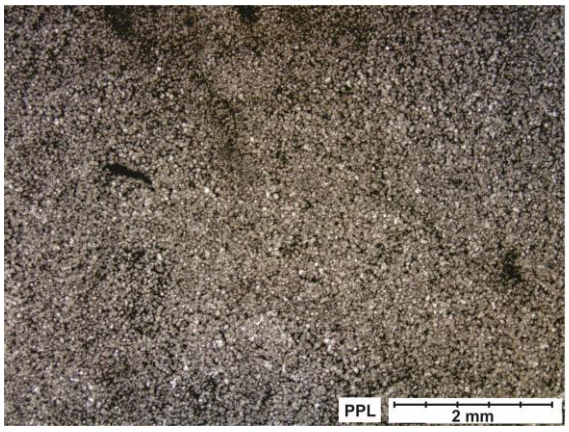

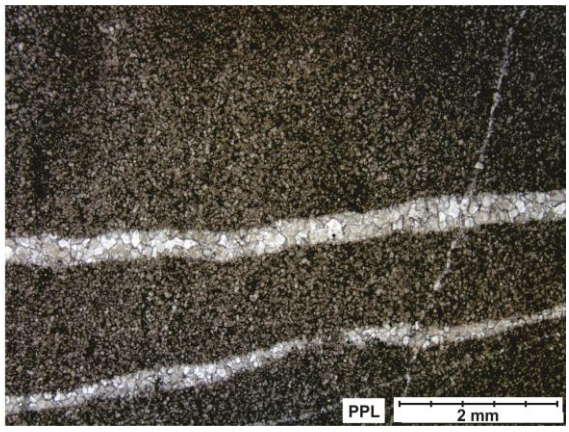

MP 2161

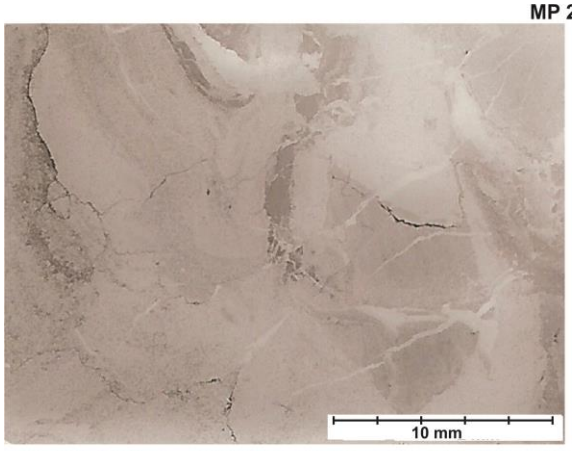

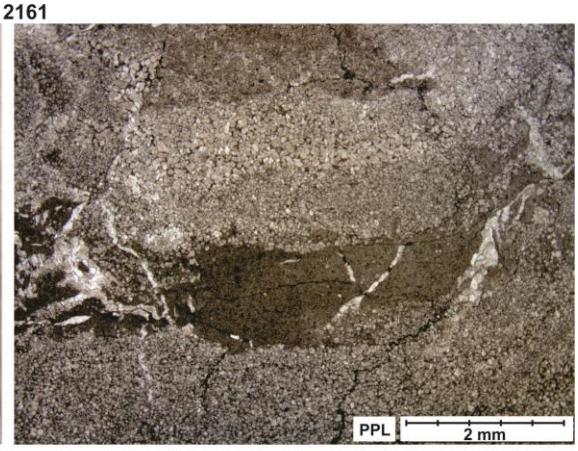

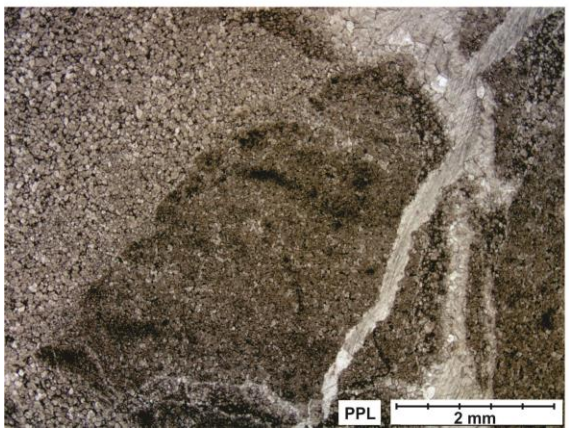

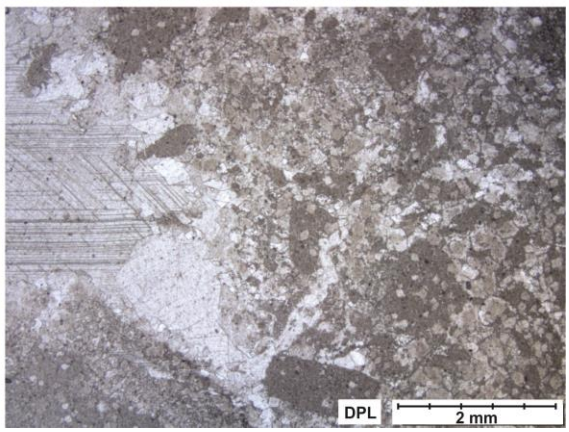

MP 2162

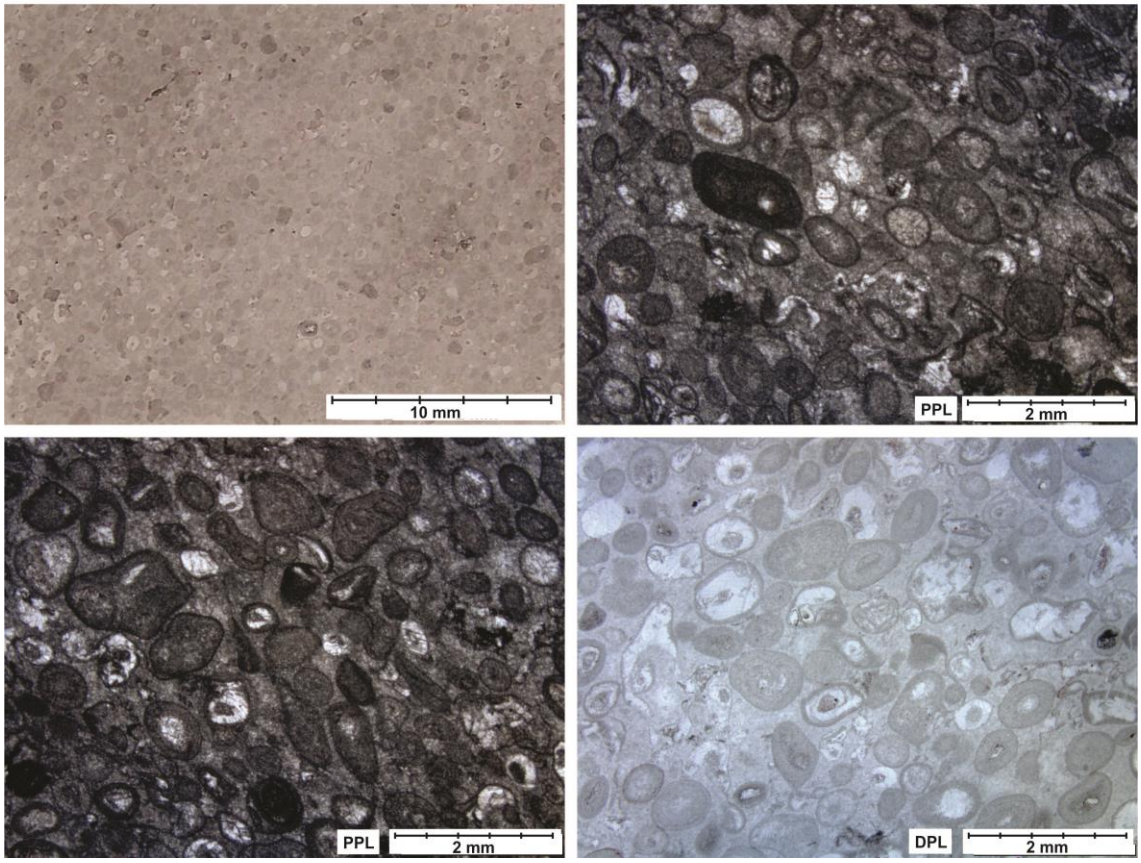

MP 2163

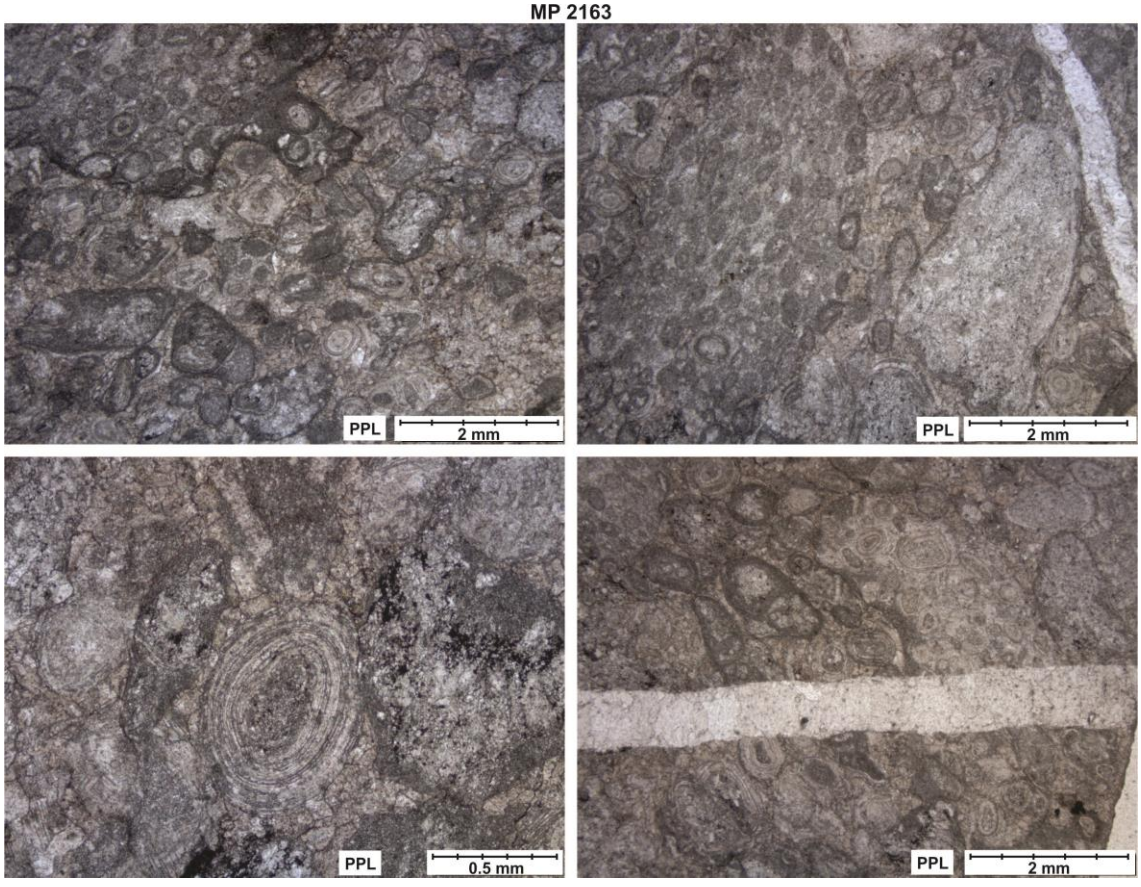

MP 2164

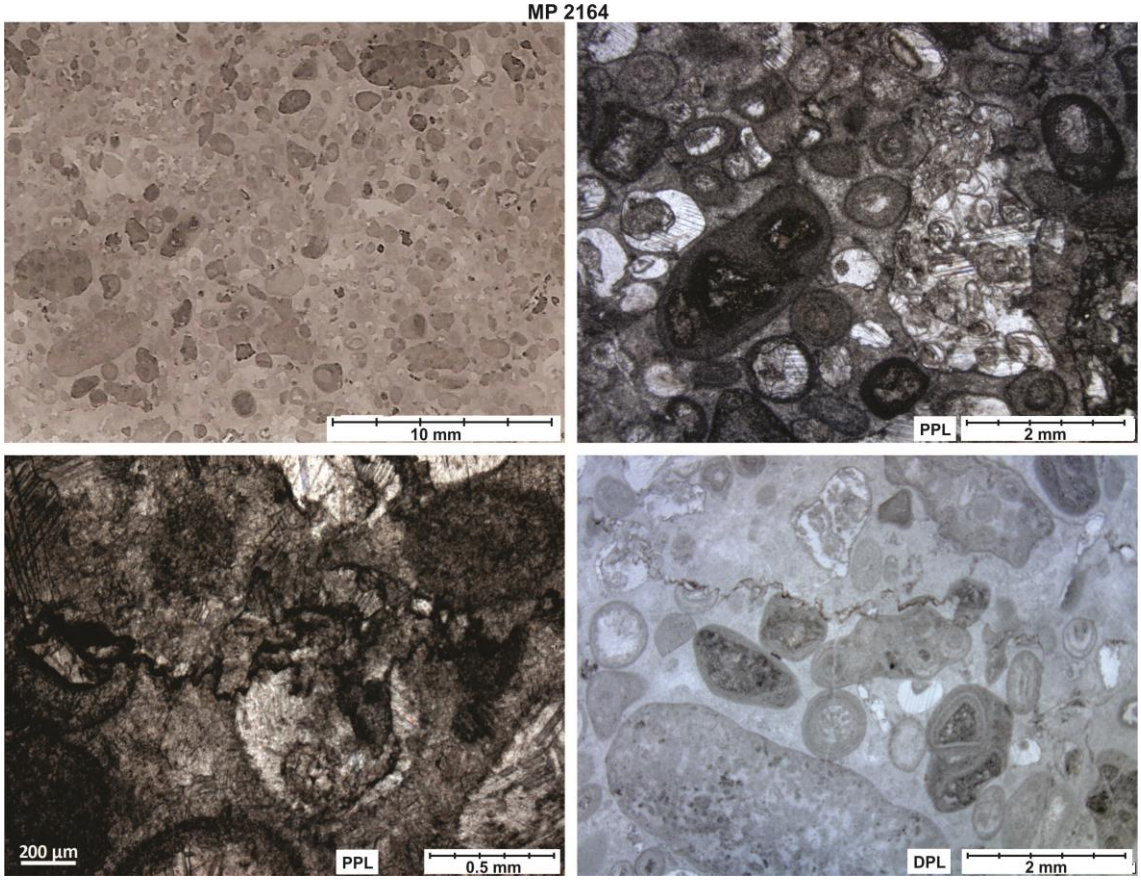

MP 1663

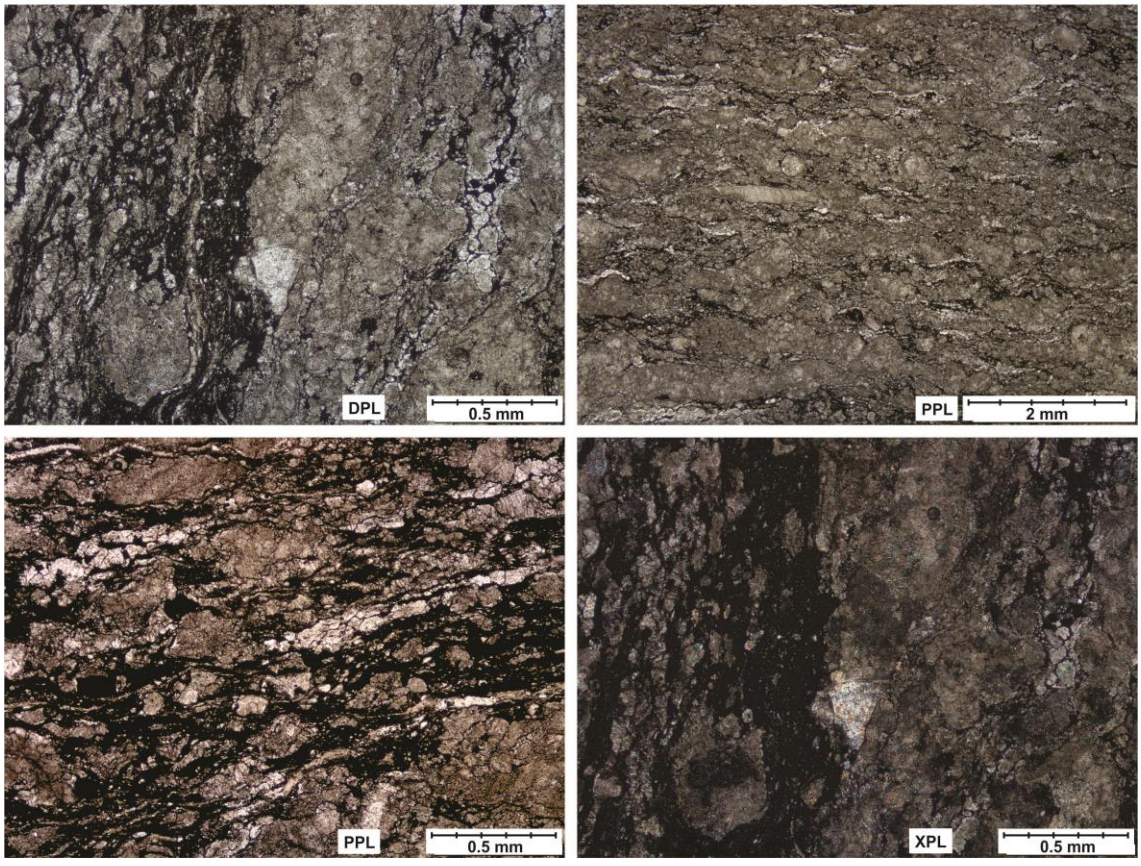

MP 1664

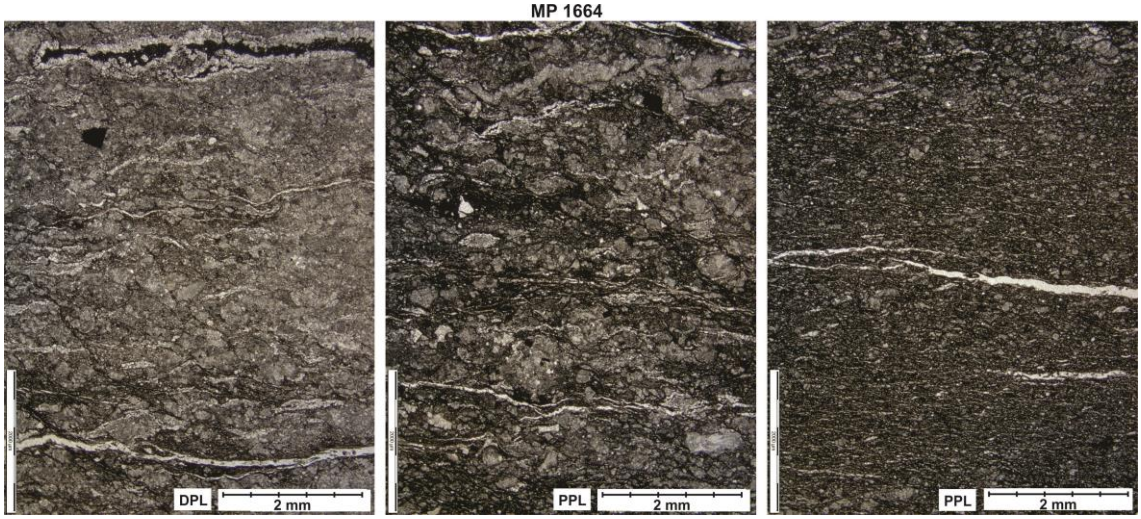

MP 1665

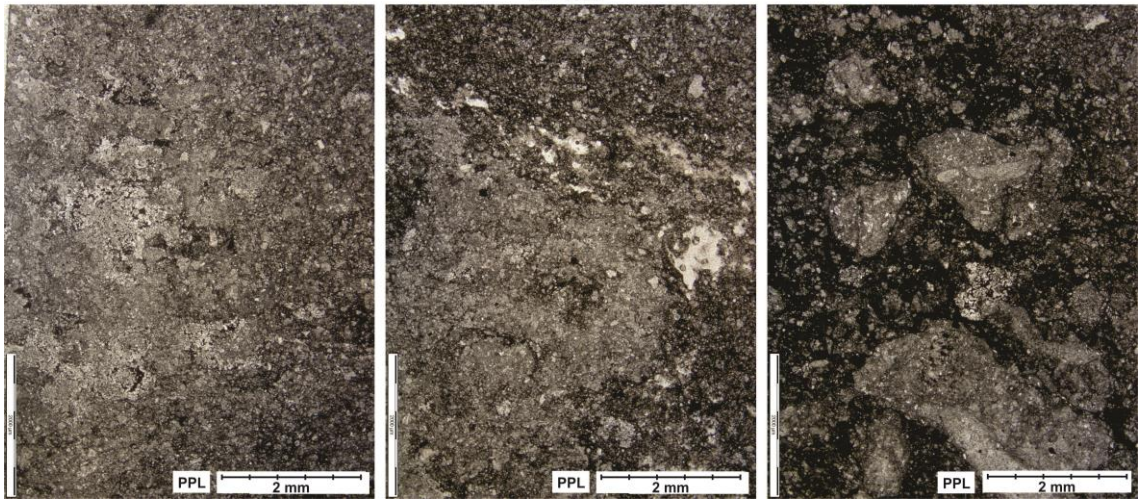

MP 1666

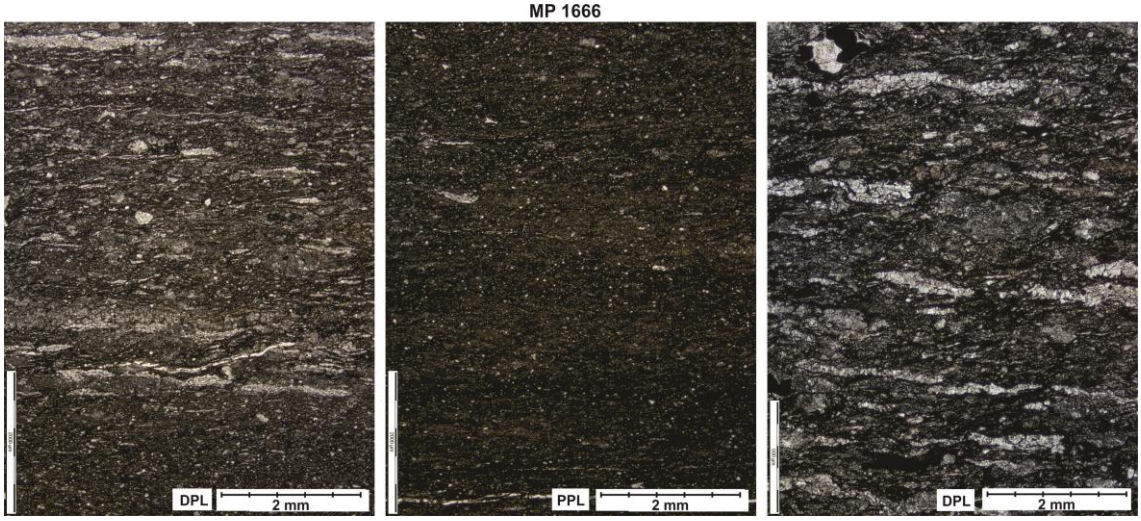

MP 1674

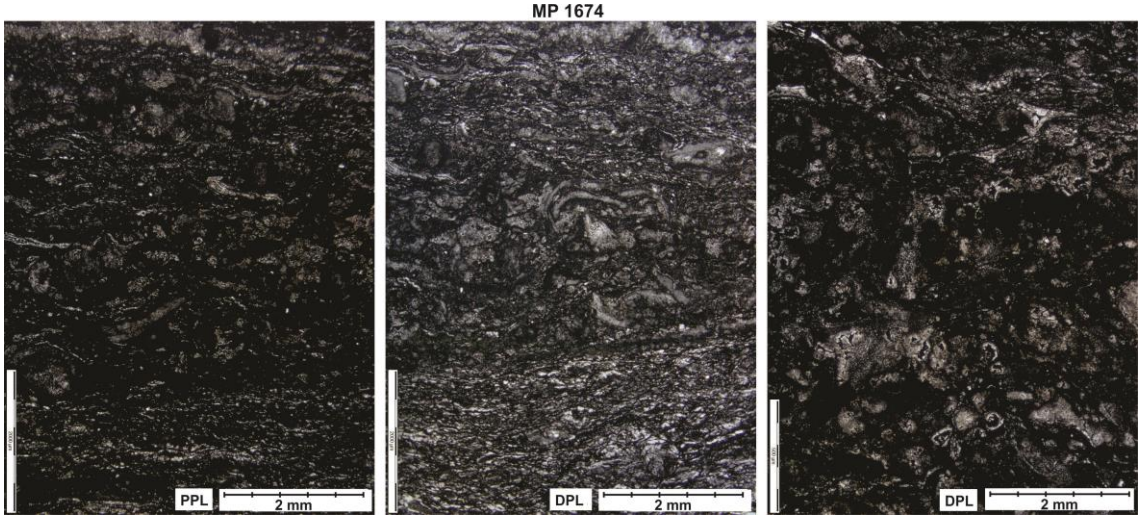

MP 1675

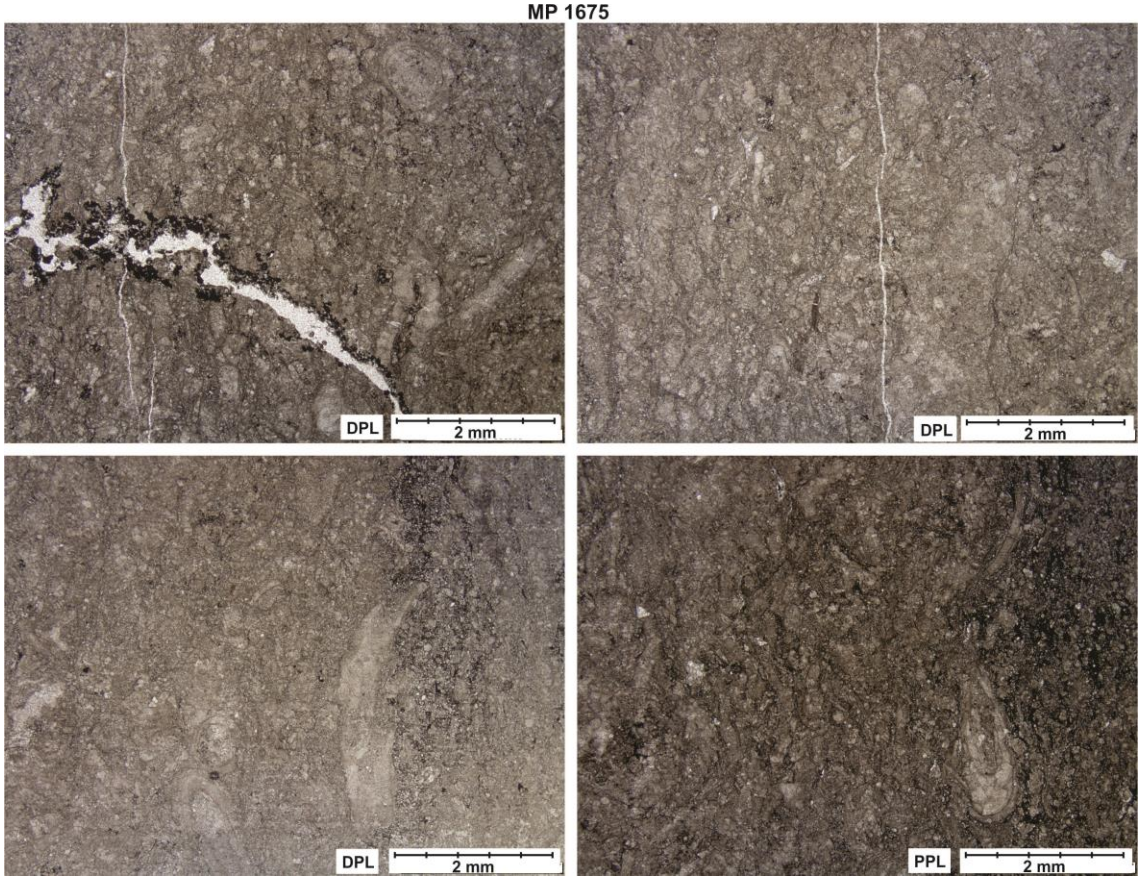

MP 1676

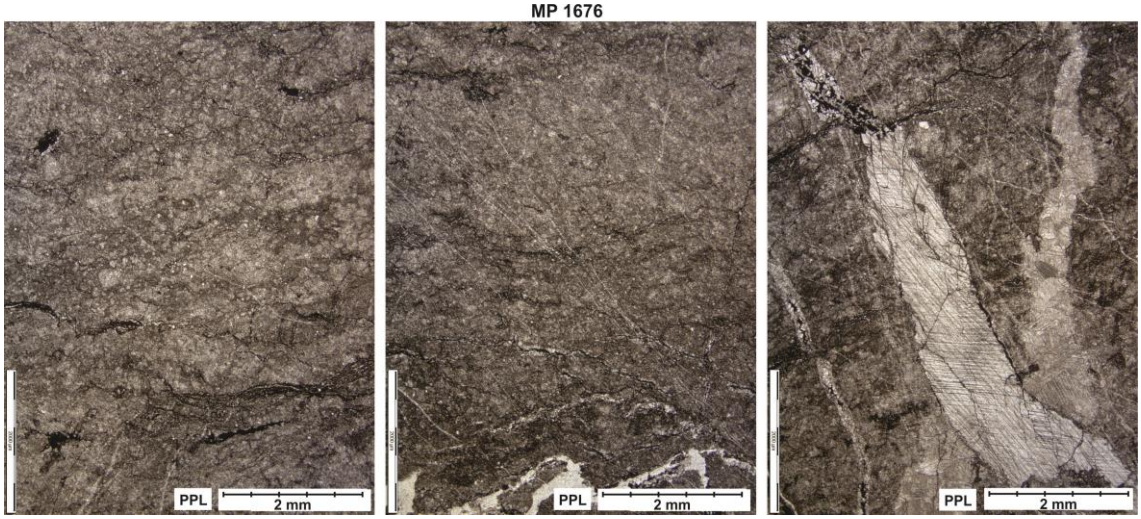

MP 1677

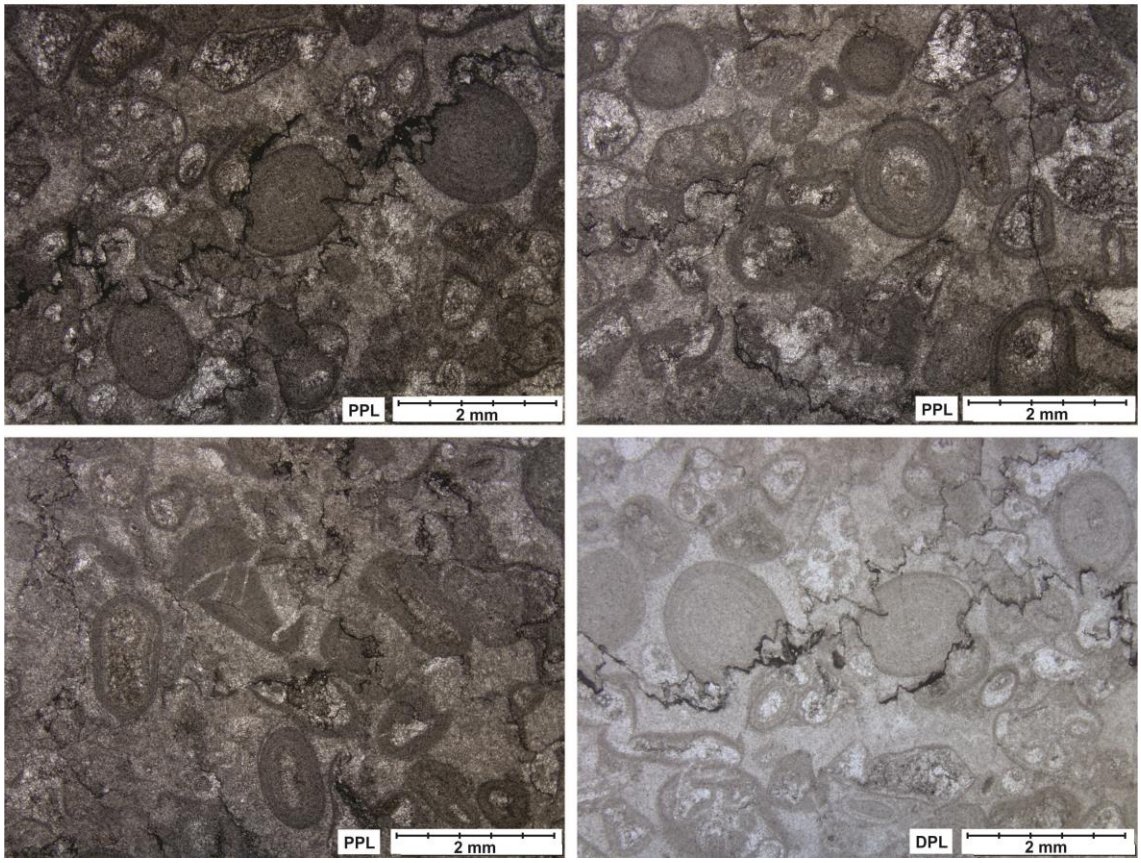

MP 1682

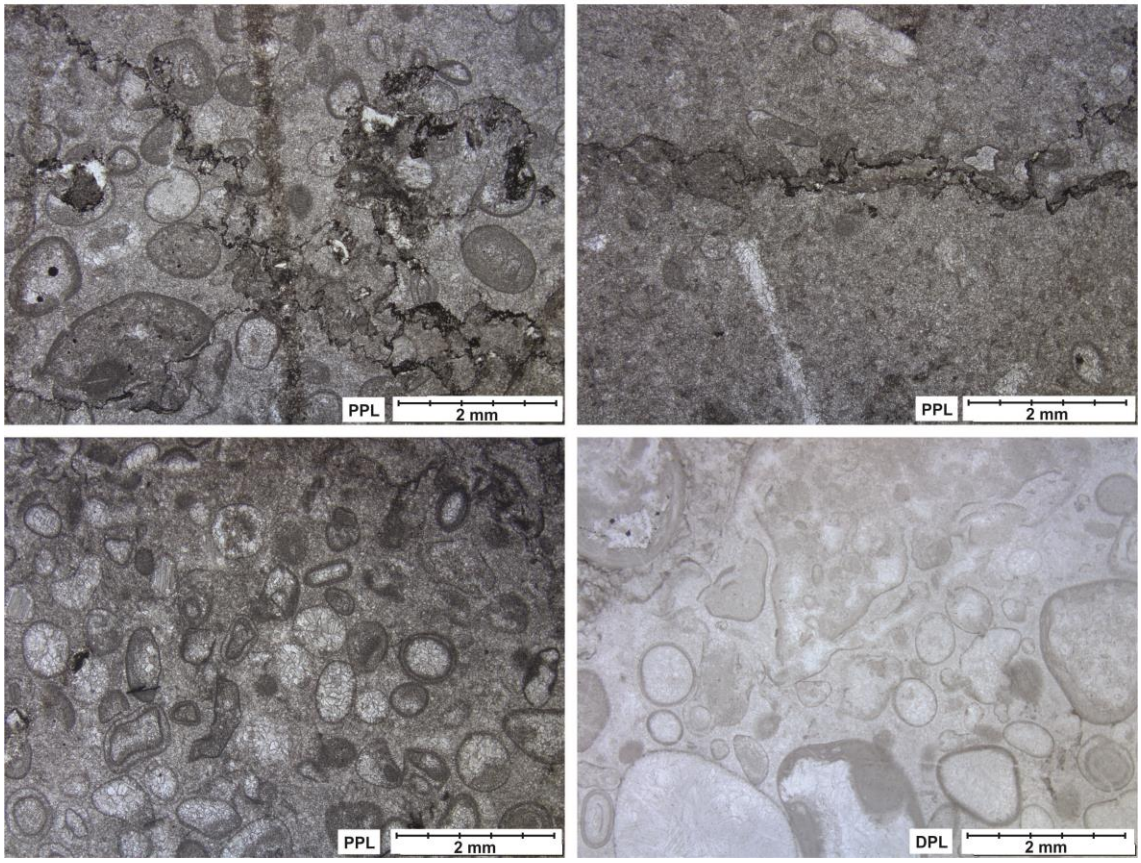

MP 1684

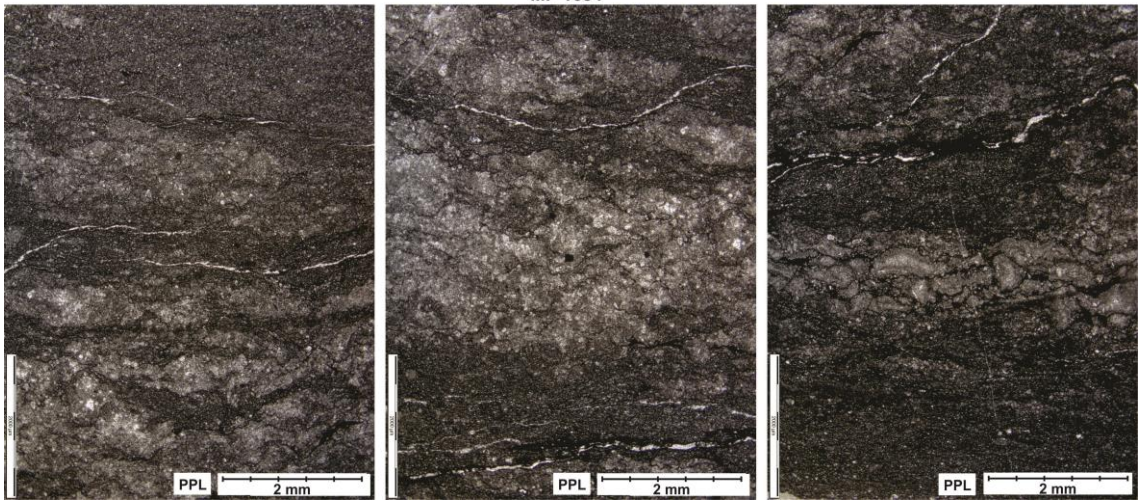

MP 1685

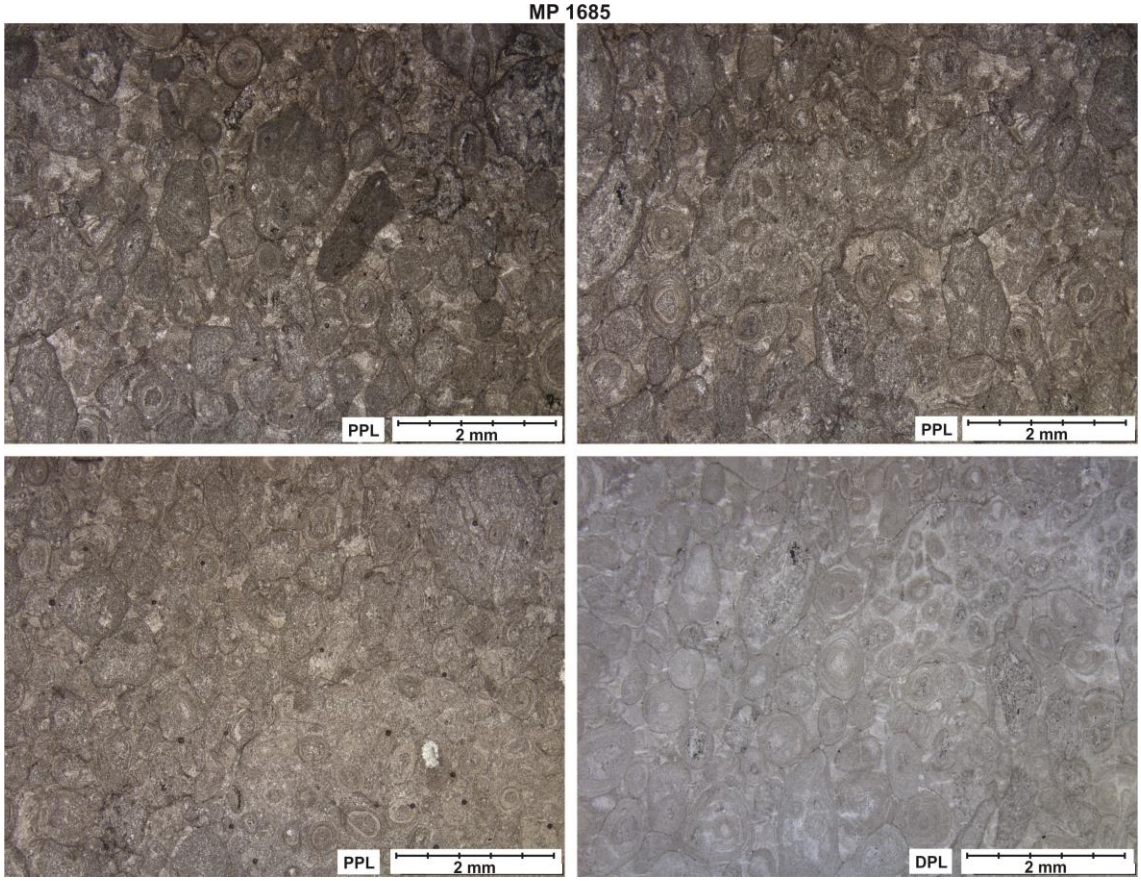

MP 1686